



**Titre:** Automatic permittivity measurement systems with cavity  
Title: perturbation techniques at 5.8 GHZ

**Auteur:** Yan Ye  
Author:

**Date:** 2004

**Type:** Mémoire ou thèse / Dissertation or Thesis

**Référence:** Ye, Y. (2004). Automatic permittivity measurement systems with cavity  
Citation: perturbation techniques at 5.8 GHZ [Mémoire de maîtrise, École Polytechnique de Montréal]. PolyPublie. <https://publications.polymtl.ca/7524/>

 **Document en libre accès dans PolyPublie**  
Open Access document in PolyPublie

**URL de PolyPublie:** <https://publications.polymtl.ca/7524/>  
PolyPublie URL:

**Directeurs de  
recherche:**  
Advisors:

**Programme:** Non spécifié  
Program:

UNIVERSITÉ DE MONTRÉAL

AUTOMATIC PERMITTIVITY MEASUREMENT SYSTEMS  
WITH CAVITY PERTURBATION TECHNIQUES AT 5.8 GHZ

YAN YE

DÉPARTEMENT DE GÉNIE ÉLECTRIQUE  
ÉCOLE POLYTECHNIQUE DE MONTRÉAL

MÉMOIRE PRÉSENTÉ EN VUE DE L'OBTENTION  
DU DIPLOME DE MAÎTRISE EN SCIENCES APPLIQUÉES  
(GÉNIE ÉLECTRIQUE)

AOÛT 2004

© YAN YE, 2004





Library and  
Archives Canada

Bibliothèque et  
Archives Canada

Published Heritage  
Branch

Direction du  
Patrimoine de l'édition

395 Wellington Street  
Ottawa ON K1A 0N4  
Canada

395, rue Wellington  
Ottawa ON K1A 0N4  
Canada

*Your file    Votre référence*

*ISBN: 0-612-97991-1*

*Our file    Notre référence*

*ISBN: 0-612-97991-1*

#### NOTICE:

The author has granted a non-exclusive license allowing Library and Archives Canada to reproduce, publish, archive, preserve, conserve, communicate to the public by telecommunication or on the Internet, loan, distribute and sell theses worldwide, for commercial or non-commercial purposes, in microform, paper, electronic and/or any other formats.

The author retains copyright ownership and moral rights in this thesis. Neither the thesis nor substantial extracts from it may be printed or otherwise reproduced without the author's permission.

#### AVIS:

L'auteur a accordé une licence non exclusive permettant à la Bibliothèque et Archives Canada de reproduire, publier, archiver, sauvegarder, conserver, transmettre au public par télécommunication ou par l'Internet, prêter, distribuer et vendre des thèses partout dans le monde, à des fins commerciales ou autres, sur support microforme, papier, électronique et/ou autres formats.

L'auteur conserve la propriété du droit d'auteur et des droits moraux qui protègent cette thèse. Ni la thèse ni des extraits substantiels de celle-ci ne doivent être imprimés ou autrement reproduits sans son autorisation.

---

In compliance with the Canadian Privacy Act some supporting forms may have been removed from this thesis.

Conformément à la loi canadienne sur la protection de la vie privée, quelques formulaires secondaires ont été enlevés de cette thèse.

While these forms may be included in the document page count, their removal does not represent any loss of content from the thesis.

Bien que ces formulaires aient inclus dans la pagination, il n'y aura aucun contenu manquant.

UNIVERSITÉ DE MONTRÉAL  
ÉCOLE POLYTECHNIQUE DE MONTRÉAL

Cette mémoire intitulée :

AUTOMATIC PERMITTIVITY MEASUREMENT SYSTEMS  
WITH CAVITY PERTURBATION TECHNIQUES AT 5.8 GHZ

présenté par : YAN YE

En vue de l'obtention du diplôme de : MAITRISE EN SCIENCES APPLIQUEES

A été dûment accepté par le jury d'examen constitué de :

M. BOSISIO, RENATO G., M. Sc. A, président

M. AKYEL, Cevdet, Ph.D., membre et directeur de recherche

M. GHANNOUCHI, Fadhel M., Ph.D., membre

## **DEDICATION**

**To my parents and my brother**

**To my husband Taijun Liu**

**To my son Xudong Liu**

## ACKNOWLEDGEMENTS

First of all, I would like to express my sincere gratitude to my advisor, Professor Cevdet Akyel, for his consistent direction, advice and encouragement during the course of my project.

Secondly, I would like to thank Mr. Jules Gauthier, Mr. Dube Steve and Mr. Brassard Roch for their assistance in the cavity fabrication and the permittivity measurement, and Mr. Rene Archambault for his help with computer software in the laboratory.

Finally, I wish also to thank my husband, Taijun Liu, for his valuable discussions and suggestions pertaining to the project.

## RÉSUMÉ

Le but de cette thèse était de développer un système automatique de mesure de constante diélectrique en utilisant l'analyseur de réseau de vecteur (VNA) à la bande de fréquence d'ISM 5.8 GHz, qui a été basé sur la technique de perturbation de cavité. Le mode  $TE_{315}$  résonnant dans une cavité rectangulaire a été choisi afin d'avoir un plus grand volume de cavité pour répondre à l'exigence de la théorie de perturbation et pour faciliter l'introduction de l'échantillon à mesurer.

Sur la base de la théorie classique de perturbation de cavité, nous avons proposé une nouvelle méthode de calibration de la mesure de constante diélectrique. Avec cette méthode de calibration, il n'est pas nécessaire de mesurer le volume d'un petit échantillon, qui élimine non seulement l'erreur de mesure du volume de l'échantillon, mais simplifie également le procédé de mesure. D'ailleurs, contrairement à la méthode traditionnelle de calibration d'un-seul-facteur de remplissage, une nouvelle méthode de calibration contenant deux facteurs remplissages a été adoptée pour améliorer l'exactitude de mesure du facteur de perte diélectrique.

Un procédé de conception d'optimisation de mode résonnant d'ordre élevé pour la cavité rectangulaire a été présenté. La fréquence de résonance mesurée de la cavité vide est 5.8066GHz. Par conséquent il y a seulement une déviation de la fréquence de 6.6MHz de la cible de conception de 5.8 GHz. Les données de mesure des modes

résonnants autour de 5.8 GHz ont démontré l'efficacité de cette méthode d'optimisation. La cavité présente un facteur de qualité élevée ( $>4000$ ) sous la condition d'une cavité vide et ce qui indique une mesure précise et fiable.

Ce système de mesure a été complètement commandé par le logiciel d'application de Windows, PermiSys, utilisé dans un PC. Le PermiSys a été développé en utilisant Microsoft VC++ et la Classe de Base de Microsoft(MFC). Il a une interface utilisateur graphique (GUI) populaire de Windows, qui a permis une opération de mesure très commode. L'interface de GPIB a été utilisée comme interface de communication entre le PC et le VNA. Le programme de communication entre le PC et le VNA a été basé sur un Logiciel d'Architecture d'Instrument Virtuel (VISA) afin d'obtenir l'indépendance de dispositif.

La méthode de curseur a été appliquée dans le PermiSys pour obtenir instantanément la constante diélectrique complexe de l'échantillon mesuré. En outre, la méthode de RCA et la méthode d'approximation Lorentziane ont été utilisées dans les données post-traitées pour réaliser des résultats de mesure plus précis.

Le système de mesure a été appliqué pour mesurer la constante diélectrique complexe de certains échantillons liquides tels que le lait, le jus d'orange, le jus de pomme, l'eau distillée, l'alcool, le méthanol et l'huile de table. Les résultats de mesure ont démontré l'efficacité et le rendement élevé de ce système de mesure automatique.

## ABSTRACT

The goal of this thesis was to develop an automatic permittivity measurement system using the Vector Network Analyzer (VNA) at the frequency band of ISM 5.8 GHz, which was based on the cavity perturbation technique. The  $TE_{315}$  resonant mode in a rectangular cavity was selected so as to have a larger cavity volume to satisfy the requirement of the perturbation theory and to make it easier to introduce the measurement sample.

On the basis of the classical cavity perturbation theory, we proposed a new calibration method of the permittivity measurement. With this calibration method, it is not necessary to measure the volume of the small sample, which not only eliminates the measurement error of the sample volume, but also simplifies the measurement procedure. Moreover, unlike the traditional one-filling-factor calibration method, a new calibration method containing two filling factors was adopted to improve the measurement accuracy of the dielectric loss factor.

An optimization design procedure of high-order resonant mode for the rectangular cavity was presented. The resonant frequency measured of the empty cavity is 5.8066GHz. Hence there is only 6.6MHz frequency deviation from the design target of 5.8 GHz. The measurement data of the resonant modes around 5.8 GHz demonstrated the effectiveness of this optimization method. The cavity exhibited a high Q-factor

(>4000) under empty cavity condition and thereby indicated an accurate and reliable measurement.

This measurement system was completely controlled by the Windows application software, PermiSys, used in a PC. The PermiSys was developed using Microsoft VC++ and Microsoft Foundation Class (MFC). It has a popular Windows Graphical User Interface (GUI), which enabled a very convenient measurement operation. The GPIB interface was used as the communication interface between PC and VNA. The communication program between PC and VNA was based on the Virtual Instrument Software Architecture (VISA) so as to obtain device independence.

The Cursor method was implemented in the PermiSys to obtain instantaneously the complex permittivity of the sample measured. In addition, the RCA method and the Lorentzian fitting method were utilized in post-data processing to achieve more accurate measurement results.

The measurement system was applied to measure the complex permittivity of some liquid samples such as milk, orange juice, apple juice, distilled water, alcohol, methanol and edible oil. The measurement results demonstrated the effectiveness and high efficiency of this automatic measurement system.



## CONDENSÉ EN FRANÇAIS

# LES SYSTÈMES DE MESURE AUTOMATIQUE DE PERMITTIVITÉ AVEC DES TECHNIQUES DE PERTURBATION DE LA CAVITÉ À 5.8 GHZ

### *0.1 Introduction*

Les permittivités de différents matériaux diélectriques jouent un rôle important dans plusieurs domaines industriels. La permittivité est un paramètre critique pour le substrat utilisé dans la conception des circuits à hautes fréquences. Ces circuits ont des applications dans les domaines de l'électronique et dans les systèmes de communication. Dans le domaine de l'ingénierie de l'agriculture, Le teneur en humidité des produits est mesuré moyennant leurs permittivités. En addition, les permittivités de ces produits permet aux biologistes en agriculture de comprendre d'avantage les caractéristiques de ces produits. Dans le domaine médical, la permittivité du sang humain change avec la variation de la santé de patient. Par conséquent, les mesures de la permittivité du patient sont utilisées par le médecin et ceci afin de juger l'état de santé du patient. En plus, la technique de mesure de la permittivité a été utilisée avec succès dans l'industrie pétrolière afin de mesurer le contenu en eau du pétrole.

Malgré l'existence de plusieurs importantes applications de la propriété de permittivité, comment faire les mesures des permittivités des différents matériaux diélectriques d'une façon efficace et précise a été un problème qui a attiré l'attention de

plusieurs chercheurs à travers le monde. Parmi les méthodes existantes, la méthode de perturbation de la cavité résonnante est la méthode la plus recommandée pour mesurer la permittivité des matériaux et ceci grâce à ses caractéristiques avantageuses. Dans ce projet, nous allons étudier cette technique de mesure en utilisant un système de mesure de la permittivité employant une cavité rectangulaire.

Cette méthode nécessite la mesure de la fréquence de résonance et la mesure du facteur de qualité de la cavité vide ainsi que de la cavité contenant l'échantillon. Cependant cette méthode présente l'inconvénient de ne pas être directe ainsi qu'elle peut engendrer des erreurs de précision sur les mesures obtenues. Par conséquent, il est nécessaire de développer un système de mesure automatique de la permittivité qui dispose d'une interface logicielle interactive et ceci afin de faciliter le procédé de mesure et le rendre automatique.

Il existe plusieurs travaux de recherche sur les mesures des permittivités avec la méthode de cavité résonnante aux fréquences centrales 915 MHz et 2.45 GHz (ISM). Il existe peu de travaux dans la littérature qui reportent des mesures de la permittivité à la fréquence centrale 5.8 GHz. Les systèmes commerciaux de communication ou d'électronique (comme les systèmes de facturation des frais de circulation dans les rues) sont de plus en plus implantés à la fréquence 5.8 GHz. Par conséquent, il est très utile d'étudier les caractéristiques diélectriques des matériaux dans cette fréquence. L'objectif principal de cette étude est de développer un système de mesure automatique de la

permittivité à 5.8 GHz en utilisant un analyseur des réseaux vectoriel (VNA) et ceci en se basant sur la technique de perturbation de la cavité.

## 0.2 Mesure de la permittivité complexe par perturbation de la cavité

Après l'introduction de l'échantillon dans une cavité, la puissance crête qui correspond à la fréquence de résonance diminue. En addition, la courbe de résonance devient plus large que la courbe originale de la cavité vide. En d'autre terme, le facteur de qualité de la cavité résonnante diminue après l'insertion de l'échantillon. Ces changements peuvent être utilisés pour calculer la permittivité complexe de l'échantillon.

Le changement de la fréquence angulaire complexe d'une cavité résonnante dû à l'introduction d'un échantillon est donné par la relation suivante:

$$\frac{\omega - \omega_0}{\omega_0} = -\left(\frac{\varepsilon_r - 1}{2}\right) \frac{\iiint_{V_s} \overline{E_0^*} \cdot \overline{E} dV}{\iiint_{V_0} |\overline{E_0}|^2 dV} \quad (0.1)$$

Avec

$\omega_0$  et  $\omega$  sont les fréquences angulaires complexes avant et après l'introduction de l'échantillon.

$\varepsilon_r$  est la permittivité complexe relative ( $\varepsilon_r = \varepsilon / \varepsilon_0$ ) de l'échantillon.

$\overline{E}_0$  et  $\overline{E}$  sont les champ électriques micro-ondes dans la cavité avant et après l'introduction de l'échantillon;

$V_0$  est le volume dans la cavité;

$V_s$  est le volume de l'échantillon;

Supposons que la permittivité complexe des matériaux est  $\varepsilon_r = \varepsilon_r' - j\varepsilon_r''$ , alors à partir de l'équation (0.1), on peut déduire :

$$\varepsilon_r' = 1 + \frac{2}{C} \left( 1 - \frac{f}{f_0} \right) \quad (0.2)$$

$$\varepsilon_r'' = \frac{1}{C} \left( \frac{1}{Q} - \frac{1}{Q_0} \right) \quad (0.3)$$

Avec

$$C = \frac{\iiint_{V_s} \overline{E}_0 \cdot \overline{E} dV}{\iiint_{V_0} |\overline{E}_0|^2 dV} \quad (0.4)$$

$Q_0$  et  $Q$  sont les facteurs de qualité de la cavité avant et après l'introduction de l'échantillon.

Dans l'équation (0.4), le champ  $\overline{E}$  de l'échantillon dépend de la permittivité, de la forme et de la taille de l'échantillon sous mesure. Par conséquent le paramètre  $C$  est un paramètre variable. Ainsi, afin d'exprimer clairement cette relation, deux paramètres  $F_1$  et  $F_2$  remplacent  $C$  sont introduits comme suit :

$$\varepsilon_r' = 1 + F_1' \frac{V_0}{V_s} \left( 1 - \frac{f}{f_0} \right) \quad (0.5)$$

$$\varepsilon_r'' = F_2' \frac{V_0}{V_s} \left( \frac{1}{Q} - \frac{1}{Q_0} \right) \quad (0.6)$$

D'une façon similaire au paramètre  $C$ , les paramètres  $F_1'$  et  $F_2'$  sont reliés à : la configuration et le mode d'opération de la cavité, la permittivité et la forme de l'échantillon et la position de l'échantillon dans la cavité.

Puisqu'il est difficile de calculer analytiquement les paramètres  $F_1(F_1')$  et  $F_2(F_2')$  pour des modes de résonance très élevés. Ces paramètres sont souvent obtenus par calibration en utilisant un échantillon standard avec une permittivité connue à l'avance. Il est à mentionner que l'échantillon standard utilisé dans la calibration doit avoir une configuration similaire à celle des échantillons à mesurer.

Dans certains cas spéciaux, la forme et le volume des échantillons mesurés sont les mêmes, comme l'exemple des échantillons de liquides versées dans des tubes minces en quartz. Ainsi dans les équations (0.5) et (0.6), on peut exprimer  $F_1'' = F_1' \frac{V_0}{V_s}$  et

$F_2'' = F_2' \frac{V_0}{V_s}$ . Ainsi, on obtient :

$$\varepsilon_r' = 1 + F_1'' \left( 1 - \frac{f}{f_0} \right) \quad (0.7)$$

$$\varepsilon_r'' = F_2'' \left( \frac{1}{Q} - \frac{1}{Q_0} \right) \quad (0.8)$$

Dans ce cas, on peut éviter de mesurer le volume de l'échantillon et le volume de la cavité. Ceci simplifie non seulement le procédé de mesure, mais aussi améliore la précision des mesures. En effet, il est souvent difficile de mesurer avec précision le volume du liquide échantillon dans un tube mince en quartz.

### ***0.3 Conception d'une cavité rectangulaire résonante***

La cavité résonnante est une partie clé dans le système automatique de mesure de la permittivité. Dans le cas de la méthode de perturbation, les cavités circulaires et rectangulaires sont les deux types de structures qui sont souvent adoptées par les chercheurs. Dans ce projet, la cavité rectangulaire est celle qui est choisie. En considérant que la fréquence centrale de résonance est 5.8 GHz. ceci correspond à une longueur d'onde de 5.17 cm. Si on utilise le mode dominant  $TE_{10x}$ , la dimension transversale de la cavité doit être de faible valeur et ceci pour satisfaire la condition de la théorie de perturbation. Par conséquent, il est important de choisir un mode de résonance de haut ordre et ceci afin d'améliorer la précision des mesures. En se basant sur l'analyse du champ électromagnétique, le mode  $TE_{315}$  est choisi dans ce projet.

La procédure de conception de la cavité résonnante rectangulaire consiste en la détermination de la largeur  $a$  et du hauteur  $b$  du guide d'onde, le calcul de la longueur  $c$

de la cavité, et la sélection du matériau de la cavité. Puisque le mode  $TE_{315}$  est un mode de haut ordre, la procédure de détermination des dimensions de la cavité est plus compliquée que dans le cas d'utilisation du mode dominant. Selon l'analyse de la longueur d'onde de coupure du guide d'onde, huit modes de haut ordre,  $TE_{01}$ ,  $TE_{20}$ ,  $TE_{11}$ ,  $TM_{11}$ ,  $TE_{21}$ ,  $TM_{21}$  et  $TE_{30}$ , existent lorsque  $a$  est égale à  $2b$  avec  $TE_{31}$  est le mode d'opération. Ainsi, il peut y avoir plusieurs modes autour de la fréquence de 5.8 GHz qui apparaissent lorsque la cavité est excitée. Ceci n'est pas ce qu'on attend. Ainsi, nous devons examiner la fréquence de résonance pour tous les modes possibles et ceci afin de garantir qu'il n'y a un gap suffisant entre la fréquence d'opération et les fréquences de résonances des autres modes de hauts ordres.

Afin d'éviter d'exciter d'autres modes résonnants au même fréquence attendue, la largeur  $a$  et la longueur  $b$  du guide d'onde doivent être judicieusement choisis. Ce processus de choix implique une procédure d'essai à erreur afin que les fréquences résonnantes de tous les autres modes soient différentes de la fréquence de résonance d'opération. Afin d'atteindre cette finalité, un programme d'optimisation a été élaboré en utilisant le logiciel Matlab. En utilisant ce programme, les dimensions de la cavité rectangulaire correspondant à la fréquence de résonance d'opération 5.8 GHz sont choisies comme suit :

$$a=127.203\text{mm}=5.008\text{in}; b=43.688\text{mm}=1.720\text{in}; c=245.339\text{mm}=9.659\text{in}.$$

En utilisant une cavité ayant les dimensions déjà mentionnées, il existe neuf autres modes  $TE_{10}$ ,  $TE_{20}$ ,  $TE_{01}$ ,  $TE_{30}$ ,  $TE/TM_{11}$ ,  $TE/TM_{21}$  et  $TE_{40}$ , qui peuvent exister mise à part le mode d'opération  $TE/TM_{31}$ . Les résultats de l'analyse du mode de la cavité résonnante ont démontré que les différences de fréquence pour toutes les autres modes de résonances sont plus grandes que 170 MHz. En plus, il existe seulement 17 modes de résonance possibles dans une bande de fréquence de 500 MHz et ceci au lieu de 27 modes de résonances possibles dans le cas où  $a$  est égale à  $2b$ .

En se basant sur des résultats de calcul du facteur de qualité pour quelques types de matériaux, l'aluminium est choisi comme le matériau de la cavité utilisée dans ce projet. Selon de l'analyse du champ électromagnétique dans cavité, la position de l'échantillon, les composants de couplage à l'entrée et à la sortie sont choisis en référence aux positions des maximums du champ. Des sondes sont sélectionnées comme des composants d'entrées et de sorties de couplage. Cette configuration est utile pour supprimer d'autres modes de hauts ou de bas ordres inattendus dans la cavité résonnante, et spécialement supprimer le mode  $TM_{315}$ .

#### ***0.4 Développement du système de mesure automatique de la permittivité --- PermiSys***

PermiSys est logiciel pour contrôler le système de mesure automatique qui a été développé en utilisant les outils de programmation Visual C++ et Microsoft Foundation



Class (MFC). La méthodologie de programmation oriente objet (OOP) a été adoptée pour attribuer au programme une architecture bien organisée et ceci afin que le logiciel soit bien facile à comprendre. La programmation OOP améliore largement l'efficacité du développement des programmes en utilisant la notion des classes des objets. En addition, l'utilisation de l'utilitaire MFC facilite la conception de l'interface interactive.

La fenêtre principale de PermiSys possède une interface usuelle, ainsi il est plus convenable pour un utilisateur de la manipuler et ceci en comparaison avec l'interface traditionnelle développée avec un système d'exploitation DOS. En addition, l'interface développée simplifie le processus de mesure : la cavité vide nécessite d'être mesurée en premier lieu et ensuite on procède directement à la mesure de la permittivité des différents matériaux. La courbe de résonance est montrée dans la fenêtre principale du logiciel et peut être sauvegardée dans un fichier \*.txt dans l'ordinateur.

### ***0.5 Traitement des données mesurées***

Comme décrit dans la section 0.2, la permittivité complexe est calculée selon la fréquence de résonance  $f$  et le facteur de qualité  $Q$  de la cavité résonnante sans et avec l'échantillon. Ainsi la précision des mesures de la permittivité complexe est complètement dépendante de la précision de la fréquence de résonance  $f$  et le facteur de qualité  $Q$ . Pour un VNA comme HP8753D ou HP8510B qui sont disponibles dans notre laboratoire, le maximum de points de mesure est 801 points. Ceci veut dire qu'il y a

uniquement 801 échantillons de fréquences pour la mesure d'un signal. Ceci détermine la résolution de mesure de la fréquence. Afin d'augmenter la résolution de la fréquence, la rangée de balayage en fréquence doit être aussi petite que possible. Par conséquent, nous devons trouver une solution pour obtenir une fréquence de résonance  $f_0$  et un facteur de qualité  $Q$  qui sont précis.

### ➤ *La méthode de Lorentzian*

Pour la méthode de Lorentzian, la variation de  $|S_{21}|$  versus la fréquence est concordée à la courbe de Lorentzian en utilisant l'algorithme des moindres carrés. La fréquence de résonance  $f_0$ , la largeur de bande  $\Delta f_{\text{Lorent}}$ , la constante  $A_1$ , la pente  $A_2$ , le facteur  $A_3$ , et l'amplitude maximum  $|S_{\text{max}}|$  sont utilisées comme des paramètres de la formule de Lorentzian :

$$|S_{21}(f)| = A_1 + A_2 f + \frac{|S_{\text{max}}| + A_3 f}{\sqrt{1 + 4 \left( \frac{f - f_0}{\Delta f_{\text{Lorent}}} \right)^2}} \quad (0.9)$$

Les paramètres de l'équation (0.11) sont déterminés par concordance des données mesurées. Ensuite l'équation (0.11) peut être utilisée pour calculer un nouveau ensemble de  $|S_{21}(f)|$ . La fréquence de résonance est donnée par la valeur moyenne des deux de fréquences correspondantes à la moitié de puissance. Puisque le terme  $|S_{21}(f)|$  est utilisé à la place de puissance, le point de moitié de puissance correspond à

$\sqrt{2}/2|S_{21}(f)|_{\max} \approx 0.707|S_{21}(f)|_{\max}$ . Le facteur de qualité  $Q$  est calculé en utilisant la formule suivante:

$$Q = \frac{f_r}{f_2 - f_1} \quad (0.10)$$

### ➤ *La méthode RCA*

Les méthodes de mesure mentionnées ci haut présentent une difficulté majeure au niveau de la détermination de la largeur de bande qui calculée à partir des fréquences de moitié de puissance. Une méthode pratique couramment utilisée consiste à mesurer directement la largeur de bande voulue. Cependant cette méthode est entachée par des erreurs sur la détermination du facteur de qualité. Afin d'améliorer la précision sur l'évaluation du facteur de qualité  $Q$  la méthode RCA (l'air de la courbe de résonance) a été proposée comme alternative. Cette méthode est basée sur le principe suivant : le facteur de perte d'un circuit de résonance est équivalent à l'intégrale en domaine fréquentiel de sa courbe de puissance de résonance. Cette méthode peut utiliser toutes les données des mesures et aussi minimiser les effets du bruit. Le facteur de qualité est déterminé par l'équation suivante :

$$Q = f_0 \frac{P_0}{S_1} \tan^{-1} \sqrt{\frac{P_0}{P(x_r)} - 1} \quad (0.11)$$

Avec

$f_0$  est la frequency de resonance,

$P_0$  est la puissance crête du circuit de sortie;

$P(x_r)$  est la puissance d'entrée du résonateur;

$S_1$  est l'air de la courbe de résonance dans le domaine fréquentiel.

## ***0.6 Procédures de mesure, résultats et discussion***

Nous avons utilisé l'analyseur des réseaux HP8753 pour mesurer le paramètre  $S_{21}$  de la cavité dans la bande de fréquence utile. Le processus de mesure est totalement contrôlé par le PermiSys à travers l'interface GPIB.

Le procédé de mesure inclut les étapes:

- Initialisation des paramètres,
- Mesure de la fréquence de résonance et du facteur de qualité  $Q$  de la cavité vide,
- Calibration du système de mesure avec un échantillon standard,
- Mesure de la fréquence de résonance et du facteur de qualité de la cavité avec échantillon, et calcul de la permittivité complexe de l'échantillon.

L'eau distillée est utilisée comme un échantillon standard pour calibrer le système de mesure. Sa permittivité à 25°C est de  $72.27 - j*20.22$  et ceci pour la fréquence d'opération 5.8 GHz. D'autres échantillons liquides comme le lait (3.25% gras), le jus d'orange, l'alcool, le méthanol et l'huile de table, sont mesurés afin de valider le système de mesure. Ces échantillons liquides sont injectés moyennant un tube à pipette en verre.

Quoique la perte de la pipette soit très faible, afin d'améliorer l'exactitude de mesure, une pipette vide est considérée comme faisant partie de la cavité vide.

## **0.7 Conclusion**

L'objectif de cette recherche est de concevoir et d'implémenter un système de mesure automatique de la permittivité des matériaux diélectriques dans la bande de fréquence 5.8 GHz. La mesure de la permittivité est basée sur la théorie de perturbation de la cavité et utilise une cavité rectangulaire opérant au mode  $TE_{315}$ . Une méthode de calibration, qui est valable pour tout mode de résonance des cavités rectangulaires ou circulaires a été proposée et implémentée dans un système de mesure automatique de permittivité dans la bande 5.8 GHz.

Une approche de conception basée sur des optimisations pour les hauts modes de résonance dans une cavité rectangulaire a été présentée. La fréquence de résonance d'une cavité vide est mesurée à 5.8066 GHz. Ainsi, il existe seulement 6.6 MHz de fréquence de déviation de la fréquence de conception de 5.8 GHz. Les résultats des mesures du mode de résonance autour de 5.8 GHz ont montré l'utilité de la procédure d'optimisation. La cavité présente un facteur de qualité ( $Q > 4000$ ) dans la condition de cavité vide, ceci prouve que les mesures sont précises et fiables.

Le logiciel PermiSys de mesure de la permittivité, dotée d'une interface graphique GUI, a été développée en utilisant les outils de programmation VC++ et MFC. La communication entre le PC et le VNA est assurée par l'interface GPIB. L'architecture des logiciels d'instrumentation (VISA) a été adoptée dans le programme de communication et ceci afin que le logiciel PermiSys soit capable de communiquer avec plusieurs programmes avec différentes cartes GPIB. En outre, le logiciel PermiSys offre un mode visuel pour configurer et contrôler le système de mesure. En suivant le menu de la fenêtre du logiciel, les mesures peuvent être effectuées étape par étape. En addition, des mesures en des instants différents peuvent être effectuées d'une façon automatique et ceci afin d'améliorer la précision des résultats. Les données des courbes de résonance et la permittivité mesurée par la méthode de Curseur sont sauvegardées dans le PC. Les données des courbes de résonance peuvent être d'avantage traité par le logiciel MATLAB avec la méthode RCA ou la méthode de Lorentizan et ceci afin d'avoir des résultats plus précis. Ce traitement par MATLAB s'effectue également moyennant une interface interactive. Le programme Matlab peut être exécuté à partir du menu du logiciel PermiSys ou directement à partir de la fenêtre principale du logiciel Windows.

Les résultats des mesures pour plusieurs exemples de liquides ont validé l'utilité et la précision du système de mesure. En outre, les résultats de traitement des données ont montré que la méthode RCA et la méthode Lorentizan sont plus précises que la méthode de Curseur.

## TABLE OF CONTENTS

DEDICATION.....	IV
ACKNOWLEDGEMENTS.....	V
RÉSUMÉ.....	VI
ABSTRACT .....	VIII
CONDENSÉ EN FRANÇAIS.....	X
0.1 INTRODUCTION .....	X
0.2 MESURE DE LA PERMITTIVITÉ COMPLEXE PAR PERTURBATION DE LA CAVITÉ .....	XII
0.3 CONCEPTION D'UNE CAVITÉ RECTANGULAIRE RÉSONANTE .....	XV
0.4 DÉVELOPPEMENT DU SYSTÈME DE MESURE AUTOMATIQUE DE LA PERMITTIVITÉ --- PERMiSYS.....	XVII
0.5 TRAITEMENT DES DONNÉES MESURÉES .....	XVIII
0.6 PROCÉDURES DE MESURE, RÉSULTANTS ET DISCUSSION.....	XXI
0.7 CONCLUSION .....	XXII
FIGURE LIST .....	XXIV
TABLE LIST .....	XXVIII
LIST OF SIGNS AND ABBREVIATION .....	XXIX
CHAPTER 1 INTRODUCTION .....	1
1.1 RESONANT CAVITY METHODS .....	2
1.2 PERMITTIVITY MEASUREMENT AT 5.8 GHZ.....	3
REFERENCES .....	6

**CHAPTER 2 COMPLEX PERMITTIVITY MEASUREMENT WITH CAVITY  
PERTURBATION TECHNIQUE ..... 8**

2.1 INTRODUCTION .....	8
2.2 A LUMPED-ELEMENT EQUIVALENT MODEL OF SAMPLE-LOADED CAVITIES .....	8
2.3 CAVITY PERTURBATION THEORY .....	10
2.4 CALIBRATION METHODS OF PERMITTIVITY MEASUREMENT.....	13
REFERENCES .....	17

**CHAPTER 3 RECTANGULAR RESONANT CAVITY DESIGN..... 19**

3.1 INTRODUCTION .....	19
3.2 RECTANGULAR RESONANT CAVITY DESIGN PROCEDURE.....	20
3.2.1 Determination of width $a$ and height $b$ of waveguide .....	20
3.2.2 Determination of length $c$ of rectangular cavity .....	23
3.2.3 Selection of cavity material.....	23
3.3 OPTIMIZATION DESIGN OF HIGH-ORDER MODE CAVITY .....	24
3.4 CAVITY OPTIMIZATION RESULTS AND RESONANT MODE ANALYSIS.....	31
3.5 DETERMINATION OF THE POSITIONS OF THE SAMPLE, THE INPUT AND THE OUTPUT COUPLING DEVICES .....	34
3.6 RESULTS OF THE PRACTICAL 5.8 GHz EMPTY RESONANT CAVITY.....	37
REFERENCES .....	39

**CHAPTER 4 DEVELOPMENT OF THE AUTOMATIC PERMITTIVITY  
MEASUREMENT SOFTWARE --- PERMISYS..... 40**

4.1 INTRODUCTION .....	40
4.2 MEASUREMENT SOFTWARE SYSTEM ARCHITECTURE .....	41
4.3 MAIN CLASSES DESIGN .....	42
4.4 GRAPHICAL USER INTERFACE (GUI) DESIGN .....	51
REFERENCES .....	58

**CHAPTER 5 SECTION 1CHAPTER 5 MEASUREMENT DATA PROCESSING..... 60**



5.1 INTRODUCTION .....	60
5.2 CURSOR METHOD .....	62
5.3 LORENTZIAN FIT METHOD .....	64
5.4 RCA METHOD.....	66
5.4.1 <i>Principle of RCA method</i> .....	66
5.4.2 <i>Software implementation of RCA method</i> .....	70
5.5 SOFTWARE DESIGN .....	73
5.5.1 <i>Graphical User interface (GUI) Design</i> .....	73
5.5.2 <i>Post data processing flow chart</i> .....	75
REFERENCES .....	78
 <b>CHAPTER 6 MEASUREMENT PROCEDURES, RESULTS AND DISCUSSION.....</b>	<b>79</b>
6.1 THE AUTOMATIC PERMITTIVITY MEASUREMENT SYSTEM.....	79
6.2 PERMITTIVITY MEASUREMENT PROCEDURES .....	80
6.2.1 <i>Parameter setting</i> .....	80
6.2.2 <i>Measuring the empty cavity</i> .....	82
6.2.3 <i>Measurement system calibration</i> .....	83
6.2.4 <i>Measuring the permittivity of the sample</i> .....	84
6.3 MEASUREMENT RESULTS AND DISCUSSION.....	88
6.3.1 <i>High loss liquid</i> .....	89
6.3.2 <i>Median loss liquid</i> .....	102
6.3.3 <i>Low loss liquid</i> .....	108
REFERENCES .....	114
 <b>CHAPTER 7 CONCLUSION AND FUTURE WORK.....</b>	<b>115</b>
 <b>APPENDIX I VNA PROGRAMMING .....</b>	<b>119</b>
<b>APPENDIX II VIRTUAL INSTRUMENT SOFTWARE ARCHITECTURE (VISA) ...</b>	<b>122</b>

## FIGURE LIST

Figure 2.1 Lumped-element equivalent circuit of a resonant cavity .....	9
Figure 2.2 A typical cavity perturbation response .....	10
Figure 2.3 Perturbation of resonant cavity (a) empty cavity; (b) cavity with a small sample .....	10
Figure 3.1 the rectangular resonant cavity .....	20
Figure 3.2 Distribution figure of cutoff wavelengths in rectangular waveguide ( $a=2b$ ) .....	22
Figure 3.3 Optimization flowchart of high-order mode rectangular cavity .....	29
Figure 3.4 waveguide width range function flowchart.....	30
Figure 3.5 Cavity resonant mode analysis flowchart .....	30
Figure 3.6 Electrical field distribution for $TE_{315}$ mode at $y=b$ plane .....	36
Figure 3.7 Magnetic field distribution for $TE_{315}$ mode at $z=0$ plane.....	36
Figure 3.8 Positions of the sample, the input and the output coupling probes.....	37
Figure 3.9 5.8GHz resonant cavity.....	38
Figure 3.10 the practical mode spectrum of the 5.8 GHz empty resonant cavity .....	39
Figure 4.1 the measurement software system architecture.....	42
Figure 4.2 Class CVectorNetworkAnalyzer CRC card.....	43
Figure 4.3 Class CMeasurementResults CRC card.....	44
Figure 4.4 Class CCurveData CRC card .....	44
Figure 4.5 Class COptionDlg CRC card .....	45
Figure 4.6 Class CCalibrationDlg CRC card .....	45
Figure 4.7 Class CAutoMeasurementDlg CRC card .....	46

Figure 4.8 Class CBrowseResultDlg CRC card.....	46
Figure 4.9 Class CMeasurementPropertyPage2 CRC card.....	47
Figure 4.10 Class CMeasurementPropertyPage2 CRC card.....	47
Figure 4.11 Class CMeasurementPropertyPage3 CRC card.....	48
Figure 4.12 Class CMeasurementPropertyPage4 CRC card.....	49
Figure 4.13 Class CPermiSysDoc CRC card .....	49
Figure 4.14 Class CPermiSysMainView CRC card.....	50
Figure 4.15 Class CMainFrame CRC card.....	50
Figure 4.16 Class CPermiSysApp CRC card.....	51
Figure 4.17 the main window of PermiSys .....	52
Figure 4.18 Empty cavity measurement wizard.....	53
Figure 4.19 Calibration dialog .....	54
Figure 4.20 Sample measurement wizard .....	55
Figure 4. 21 automatic measurement dialog .....	56
Figure 4.22 Option setting dialog.....	57
Figure 4.23 Browse result dialog .....	58
Figure 5. 1 Cursor method.....	63
Figure 5.2 Lorentzian resonance curve .....	64
Figure 5.3 A typical Lorentzian fit curve.....	65
Figure 5.4 Finite range integration for RCA method.....	68
Figure 5.5 A typical curve fit for RCA .....	71
Figure 5.6 Post data processing GUI.....	76
Figure 5.7 Post data processing flow chart .....	77
Figure 6.1 the diagram of the automatic permittivity measurement system .....	79

Figure 6.2 the photo of the automatic permittivity measurement system .....	80
Figure 6.3 Parameter setting.....	81
Figure 6.4 Empty cavity measurement.....	82
Figure 6.5 Calibration dialog .....	84
Figure 6.6 Permittivity measurement wizard (a) measure cavity with sample (b) calculate the permittivity .....	86
Figure 6.7 Automatic multi-time measurement .....	87
Figure 6.8 The measurement results displayed in the main window .....	88
Figure 6.9 Dielectric constant of distilled water at 5.8 GHz.....	92
Figure 6.10 Dielectric loss factor of distilled water at 5.8 GHz.....	92
Figure 6.11 Dielectric constant of 3.25% milk at 5.8 GHz.....	95
Figure 6.12 Dielectric loss factor of 3.25% milk at 5.8 GHz.....	95
Figure 6.13 Dielectric constant of orange juice at 5.8 GHz.....	98
Figure 6.14 Dielectric loss factor of orange juice at 5.8 GHz.....	98
Figure 6.15 Dielectric constant of apple juice at 5.8 GHz .....	101
Figure 6.16 Dielectric loss factor of apple juice at 5.8 GHz.....	101
Figure 6.17 Dielectric constant of methanol at 5.8GHz.....	104
Figure 6.18 Dielectric loss factor of methanol at 5.8 GHz .....	104
Figure 6.19 Dielectric constant of 70% alcohol at 5.8 GHz .....	107
Figure 6.20 Dielectric loss factor of 70% alcohol at 5.8 GHz .....	107
Figure 6.21 Dielectric constant of Canola oil at 5.8 GHz.....	110
Figure 6.22 Dielectric loss factor of Canola oil at 5.8 GHz.....	110
Figure 6.23 Dielectric constant of vegetable oil at 5.8 GHz.....	113
Figure 6.24 Dielectric loss factor of vegetable oil at 5.8 GHz.....	113

Figure A-1 VISA implementation context .....	122
--	-----

## TABLE LIST

Table 3.1 Resonant mode analysis within 500 MHz frequency difference .....	25
Table 3.2 cutoff wavelengths of the related waveguide modes .....	32
Table 3.3 Resonant mode analysis within 500 MHz frequency difference ( $a \approx 2.9b$ ) ..	32
Table 3.4 The quality factors of the cavity with different materials for TE <sub>315</sub> resonant mode .....	33
Table 5.1 Typical measurement results the resonant frequency $f_0$ and the quality factor Q .....	61
Table 6.1 Permittivity of distilled water at 5.8 GHz .....	91
Table 6.2 Permittivity of 3.25%-fat milk at 5.8 GHz.....	94
Table 6.3 Permittivity of orange juice at 5.8 GHz .....	97
Table 6.4 Permittivity of apple juice at 5.8 GHz .....	100
Table 6.5 Permittivity of methanol at 5.8 GHz .....	103
Table 6.6 Permittivity of 70% alcohol at 5.8 GHz.....	106
Table 6.7 Permittivity of Canola oil at 5.8 GHz .....	109
Table 6.8 Permittivity of vegetable oil at 5.8 GHz .....	112

## LIST OF SIGNS AND ABBREVIATION

ADT	Abstract Data Type
API	Application-Programming Interface
COM	Component Object Model
CRC	Class Responsibilities Collaborators
$f_0$	resonant frequency
GPIB	General Purpose Interface Bus, IEEE488.1
GUI	Graphical User Interface
ISM	Industrial, Scientific and Medical
Q	Quality factor
MDI	Multiple Document Interface
MFC	Microsoft Foundation Class
OOP	Object-Oriented Programming
PC	Personnel Computer
RCA	Resonance Curve Area
SDI	Signal Document Interface
VC++	Visual C++
VISA	Virtual Instrument Software Architecture
VNA	Vector Network Analyzer
$\varepsilon_r'$	relative dielectric constant
$\varepsilon_r''$	loss factor of materials

## Chapter 1 Introduction

Dielectric parameters of various dielectric materials are found more and more important applications in different industrial fields. They are critical parameters of the substrate for high frequency circuit design in electronic and communication areas. In agricultural engineering, the moisture contents of the agro-products are measured depending on the permittivity. The agrobiologists can further understand the characteristics of the different agro-products or soils based on their permittivities. In medical field, the complex permittivity of human blood will change with the variation of the health condition of the examinee. Hence, the measurement results of the permittivity of the patient are helpful for the doctor to judge the health situation of the patient. Moreover, the permittivity measurement technique has been successfully used in petroleum industry to measure the water content of the petroleum.

Although there are so many important applications for permittivity measurement, how to measure the permittivity of different dielectric materials accurately and more efficiently has been an important issue for many researchers in the world. There are many permittivity measurement methods that have been presented in papers [1][2] or in the electromagnetic technique books [3][4]. They can be classified as waveguide methods, resonant cavity methods, open-ended coaxial probe methods, and impedance methods[3].



Among these methods, the resonant cavity method is a popular permittivity measurement method due to its high accuracy. We will make a brief review for this method in the following section.

### **1.1 Resonant cavity methods**

The resonant cavity method applies the cavity perturbation technique to measure the permittivity of the dielectric materials. In fact, the perturbation of a resonant cavity caused by the insertion of a dielectric sample can be employed to calculate the complex permittivity by measuring the change in resonant frequency and its quality factor.

The cavity perturbation theory was first proposed by Bethe and Schwinger in 1943[6]. The perturbation is caused by the insertion of small dielectric sample into a cavity and by a small variation of the electromagnetic boundary of the cavity. In 1960, Waldron presented the detailed perturbation formula with necessary approximations[7]. He pointed out that the high accuracy perturbation formula would only be possible if the sample is properly shaped and positioned in the resonant cavity. The sensitivity of measurement can be increased through putting the sample in the strong field region. The cavity perturbation method was summarized by Chao in 1985[8]. Moreover, a cavity perturbation technique, in which high temperature measurements can be processed, was described by Akyel and Bosisio in 1989[9].

The cavity perturbation technique belongs to two-port techniques and is suitable for different kind of samples including solid and liquid samples. It can provide a measurement result with high accuracy. This method is suitable for low loss materials and can provide more accurate measurements, however, measurements are limited to the resonant frequency of the cavity.

## **1.2 Permittivity measurement at 5.8 GHz**

There are a large amount of permittivity measurement researches with the resonant cavity methods at ISM 915 MHz and 2.45 GHz frequency band. However, at ISM 5.8 GHz frequency band, we have not found any dedicated reports about the permittivity measurement at this ISM frequency band. Since there is stronger interference at 915 MHz and 2.45 GHz, more and more commercial electronic or communication systems, such as road billing systems and WLAN, are implemented at 5.8 GHz. For this reason, it is significant to study the dielectric characteristics of materials at ISM 5.8 GHz frequency band.

Since the resonant cavity method is one of the most accurate permittivity measurement methods, it will be taken as the main approach in this project. The rectangular cavity perturbation theory will be reviewed and some useful measurement formula will be deduced in Chapter 2.

To design the cavity using the dominant cavity mode, the cavity will become smaller and smaller as the resonant frequency increases. However, the permittivity measurement with the resonant cavity method is based on the perturbation theory. In order to satisfy the perturbation condition, the volume of the cavity should be as large as possible. Therefore, the resonant mode has to be high-order resonant mode instead of the dominant mode. This makes the cavity design become far more complicated than in low frequency band. The details about the high-order mode cavity design will be discussed in Chapter 3.

Whatever which measurement method is adopted, generally the measurement process is tedious and easy to make error, especially when it is necessary to make multi-time measurement for a sample. Consequently, in order to solve these problems, the research target of this project is to set up an automatic cavity permittivity measurement system at 5.8 GHz. Measurement control software, PermiSys, will be developed with VC++. The design process of PermiSys will be presented in Chapter 4.

In order to improve the accuracy of the measurement results, there are several special data processing techniques that have been implemented to produce a more accurate result. The details are presented in Chapter 5.

In Chapter 6, the measurement procedure is given and several liquid samples have been measured to validate the measurement system. Finally, from our experimental results, we draw some conclusions in Chapter 7.

## References

- [1] Afar M N, Birch J R and Clarke R N, The measurements of properties of materials  
*Proc. IEEE* 74 pp.183, 1986
- [2] Stuchly M A and Stuchly S S, Coaxial line reflection methods for measuring  
dielectric properties of biological substances at radio and microwave frequencies  
*IEEE Trans. Instrum. Meas.* 29, pp.176–83, 1980
- [3] Sucher M and Fox J, *Handbook of Microwave Measurements* vol II (Polytechnic  
Press Institute of Brooklyn) pp. 495, 1963
- [4] Roussy G and Pearce J A, *Foundations and Industrial Applications of microwaves  
and Radio Frequency Fields* (New York: Wiley) pp.331, 1995
- [5] A.W. Kraszewski, Microwave Aquametry-a review, *Jounal of Microwave Power*,  
vol.15, no.4, pp209-220, 1980.
- [6] H.A. Bethe and J. Schwinger, “Perturbation Theory for Cavities,” National Defense  
Research Committee, Contractor’s Report #D1-117, Cornell Univ., March 1943.
- [7] R. A. Waldron, “Errors due to the uncertainty principle in swept frequency cavity  
measurements of properties of materials,” *IEEE Trans. Microwave Theory Tech.*,  
vol. MTT–16, pp. 314–315, 1968.
- [8] S. H. Chao, “Measurements of microwave conductivity and dielectric constant by  
the cavity perturbation method and their errors,” *IEEE Trans. Microwave Theory  
Tech.*, vol. MTT-33, pp. 519–526, 1985.

- [9] Akyel, C.; Bosisio, R.G., "New developments on automated-active circuits for permittivity measurements at microwave frequencies Instrumentation and measurement", IEEE Transactions on MTT, vol. 38, Issue: 2, pp. 496 –504, 1989.

## **Chapter 2   Complex Permittivity Measurement with Cavity Perturbation Technique**

### ***2.1 Introduction***

The cavity perturbation technique was originally developed by Bethe and Schwinger in 1943 [1]. Then it is widely used in the study of the electromagnetic properties of dielectrics, semiconductors, magnetic materials and composite materials [2]-[7]. For the permittivity measurement with this method, the sample under test is introduced into a resonant cavity, and its complex permittivity can be determined from the variation of the resonant frequency and the quality factor of the cavity caused by the insertion of the sample.

In this chapter we will discuss the lumped-element equivalent model of a sample-loaded resonant cavity at first. Then the deduction of the cavity perturbation formulas for permittivity measurements will be reviewed. At last, new two-filling-factor calibration method is proposed based on the perturbation formulas.

### ***2.2 A Lumped-Element Equivalent Model of Sample-Loaded Cavities***

A resonant cavity can be represented by a lumped-element equivalent circuit, which consists of inductance  $L$ , resistance  $R$  and capacitance  $C$ , as shown in Figure 2.1 [7]. In this figure, the equivalent capacitance  $C$  includes a major part  $C_1$  and a minor part  $C_2$ .

We can assume that the introducing a sample into the cavity is equivalent to inserting the sample into the capacitor  $C_2$ , so only the minor part  $C_2$  is affected by the sample. Then the resonant frequency  $f$  and the quality factor  $Q$  of the resonant cavity can be computed as follows[8]:

$$f = \frac{1}{2\pi\sqrt{L(C_1 + C_2)}} \quad (2.1)$$

$$Q = R\sqrt{\frac{C_1 + C_2}{L}} \quad (2.2)$$

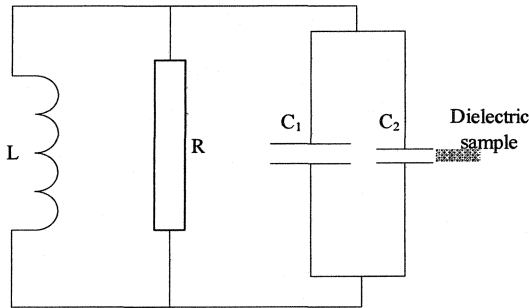


Figure 2.1 Lumped-element equivalent circuit of a resonant cavity

Hence the resonant frequency  $f$  will decrease after inserting a sample in the cavity according to the equation(2.1). The overall effects of the increase of capacitance  $C$  and the decrease of resistance  $R$  will determine the change of the quality factor  $Q$  caused by inserting the sample into the cavity. Generally, the overall effects always cause  $Q$  to decrease. A typical example of a cavity perturbation response is shown in Figure 2.2 in terms of the resonance frequency  $f$  and the quality factor  $Q$ .



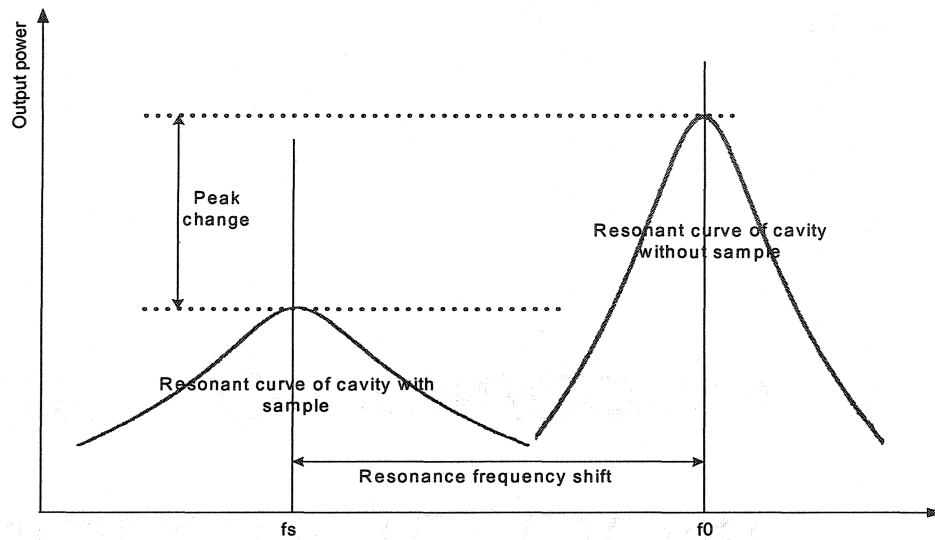
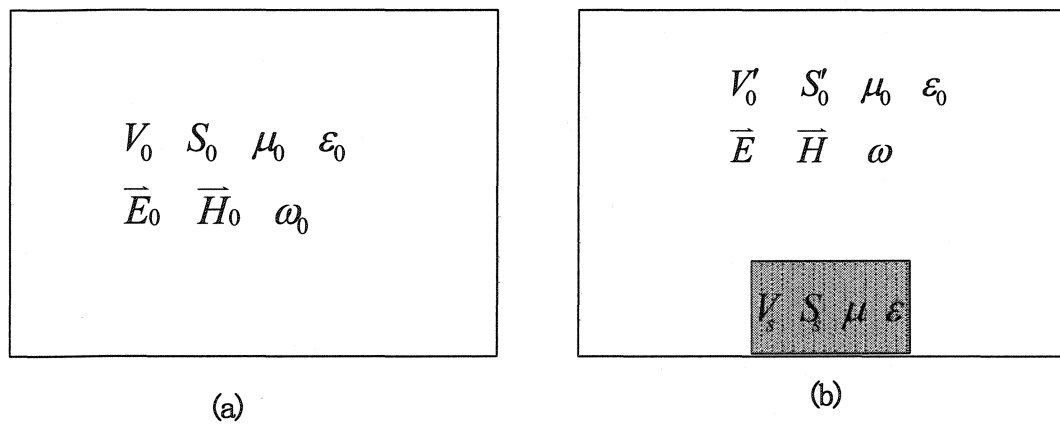


Figure 2.2 A typical cavity perturbation response



Fi

Figure 2.3 Perturbation of resonant cavity (a) empty cavity; (b) cavity with a small sample

### 2.3 Cavity Perturbation Theory

A cavity perturbation with a small sample is shown in Figure 2.3.  $V_0$  is the volume of the empty cavity.  $S_0$  is the area of the inner surface of the empty cavity.  $\epsilon_0$  is the

dielectric constant of air.  $\mu_0$  is the permeability of air.  $\overline{E}_0$ ,  $\overline{H}_0$  and  $\omega_0$  are electrical field intensity, magnetic field intensity and the resonant frequency in the empty cavity, respectively.  $V_s$  is the volume of the sample and  $S_s$  is the surface area of the sample.  $\varepsilon$  is the dielectric constant of the sample.  $\mu$  is the permeability of the sample.  $\overline{E}$ ,  $\overline{H}$  and  $\omega$  are electrical field intensity, magnetic field intensity and the resonant frequency in the cavity after introducing the small sample, respectively.

From Maxwell equations [8], we have

For empty cavity:

$$\left. \begin{aligned} \nabla \times \overline{H}_0 &= j\omega_0 \varepsilon_0 \overline{E}_0 \\ \nabla \times \overline{E}_0 &= -j\omega_0 \mu_0 \overline{H}_0 \end{aligned} \right\} \quad (2.3)$$

For cavity with the sample:

$$\left. \begin{aligned} \nabla \times \overline{H} &= j\omega \varepsilon_0 \overline{E} \quad (\text{outside } V_s) \\ \nabla \times \overline{H} &= j\omega \varepsilon \overline{E} \quad (\text{inside } V_s) \end{aligned} \right\} \quad (2.4)$$

$$\left. \begin{aligned} \nabla \times \overline{E} &= -j\omega \mu_0 \overline{H} \quad (\text{outside } V_s) \\ \nabla \times \overline{E} &= -j\omega \mu \overline{H} \quad (\text{inside } V_s) \end{aligned} \right\} \quad (2.5)$$

Making the scalar products of  $\overline{E}_0^*$  with equation (2.4):

$$\left. \begin{aligned} \overline{E}_0^* \cdot \nabla \times \overline{H} &= j\omega \varepsilon_0 \overline{E}_0^* \cdot \overline{E} \quad (\text{outside } V_s) \\ \overline{E}_0^* \cdot \nabla \times \overline{H} &= j\omega \varepsilon \overline{E}_0^* \cdot \overline{E} \quad (\text{inside } V_s) \end{aligned} \right\} \quad (2.6)$$

Making the scalar products of  $\overline{H}_0^*$  with equation (2.5):

$$\left. \begin{aligned} \overline{H}_0^* \cdot \nabla \times \overline{E} &= -j\omega \mu_0 \overline{H}_0^* \cdot \overline{H} \quad (\text{outside } V_s) \\ \overline{H}_0^* \cdot \nabla \times \overline{E} &= -j\omega \mu \overline{H}_0^* \cdot \overline{H} \quad (\text{inside } V_s) \end{aligned} \right\} \quad (2.7)$$

Making the scalar products of  $\overline{E}$  and  $\overline{H}$  with equation (2.3), respectively, we have

$$\left. \begin{aligned} \bar{E} \cdot \nabla \times \bar{H}_0^* &= -j\omega_0 \varepsilon_0 \bar{E} \cdot \bar{E}_0^* \\ \bar{H} \cdot \nabla \times \bar{E}_0^* &= j\omega_0 \mu_0 \bar{H} \cdot \bar{H}_0^* \end{aligned} \right\} \quad (2.8)$$

Integrating  $\left[ \left( \bar{E}_0^* \cdot \nabla \times \bar{H} + \bar{E} \cdot \nabla \times \bar{H}_0^* \right) - \left( \bar{H}_0^* \cdot \nabla \times \bar{E} + \bar{H} \cdot \nabla \times \bar{E}_0^* \right) \right]$  over volume  $V_0$ , we obtain

$$\begin{aligned} & \iiint_{V_0} \left[ \left( \bar{E}_0^* \cdot \nabla \times \bar{H} + \bar{E} \cdot \nabla \times \bar{H}_0^* \right) - \left( \bar{H}_0^* \cdot \nabla \times \bar{E} + \bar{H} \cdot \nabla \times \bar{E}_0^* \right) \right] dv \\ &= \iiint_{V-V_s} \left[ j\varepsilon_0 (\omega - \omega_0) \bar{E}_0^* \cdot \bar{E} + j\mu_0 (\omega - \omega_0) \bar{H}_0^* \cdot \bar{H} \right] dv \\ &+ \iiint_{V_s} \left[ j(\omega\varepsilon - \omega_0\varepsilon_0) \bar{E}_0^* \cdot \bar{E} + j(\omega\mu - \omega_0\mu_0) \bar{H}_0^* \cdot \bar{H} \right] dv \end{aligned} \quad (2.9)$$

We now use the vector identity:

$$\nabla \cdot (\bar{A} \times \bar{B}) = \bar{B} \cdot (\nabla \times \bar{A}) - \bar{A} \cdot (\nabla \times \bar{B}) \quad (2.10)$$

The left-hand side of equation (2.9) becomes

$$\begin{aligned} & \iiint_{V_0} \left[ \left( \bar{E}_0^* \cdot \nabla \times \bar{H} + \bar{E} \cdot \nabla \times \bar{H}_0^* \right) - \left( \bar{H}_0^* \cdot \nabla \times \bar{E} + \bar{H} \cdot \nabla \times \bar{E}_0^* \right) \right] dv \\ &= - \iiint_{V_0} \left[ \nabla \cdot (\bar{E}_0^* \times \bar{H}) + \nabla \cdot (\bar{E} \times \bar{H}_0^*) \right] dv \\ &= \oint_{S_0} \left[ (\bar{E}_0^* \times \bar{H}) + (\bar{E} \times \bar{H}_0^*) \right] \cdot \hat{n} ds \end{aligned} \quad (2.11)$$

where  $\hat{n}$  is the unit normal vector of the inside wall of the cavity. Since  $\hat{n} \times \bar{E} = 0$  at the inside wall of the cavity, the area integral at the right-hand side of the equation (2.11) equals to zero. Thus from equation (2.9) we obtain

$$\begin{aligned} & \iiint_{V-V_s} \left[ j\varepsilon_0 (\omega - \omega_0) \bar{E}_0^* \cdot \bar{E} + j\mu_0 (\omega - \omega_0) \bar{H}_0^* \cdot \bar{H} \right] dv \\ &+ \iiint_{V_s} \left[ j(\omega\varepsilon - \omega_0\varepsilon_0) \bar{E}_0^* \cdot \bar{E} + j(\omega\mu - \omega_0\mu_0) \bar{H}_0^* \cdot \bar{H} \right] dv = 0 \end{aligned} \quad (2.12)$$

As  $V_s$  is very small, the integral over the volume  $(V_0 - V_s)$  can be approximated by the integral over the volume  $V_0$ . Moreover, considering  $(\omega\varepsilon - \omega_0\varepsilon_0) \approx \omega_0(\varepsilon - \varepsilon_0)$  and

$(\omega\mu - \omega_0\mu_0) \approx \omega_0(\mu - \mu_0)$ , equation (2.12) then becomes

$$\frac{\omega - \omega_0}{\omega_0} = - \frac{\iiint_{V_s} [(\varepsilon - \varepsilon_0) \overline{E_0^*} \cdot \overline{E} + (\mu - \mu_0) \overline{H_0^*} \cdot \overline{H}] dV}{\iiint_{V_0} (\varepsilon_0 \overline{E_0^*} \cdot \overline{E} + \mu_0 \overline{H_0^*} \cdot \overline{H}) dV} \quad (2.13)$$

Equation (2.13) expresses the relative change of complex angular frequency of a resonant cavity due to the introduction of a sample into the cavity[9], [10]. It should be noted that this equation is based on the assumptions that the cavity wall is perfect conductor and the perturbation is very small.

In this project, we will only study the characterizations of dielectrics (nonmagnetic materials), so  $\mu = \mu_0$ . We assume  $\varepsilon = \varepsilon_r \varepsilon_0$ , where  $\varepsilon_r$  is the relative complex permittivity of the sample. Therefore, equation (2.13) can be written as

$$\frac{\omega - \omega_0}{\omega_0} = - \left( \frac{\varepsilon_r - 1}{2} \right) \frac{\iiint_{V_s} \overline{E_0^*} \cdot \overline{E} dV}{\iiint_{V_0} |\overline{E_0}|^2 dV} \quad (2.14)$$

## 2.4 Calibration Methods of Permittivity Measurement

The relationship between the complex angular frequency and the quality factor of a resonant cavity can be expressed as follows [10]

$$\omega = \omega_r + j\omega_i \quad (2.15)$$

$$\omega_r = 2\pi f \quad (2.16)$$

$$Q = \frac{\omega_r}{2\omega_i} \quad (2.17)$$

If we suppose that  $\omega_{r0} \approx \omega_r$  and  $\omega_{i0} \ll \omega_{r0}$ , then we have

$$\begin{aligned} \frac{\omega - \omega_0}{\omega_0} &= \frac{(\omega_r - \omega_{r0}) + j(\omega_i - \omega_{i0})}{\omega_{r0} \left( 1 + j \frac{\omega_{i0}}{\omega_{r0}} \right)} \\ &\approx \left[ \left( \frac{f - f_0}{f_0} \right) + j \left( \frac{1}{2Q} - \frac{1}{2Q_0} \right) \right] \left( 1 - j \frac{1}{2Q_0} \right) \\ &\approx \left( \frac{f - f_0}{f_0} \right) + j \left( \frac{1}{2Q} - \frac{1}{2Q_0} \right) \end{aligned} \quad (2.18)$$

In equation (2.18) we assume  $Q_0 \gg 1$ . Comparing equation (2.14) with equation (2.18), we have

$$\left( \frac{f - f_0}{f_0} \right) + j \left( \frac{1}{2Q} - \frac{1}{2Q_0} \right) = - \left( \frac{\epsilon_r - 1}{2} \right) \frac{\iiint_{V_s} \overline{E_0^*} \cdot \overline{E} dV}{\iiint_{V_0} |\overline{E_0}|^2 dV} \quad (2.19)$$

Suppose the complex permittivity of the material is  $\epsilon_r = \epsilon_r' - j\epsilon_r''$ , and then equation (2.19) can be rewritten as follows:

$$2 \left( \frac{f_0 - f}{f_0} \right) = (\epsilon_r' - 1) C \quad (2.20)$$

$$\frac{1}{Q} - \frac{1}{Q_0} = \epsilon_r'' C \quad (2.21)$$

where

$$C = \frac{\iiint_{V_s} \overline{E_0^*} \cdot \overline{E} dV}{\iiint_{V_0} |\overline{E_0}|^2 dV} \quad (2.22)$$

Equation (2.20) and (2.21) can also be written as

$$\varepsilon_r' = 1 + \frac{2}{C} \left( 1 - \frac{f}{f_0} \right) \quad (2.23)$$

$$\varepsilon_r'' = \frac{1}{C} \left( \frac{1}{Q} - \frac{1}{Q_0} \right) \quad (2.24)$$

In equation (2.25) and (2.26), the parameter  $C$  is generally assumed to be a constant, which is dependent on the geometry and the location of the sample and the resonant mode in the cavity, but approximately independent of the permittivities of samples. However, it is well known that the perturbed field  $E$  in the sample is a function of the permittivity and geometry of the sample under test. Therefore, in order to obtain more accurate measurement results, two parameters  $F_1$  and  $F_2$ , instead of one parameter  $C$ , are introduced to equations (2.20)-(2.24) as follows:

$$\frac{f_0 - f}{f_0} = F_1 \left( \varepsilon_r' - 1 \right) \frac{V_s}{V_0} \quad (2.27)$$

$$\frac{1}{Q} - \frac{1}{Q_0} = F_2 \varepsilon_r'' \frac{V_s}{V_0} \quad (2.28)$$

Or

$$\varepsilon_r' = 1 + F_1' \frac{V_0}{V_s} \left( 1 - \frac{f}{f_0} \right) \quad (2.29)$$

$$\varepsilon_r'' = F_2' \frac{V_0}{V_s} \left( \frac{1}{Q} - \frac{1}{Q_0} \right) \quad (2.30)$$

Where  $F_1' = 1/F_1$  and  $F_2' = 1/F_2$ . Similar to parameter C, parameters  $F_1(F_1')$  and  $F_2(F_2')$  are the function of the configurations and the resonant mode of the cavity, the geometry of the sample, and the sample's location in the cavity. Since it is very complicated to calculate the parameters  $F_1(F_1')$  and  $F_2(F_2')$  using classical electromagnetic analytical methods when the resonant mode is a high-order mode,  $F_1(F_1')$  and  $F_2(F_2')$  are usually acquired by a calibration method with a known permittivity sample as standard[11]. By the help of the variations of the resonant frequency  $f$  and the quality factor  $Q$  caused by the insertion of the standard sample,  $F_1(F_1')$  and  $F_2(F_2')$  can be determined using equation (2.27) and (2.28) or equation (2.29) and (2.30). It should be pointed out that the standard sample should be as small as possible and should have a similar geometry with the samples to be measured so as to improve the measurement accuracy.

It is well known that the low measurement accuracy of the volume of the small sample is one of the main error sources with the permittivity measurement using equation (2.29) and (2.30). However, in some special cases, the shape and volume of the measured samples always are same, for example, to measure the liquid samples with a thin quartz tube. Hence in equation (2.29) and (2.30) we can let  $F_1'' = F_1' \frac{V_0}{V_s}$  and

$F_2'' = F_2' \frac{V_0}{V_s}$ . Then we have

$$\varepsilon_r' = 1 + F_1'' \left( 1 - \frac{f}{f_0} \right) \quad (2.31)$$

$$\varepsilon_r'' = F_2'' \left( \frac{1}{Q} - \frac{1}{Q_0} \right) \quad (2.32)$$

In this case, a liquid standard, such as pure water, can be used to calibrate the measurement system so as to get  $F_1''$  and  $F_2''$  from equation (2.31) and (2.32). In this way, we can avoid measuring the volume of the sample and the volume of the cavity. Therefore, using equation (2.31) and (2.32) to compute the complex permittivity is able to improve the accuracy of the measurement since it is difficult to accurately measure the volume of the small liquid sample.

After calibrating with a standard sample, we can take advantage of equation (2.31) and (2.32) to compute the permittivity of a new sample with the same volume and shape. Consequently, the errors that caused by the measurement procedures of volume of the cavity and the sample can be avoided.

## References:

- [1] H.A. Bethe and J. Schwinger, "Perturbation Theory for Cavities," National Defense Research Committee, Contractor's Report #D1-117, Cornell Univ., March 1943.
- [2] *Dielectric Materials and Applications*, A. R. Von Hippel, Ed. Norwood, MA; Artech House, 1995.
- [3] J. N. Dahiya and R. W. Freeman, "Computer interfacing of a microwave resonant



- cavity for temperature measurements during dielectric relaxation,” *Comput. Phys.*, pp. 49–54, July/Aug. 1989.
- [4] W. Bauhofer, “Determination of semiconductor energy gaps using the microwave cavity perturbation method,” *J. Phys. E: Sci. Instrum.*, vol. 14, pp. 934–938, 1981.
- [5] A. J. B. Fuller, *Ferrites at Microwave Frequencies*. Stevenage, U.K.: Peregrinus, 1987, pp. 235-255.
- [6] B. Meng, J. Booske, and R. Cooper, “A system to measure complex permittivity of low loss ceramics at microwave frequencies and over large temperature ranges” *Rev. Sci. Instrum.*, vol. 66, no. 2, 1995, pp. 1068–1071.
- [7] Linfeng Chen; Ong, C.K.; Tan, B.T.G; “Amendment of cavity perturbation method for permittivity measurement of extremely low-loss dielectrics”, *IEEE Trans. on Instrum. Meas.*, vol.48, no.6, pp.1031-1037, Dec. 1999
- [8] R. E. Collin, *Foundations for microwave engineering*. New York: McGraw-Hill, 1992
- [9] R. A. Waldron, *Theory of guided electromagnetic waves*. London, U.K.: Van Nostrand Reinhold, 1969, ch. 6.
- [10] M. Sucher and J. Fox, *Handbook of Microwave Measurements*, 3rd ed. Brooklyn, NY: Polytechnic Press, 1963.
- [11] C. Akyel, and R. G. Bosisio, “New developments on automated-active circuits for permittivity measurements at microwave frequencies”, *IEEE Trans. Instrum. Meas.*, vol.38, no.2, pp.496-504, April 1989

## Chapter 3 Rectangular Resonant Cavity Design

### 3.1 Introduction

The rectangular resonant cavity is a key part in this automatic permittivity measurement system. Since the resonant frequency of the cavity is 5.8 GHz, it corresponds to a wavelength of 5.17 cm. If we use dominant  $TE_{10x}$  mode as what people did in 2.45 GHz[1], the transverse size would be too small to satisfy the condition of perturbation theory. For this reason, we have to select high-order resonant mode in order to improve the measurement accuracy. In this project, the  $TE_{315}$  mode was selected and the mode selection criterion will be presented in the following section. However, the design procedure of this high-order mode is more complicated than that using the dominant mode.

In this chapter we will review the design procedure of the rectangular resonant cavity using the classical electromagnetic field theory. Then the optimization of the high-order mode cavity design will be discussed and the optimization results will be given. According to the electromagnetic field distribution of the selected mode in the cavity, we will determine the position of the sample inserted as well as the positions of the input and the output probes.

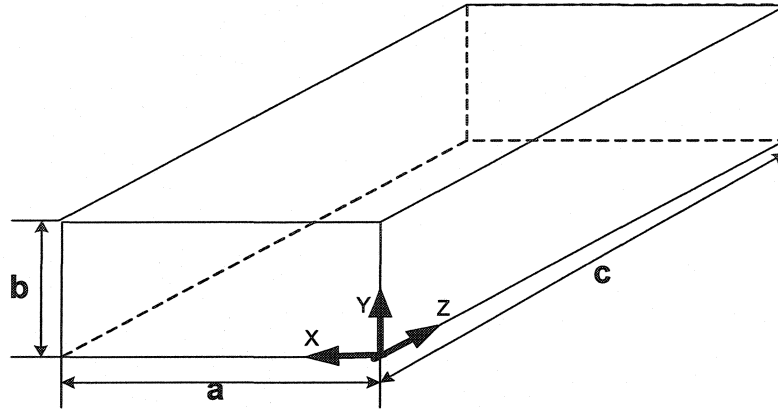


Figure 3.1 the rectangular resonant cavity

### 3.2 Rectangular resonant cavity design procedure

#### 3.2.1 Determination of width a and height b of waveguide

A rectangular resonant cavity is shown in Figure 3.1. a, b and c are the width, height and length of the rectangular cavity respectively. At first, the width a and the height b of the waveguide should be determined by classical electromagnetic field theory of waveguide. It is well known that the cut-off wavelength of the rectangular waveguide is[2]:

$$\lambda_c = \frac{2}{\sqrt{\left(\frac{m}{a}\right)^2 + \left(\frac{n}{b}\right)^2}} \quad (3.1)$$

Where m and n are called the mode index, and they stands for the number of half-waves in the x and y direction in the Figure 3.1.  $\lambda_c$  is only the function of m, n, a and b.

When the width  $a$  and the height  $b$  of the waveguide are fixed, the cutoff wavelength will decrease as  $m$  and  $n$  increase.

If the ratio  $a/b$  is assumed to be a fixed value, then the cutoff wavelengths of all of the modes can be computed from equation (3.1). The relationship between the cutoff wavelength of the work mode and the cutoff wavelengths of other modes is determined. A distribution chart of the cutoff wavelengths can be obtained from these calculation results. For example, suppose  $a/b=2$ , then the cutoff wavelength of  $TE/TM_{31}$  mode is:  $\lambda_{CTE31}=0.5547a$ . The dominant modes and the low-order mode that have longer cutoff wavelengths than that of  $TE/TM_{31}$  are  $TE_{10}$ ,  $TE_{20}$ ,  $TE_{01}$ ,  $TE_{30}$ ,  $TE_{11}/TM_{11}$ , and  $TE_{21}/TM_{21}$ . Their cutoff wavelengths are:  $\lambda_{CTE10}=2a$ ;  $\lambda_{CTE20}=\lambda_{CTE01}=a$ ;  $\lambda_{CTE30}=0.6667a$ ;  $\lambda_{CTE11}=\lambda_{CTM11}=0.8944a$ ; and  $\lambda_{CTE21}=\lambda_{CTM21}=0.7071a$ , respectively,. These eight modes ( $TE_{10}$ ,  $TE_{01}$ ,  $TE_{20}$ ,  $TE_{11}$ ,  $TM_{11}$ ,  $TE_{21}$ ,  $TM_{21}$ ,  $TE_{30}$ ) always exist whatever  $TE_{31}$  or  $TM_{31}$  mode is employed.

The nearby high-order modes that have shorter cutoff wavelengths than that of  $TE/TM_{31}$  are  $TE_{40}$ ,  $TE_{02}$ ,  $TE_{22}/TM_{22}$ ,  $TE_{41}/TM_{41}$ ,  $TE_{12}/TM_{12}$ ,  $TE_{50}$  and etc. Their cutoff wavelengths are:  $\lambda_{CTE40}=\lambda_{CTE02}=0.5a$ ;  $\lambda_{CTE12}=\lambda_{CTM12}=0.4851a$ ;  $\lambda_{CTE22}=\lambda_{CTM22}=\lambda_{CTE41}=\lambda_{CTM41}=0.4472a$ ;  $\lambda_{CTE50}=0.4a$ . These high-order modes can be avoid if the wavelength  $\lambda$  of the work mode  $TE/TM_{31}$  is longer than  $\lambda_{CTE40}=\lambda_{CTE02}=0.5a$ . The distribution chart of the cutoff wavelengths of all these modes is shown in Figure 3.2. Hence the wavelength  $\lambda_0$  of the work mode  $TE_{31}/TM_{31}$  has to satisfy following condition:

$$\lambda_{TE40} < \lambda_0 < \lambda_{TE31} \quad (3.2)$$

That is:  $0.5a < \lambda_0 < 0.5547a$

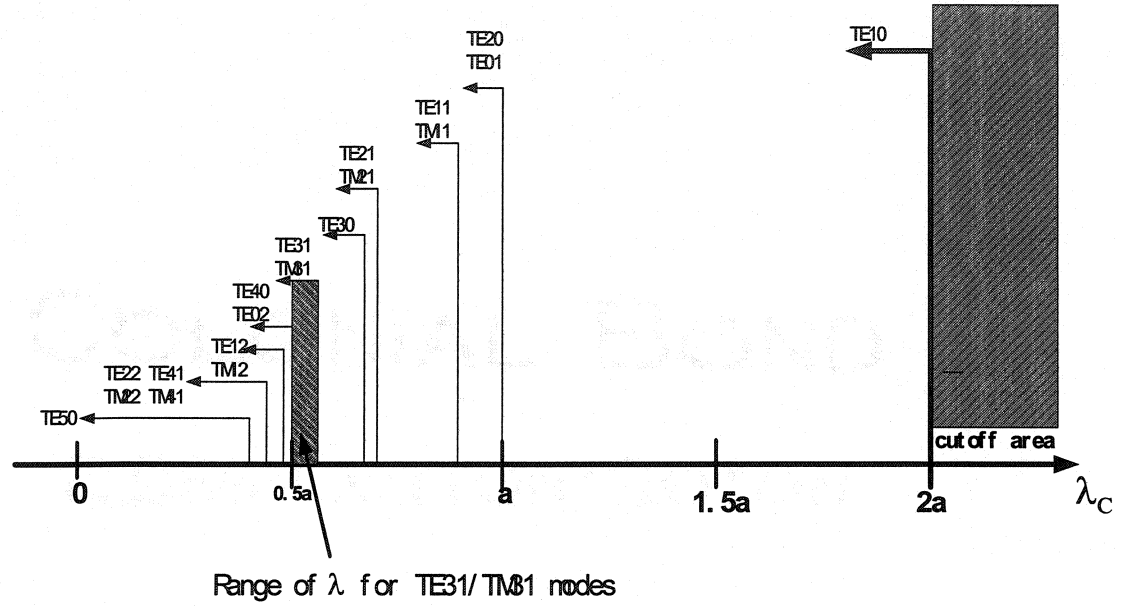


Figure 3.2 Distribution figure of cutoff wavelengths in rectangular waveguide ( $a=2b$ )

Therefore,

$$\frac{\lambda_0}{0.5547} < a < \frac{\lambda_0}{0.5} \quad (3.3)$$

Since the resonant frequency  $f_0$  equals to 5.8 GHz in this project, the wavelength  $\lambda_0$  of the work mode  $TE_{31}/TM_{31}$  is  $\lambda_0 = v/f_0 = 3.0 \times 10^8 / (5.8 \times 10^9) = 0.0517$  m.

Therefore,  $0.0932 < a < 0.1034$  m. Suppose we selected  $a = 0.0983$  m, then  $b = 0.0492$  m.

### 3.2.2 Determination of length c of rectangular cavity

The second step is to calculate the length c of the rectangular cavity. Once a and b are fixed, the length c of the cavity can be obtained by the following equations[2]:

$$\lambda_0 = \frac{2}{\sqrt{\left(\frac{m}{a}\right)^2 + \left(\frac{n}{b}\right)^2 + \left(\frac{k}{c}\right)^2}} \quad (3.4)$$

Hence

$$c = \frac{k}{\sqrt{\left(\frac{2}{\lambda_0}\right)^2 - \left(\frac{m}{a}\right)^2 - \left(\frac{n}{b}\right)^2}} \quad (3.5)$$

where m, n and k are the number of the half-waves in the x, y and z direction in Figure 3.1.  $\lambda_0$  is the resonant wavelength and it can be found by

$$\lambda_0 = \frac{v_0}{f_0} \quad (3.6)$$

where  $v_0 = 3 \times 10^8 \text{ m/s}$  is the light speed in vacuum and  $f_0$  is the resonant frequency.

In the previous example,  $f_0 = 5.8 \text{ GHz}$ ,  $\lambda_0 = 0.0517 \text{ m}$ ,  $a = 0.0983 \text{ m}$  and  $b = 0.0492 \text{ m}$ .

For  $\text{TE}_{315}/\text{TM}_{315}$  mode,  $m=3$ ,  $n=1$ ,  $k=5$ , using equation (3.5) we can get  $c=0.4068 \text{ m}$ .

### 3.2.3 Selection of cavity material

The last step is to select a suitable cavity material according to the quality factor of the cavity designed. With the different materials, the quality factors of the cavity that has

same geometric dimensions are totally different. The selection criterion of the cavity material will base on the following factors: higher quality factor, cheaper price and easier fabrication. The quality factor  $Q$  of TE mode in a rectangular cavity is given by[3]

$$Q = \frac{\lambda_0}{\delta} \cdot \frac{abc}{4} \frac{(p^2 + q^2)(p^2 + q^2 + r^2)^{3/2}}{ac[p^2 r^2 + (p^2 + q^2)^2] + bc[q^2 r^2 + (p^2 + q^2)^2] + abr^2(p^2 + q^2)} \quad (3.7)$$

where

$$p=m/a \quad q=n/b \quad r=k/c;$$

$$\delta = \left( \frac{2}{2\pi f_0 \mu_0 \sigma} \right)^{1/2} \text{ is skin depth;}$$

$\sigma$  is the conductivity of the material;

$\mu_0 = 1.257 \times 10^{-6} H/m$  is the permeability of free space (a vacuum).

### 3.3 Optimization design of high-order mode cavity

In the example of the previous section, there are eight high-order modes ( $TE_{10}$ ,  $TE_{01}$ ,  $TE_{20}$ ,  $TE_{11}$ ,  $TM_{11}$ ,  $TE_{21}$ ,  $TM_{21}$ ,  $TE_{30}$ ) that always exist whatever  $TE_{31}$  or  $TM_{31}$  mode is used. Therefore, there may be many resonant modes around the work frequency 5.8 GHz when the cavity is excited. This is not what we expected. Thus we have to check the resonant frequency of all of the possible modes to guarantee there is an enough gap between the work frequency and the resonant frequencies of all other possible modes.

The resonant mode analysis results within 500 MHz frequency band for this example are given in Table 3.1. From the Table 3.1, we can see that there are 3 resonant modes,  $TE_{1-0-15}$ ,  $TE_{3-0-10}$  and  $TE_{1-1-13}$ , which resonant frequency difference is smaller than 85 MHz. Especially for  $TE_{1-0-15}$  mode, the resonant frequency difference is only 62.7427 MHz. Moreover,  $TE_{10}$  mode is the dominant mode of the waveguide, so it will have stronger field components than those of  $TE_{31}$  mode. Therefore, the cavity size in this example cannot meet our design requirements.

Table 3.1 Resonant mode analysis within 500MHz frequency difference

Resonant Mode	Resonant Frequency(GHz)	Frequency Difference(MHz)
$TE/TM_{3-1-1}$	5.51154	288.459
$TE/TM_{3-1-2}$	5.54842	251.582
$TE/TM_{3-1-3}$	5.60934	190.658
$TE/TM_{3-1-4}$	5.69354	106.459
<b><math>TE/TM_{3-1-5}</math></b>	<b>5.8</b>	<b>0</b>
$TE_{3-1-6}$	5.92752	127.521
$TE/TM_{3-1-7}$	6.07478	274.777
$TE/TM_{3-1-8}$	6.24037	440.37200
$TE_{3-0-8}$	5.44401	355.98600
$TE/TM_{2-1-9}$	5.44264	357.36500
$TE_{3-0-9}$	5.6523	147.69800
$TE/TM_{2-1-10}$	5.67498	125.018
<b><math>TE_{3-0-10}</math></b>	<b>5.87637</b>	<b>76.365</b>
$TE/TM_{2-1-11}$	5.92119	121.189
$TE_{3-0-11}$	6.11447	314.468
$TE_{0-1-12}$	5.37424	425.757
$TE_{2-0-12}$	5.37424	425.757



TE/TM <sub>1-1-12</sub>	5.58648	213.523
TE/TM <sub>2-1-12</sub>	6.1796	379.599
TE <sub>0-1-13</sub>	5.68167	118.331
TE <sub>2-0-13</sub>	5.68167	118.331
<b>TE/TM<sub>1-1-13</sub></b>	<b>5.88282</b>	<b>82.8226</b>
TE <sub>0-1-14</sub>	5.99601	196.011
TE <sub>1-0-14</sub>	5.3827	417.303
TE <sub>2-0-14</sub>	5.99601	196.011
TE/TM <sub>1-1-14</sub>	6.18695	386.953
<b>TE<sub>1-0-15</sub></b>	<b>5.73726</b>	<b>62.7427</b>
TE <sub>1-0-16</sub>	6.0935	293.499

In fact, for the high-order mode resonant cavity design, it is far more difficult than the dominant mode cavity since there are many other resonant modes that could exist when the cavity is excited. In order to avoid exciting other resonant modes around the work resonant frequency, the ratio  $a/b$  of the waveguide should be very carefully selected. This selection process includes an error-and-try procedure to make the resonant frequencies of all of the other possible resonant modes deviate from the work resonant frequency as far as possible. For this reason, an optimization program has been developed using Matlab.

The flow-chart of the optimization program is shown in Figure 3.3. The ratio  $a/b$  will be swept from  $R_{min}$  to  $R_{max}$  during the optimization process. At first, the ratio  $a/b$  will be set to  $R_{min}$ . Then the program will call waveguide-width-range function.

The flowchart of the waveguide-width-range function is shown in Figure 3. 4. In this function, the highest mode considered will be defined at first. Then the cutoff wavelengths of all of the modes will be calculated using equation (3.1). At last, the cutoff wavelength of the work mode ( $TE_{315}/TM_{315}$ ) will be compared with the cutoff wavelengths of other modes to find the nearest high-order mode which cutoff wavelength is just shorter than that of  $TE_{315}/TM_{315}$ . In this way, the value range of the width  $a$  of the waveguide can be determined. Here we suppose the width range is from  $A_{min}$  to  $A_{max}$ . Then the width  $a$  of the waveguide will be swept from  $A_{min}$  to  $A_{max}$  and the height  $b$  of the waveguide can be determined accordingly.

The optimization program will be able to calculate the length  $c$  of the rectangular cavity from equation (3.5). Then the resonant frequencies of all possible modes will be estimated from equation (3.4) and (3.6). Here we define the modes, which cutoff wavelength is shorter than that of the work mode, but longer than those of all other high-order modes, as the nearest high-order mode. Considering the nearest high-order mode is very close to our work mode  $TE_{315}$ , we also included it in the mode check list during the optimization process. After that, all of these resonant frequencies will be compared with the work resonant frequency  $f_0=5.8$  GHz to check whether all of the frequency differences are larger than a predefined threshold (e.g, 150 MHz). If all of other resonant frequencies are far enough from the work frequency, this group of cavity dimension will be save to a text file. Otherwise, the dimension will be discarded.

This optimization iteration process will continue until all of the width  $a$  and all of the ratio  $a/b$  are swept. All of the qualified cavity dimensions will be saved in the result text file. Based on these initial optimization results, the ratio  $a/b$  and the frequency difference threshold can be modified. Then a new optimization process as described above can be executed until satisfactory results are obtained.

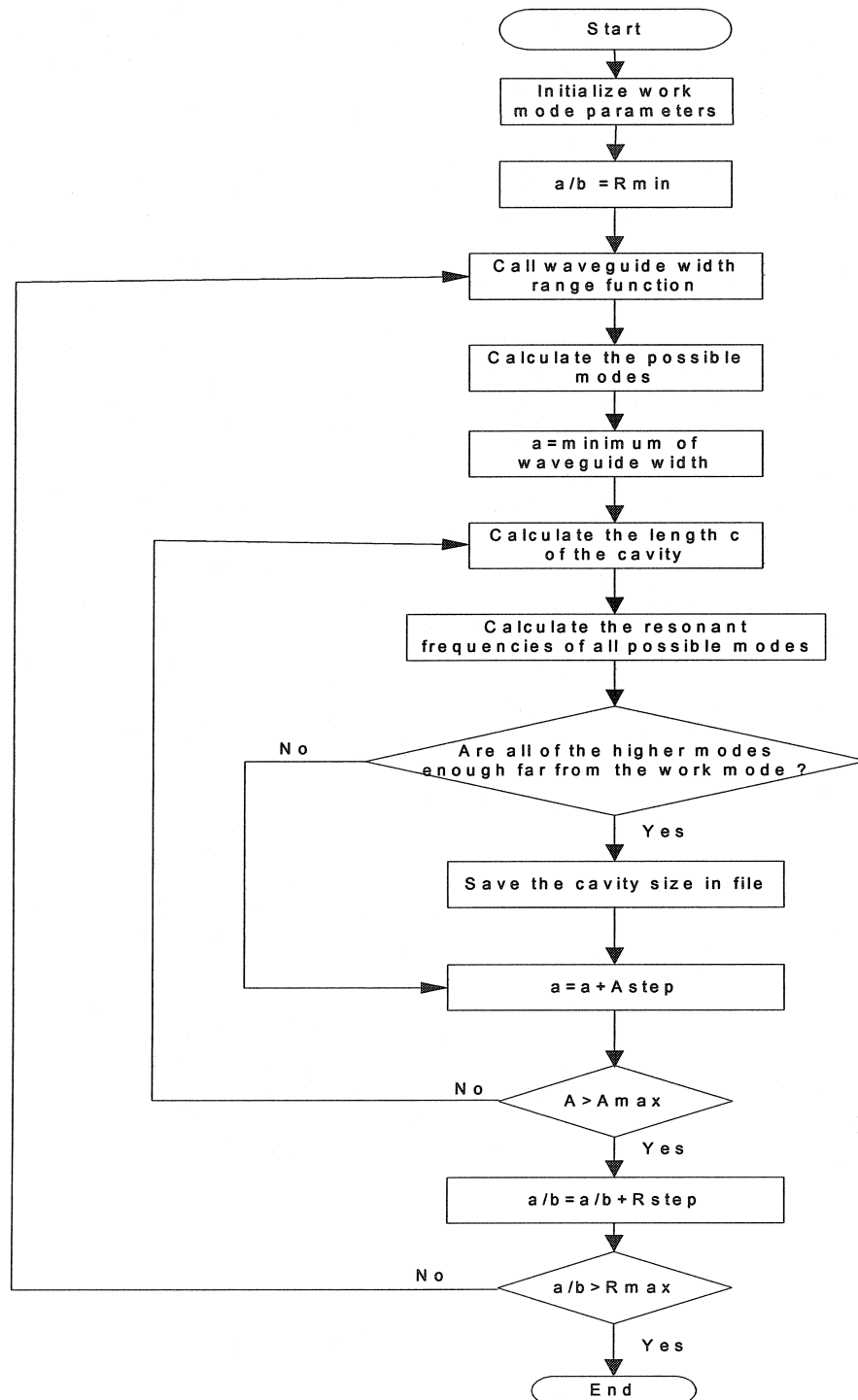


Figure 3.3 Optimization flowchart of high-order mode rectangular cavity

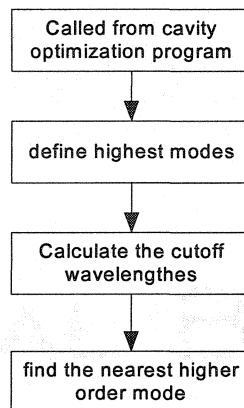


Figure 3. 4 waveguide width range function flowchart

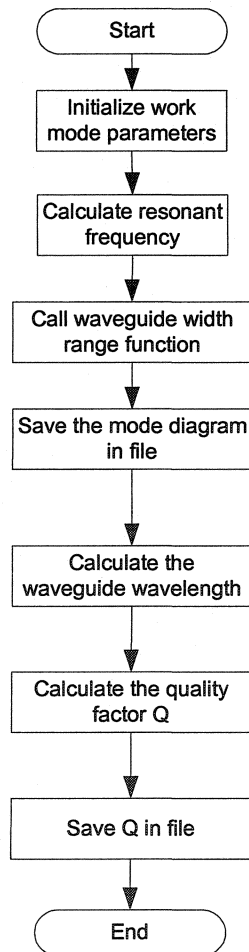


Figure 3.5 Cavity resonant mode analysis flowchart

### 3.4 Cavity optimization results and resonant mode analysis

Using the optimization method described in the previous section, the rectangular cavity dimensions for a work resonant frequency at 5.8 GHz are selected as following:

$$a=127.203\text{mm}=5.008\text{in}; \quad b=43.688\text{mm}=1.720\text{in}; \quad c=245.339\text{mm}=9.659\text{in}.$$

The cutoff wavelengths of the related waveguide modes are listed in Table 3.2. Hence excluding the work mode TE/TM<sub>31</sub>, there are 9 other modes, TE<sub>10</sub>, TE<sub>20</sub>, TE<sub>01</sub>, TE<sub>30</sub>, TE/TM<sub>11</sub>, TE/TM<sub>21</sub>, and TE<sub>40</sub>, which could exist. Having obtained the resonant cavity dimension, the cavity resonant mode analysis and the quality factors of the cavity with different materials can be calculated as the program flow in Figure 3.5. Here The quality factor  $Q$  is estimated by equation (3.7). The resonant mode analysis results are shown in Table 3.3. We observed that the frequency differences between the work mode TE/TM<sub>315</sub> and all of the other possible resonant modes are larger than 170 MHz. Moreover, there are only 17 possible resonant modes within 500 MHz frequency range, instead of 27 possible resonant modes in the previous example ( $a=2b$ ). The quality factors of the cavity with different materials for TE<sub>315</sub> resonant mode are listed in Table 3.4. From Table 3.4 we note that aluminium has higher  $Q$  factor, which is 16890 for this cavity in theory. Moreover, aluminium is cheaper than other materials listed in the table and also easy to manufacture. Therefore, aluminium was selected as the cavity material in this project.

Table 3.2 cutoff wavelengths of the related waveguide modes

<i>Waveguide modes</i>	<i>Cutoff wavelength</i>	<i>Notes</i>
TE <sub>10</sub>	2a	Exist
TE <sub>20</sub>	a	Exist
TE <sub>01</sub>	0.6869a	Exist
TE <sub>30</sub>	0.6667a	Exist
TE/TM <sub>11</sub>	0.6497a	Exist
TE/TM <sub>21</sub>	0.5662a	Exist
TE <sub>40</sub>	0.5a	Exist
<b><i>TE/TM<sub>31</sub></i></b>	<b><i>0.4784a</i></b>	<i>Work mode</i>
TE/TM <sub>41</sub>	0.4042a	Nearest high-order mode
TE <sub>50</sub>	0.4a	

Table 3.3 Resonant mode analysis within 500MHz frequency difference ( $a \approx 2.9b$ )

<b>Resonant Mode</b>	<b>Resonant Frequency(GHz)</b>	<b>Frequency Difference(MHz)</b>
TE <sub>4-0-4</sub>	5.31317	487.581
TE <sub>4-0-5</sub>	5.62086	179.891
TE/TM <sub>3-1-4</sub>	5.50313	297.623
<b><i>TE/TM<sub>3-1-5</sub></i></b>	<b><i>5.80075</i></b>	<b><i>0</i></b>
TE/TM <sub>3-1-6</sub>	6.14496	344.216
TE/TM <sub>2-1-6</sub>	5.55048	250.267

TE4-0-6	5.97545	174.69700
TE0-1-7	5.48682	313.93000
TE/TM1-1-7	5.61211	188.64300
TE/TM2-1-7	5.97222	171.46800
TE3-0-7	5.55262	248.125
TE0-1-8	5.97598	175.23
TE/TM1-1-8	6.09121	290.464
TE2-0-8	5.4301	370.644
TE3-0-8	6.03645	235.706
TE1-0-9	5.62753	173.214
TE2-0-9	5.98672	185.97
TE1-0-10	6.22668	425.931

Table 3.4 The quality factors of the cavity with different materials for TE<sub>315</sub> resonant mode

<i>Material</i>	<i>Conductivity (s/m)</i>	<i>Quality factor <math>Q_0</math></i>
Copper	$5.813 \times 10^7$	20846
Aluminium	$3.816 \times 10^7$	16890
Brass	$1.11 \times 10^7$	9109
Silver	$6.173 \times 10^7$	21482



### 3.5 *Determination of the positions of the sample, the input and the output coupling devices*

In this project, TE/TM<sub>315</sub> resonant mode was selected due to the high work frequency (5.8 GHz) and the requirements of the perturbation theory as described above. However, considering the sample should be put in the strongest position of the electrical field and paralleled with the direction of the electrical field so as to cause large frequency shift for a small sample, so TE<sub>315</sub> mode was adopted as the work mode instead of TM<sub>315</sub> mode.

According to classical electromagnetic field theory, the field components of TE<sub>315</sub> in the rectangular cavity are represented as following[2]:

$$E_x = \frac{j\omega\mu\pi}{K_c^2 b} H_{315} \cos\left(\frac{3\pi}{a}x\right) \sin\left(\frac{\pi}{b}y\right) \sin\left(\frac{5\pi}{c}z\right) \quad (3.8)$$

$$E_y = \frac{-3j\omega\mu\pi}{K_c^2 a} H_{315} \sin\left(\frac{3\pi}{a}x\right) \cos\left(\frac{\pi}{b}y\right) \sin\left(\frac{5\pi}{c}z\right) \quad (3.9)$$

$$E_z = 0 \quad (3.10)$$

$$H_x = \frac{-15\pi^2}{K_c^2 ac} H_{315} \sin\left(\frac{3\pi}{a}x\right) \cos\left(\frac{\pi}{b}y\right) \cos\left(\frac{5\pi}{c}z\right) \quad (3.11)$$

$$H_y = \frac{-5\pi^2}{K_c^2 bc} H_{315} \cos\left(\frac{3\pi}{a}x\right) \sin\left(\frac{\pi}{b}y\right) \cos\left(\frac{5\pi}{c}z\right) \quad (3.12)$$

$$H_z = H_{315} \cos\left(\frac{3\pi}{a}x\right) \cos\left(\frac{\pi}{b}y\right) \sin\left(\frac{5\pi}{c}z\right) \quad (3.13)$$

where

$$K_c^2 = \left(\frac{3\pi}{a}\right)^2 + \left(\frac{\pi}{b}\right)^2 \quad (3.14)$$

Suppose coefficient  $H_{315}$  equals to 1. Making a Matlab program, the distribution of the field components in space can be displayed in 3D space. The electrical field distribution at  $y=b$  plane is shown in Figure 3.6. The distribution of the magnitude of the magnetic field at  $z=0$  plane is shown in Figure 3.7. With the help of the excellent 3D visualization of Matlab 3D figure, the field distribution in the space becomes concrete and very easy to distinguish where is the strongest point of the electrical field or the magnetic field. Based on the field structure analysis, the position of the sample, the input and output coupling devices was selected at the peak positions of the electrical field as shown in

Figure 3.8 to provide the largest resonant frequency shift and the strongest input and output energy coupling. Electrical probes are selected as the input and output coupling devices. This configuration is helpful to suppress other unexpected resonant modes in the cavity, especially to avoid exciting  $TM_{315}$  mode.

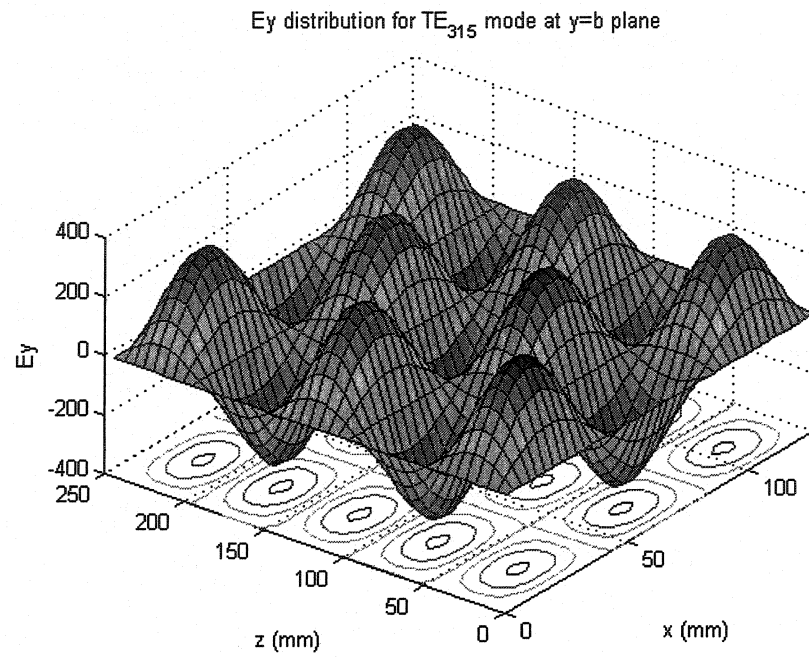


Figure 3.6 Electrical field distribution for  $TE_{315}$  mode at  $y=b$  plane

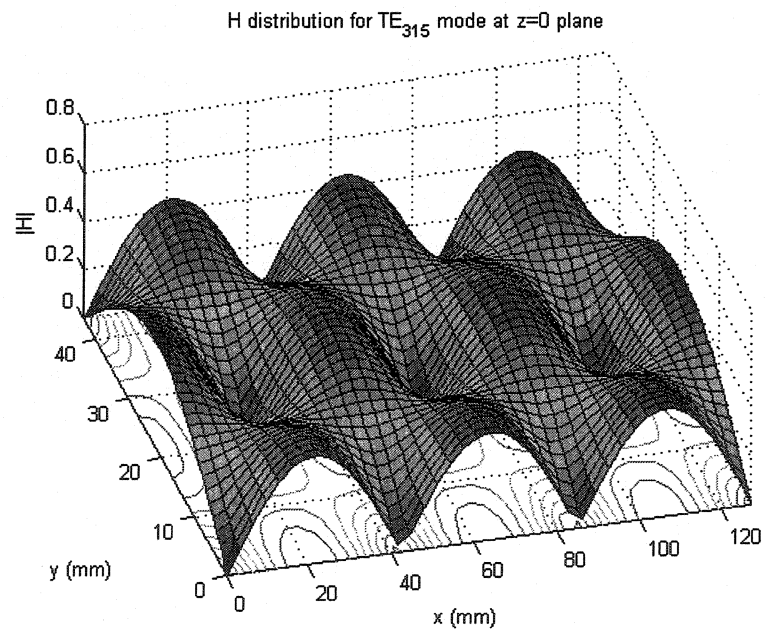


Figure 3.7 Magnetic field distribution for  $TE_{315}$  mode at  $z=0$  plane

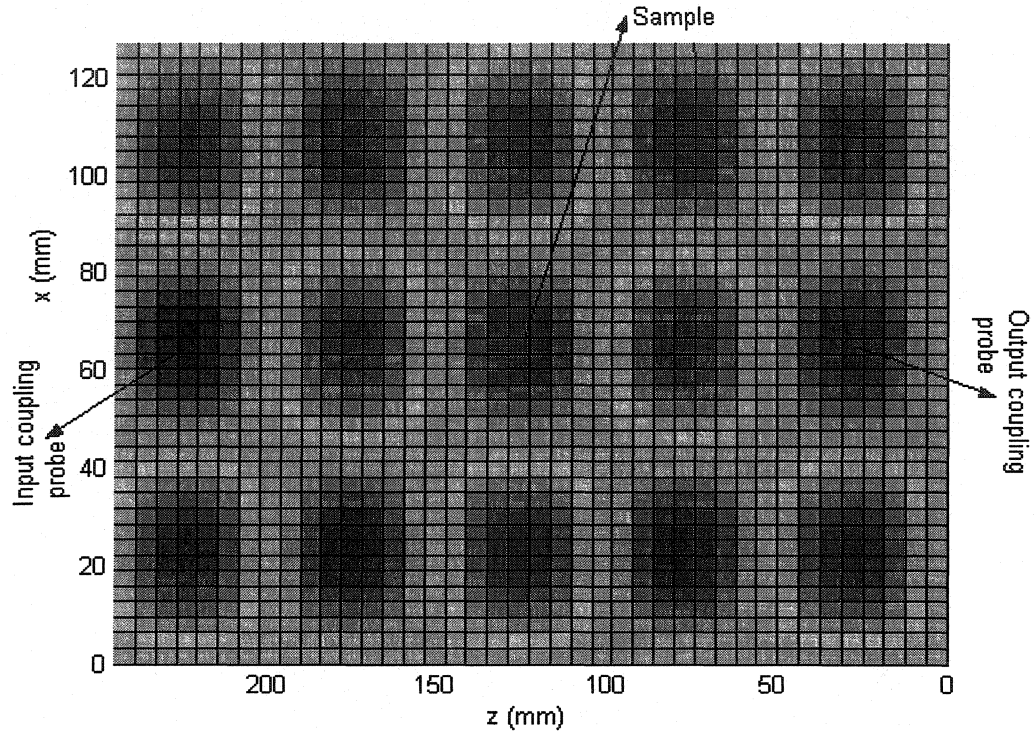


Figure 3.8 Positions of the sample, the input and the output coupling probes

### 3.6 Results of the practical 5.8 GHz empty resonant cavity

Based on the above design data, we fabricated the resonant cavity in our lab. The practical 5.8GHz rectangular resonant cavity is shown in Figure 3.9. The resonant frequency of the empty cavity is about 5.8066GHz. There is only 6.6MHz deviation from the design target. The result of the resonant mode analysis around 5.8 GHz is in Figure 3.10. We can see that the resonant frequency of the nearest other mode is about 5.925GHz. Hence the frequency difference between the work mode and the nearest other

mode is larger than 110 MHz. This frequency gap can satisfy the permittivity measurement requirements. Therefore, these results demonstrated the proposed optimization design of the cavity is successful.

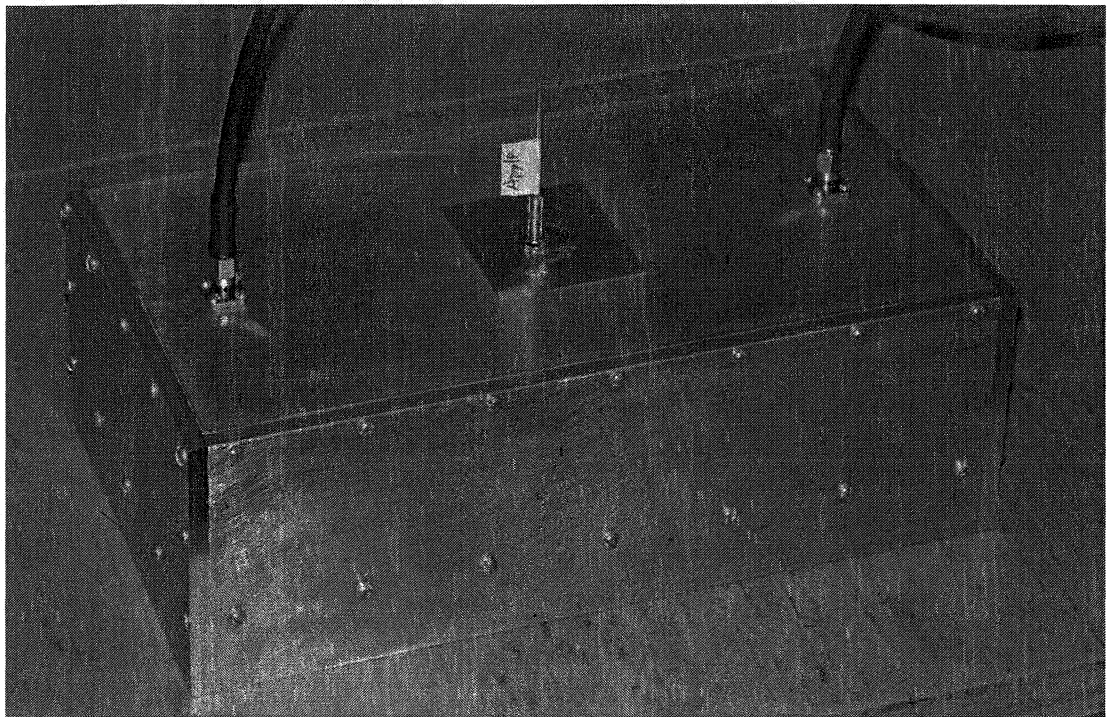


Figure 3.9 5.8 GHz resonant cavity

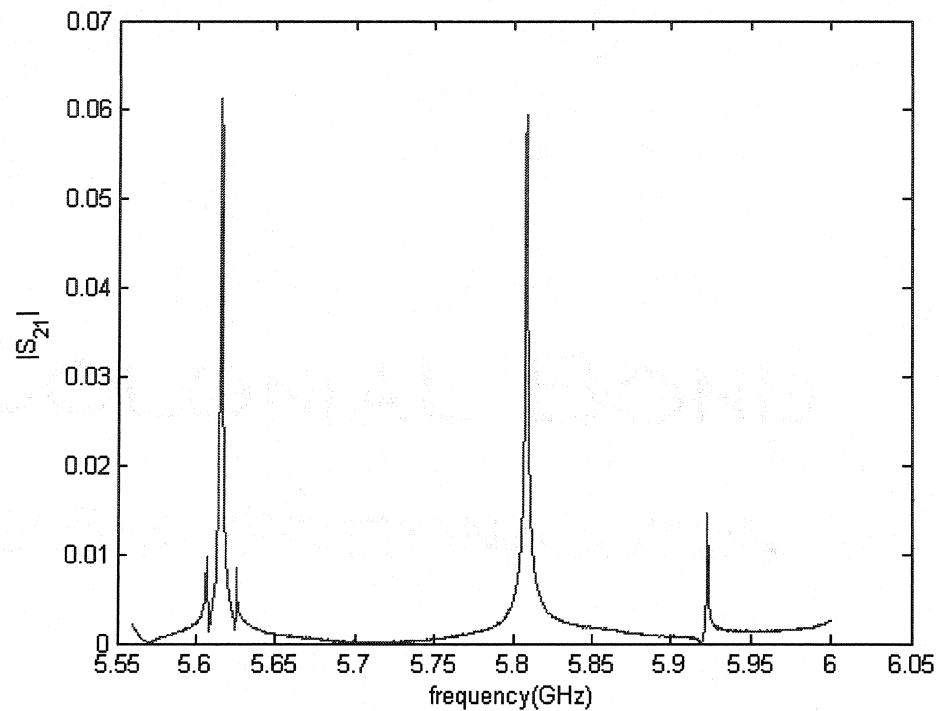


Figure 3.10 the practical mode spectrum of the 5.8 GHz empty resonant cavity

## References:

- [1] R. C. Labelle, Automatic permittivity measurements of moistened dielectric materials in a high-power microwave resonant cavity, Mémoire de maîtrise, Ecole polytechnique de Montréal, 1984
- [2] D. M. Pozar, *Microwave engineering*, 2<sup>nd</sup> edition, New York : Wiley, 1998
- [3] H. Rapaport, M. Wind, *Handbook of microwave measurements*, 2<sup>nd</sup> edition, Brooklyn : Polytechnic Institute of Brooklyn, Microwave Research Institute, 1955

## **Chapter 4 Development of the automatic permittivity measurement software --- PermiSys**

### ***4.1 Introduction***

PermiSys is an automatic permittivity measurement system software developed using Visual C++ and Microsoft Foundation Class (MFC)[1] in this project to control the measurement process, record the resonant curve data of the cavity and calculate the permittivity based on these data. Compared with the traditional Dos interface measurement software, it is more convenient for people to use permiSys due to its popular Windows interface. Moreover, since it simplifies the measurement process, the empty cavity only need to be measured once, and then we can measure the permittivity of the different materials directly. The resonant curve is displayed in the windows and saved as a .txt file in the PC. In order to get more accurate measurement results, the resonant curve can be further processed with other software tools such as Matlab. This data processing approach will be discussed in details in the next chapter.

During the software development process, the Object–Oriented Programming (OOP) technique has been employed to organize and manage the code because of the complication of the Windows system[2]-[10]. The basic units for OOP are objects, which are the instances of classes. Classes are abstraction descriptions of objects. The

utilization of classes is the most important characteristics of OOP language such as C++. By the help of the inheritance property of the class, the code reuses in OOP become very convenient. A class consists of member data or properties, and member function or methods. These properties and methods can be divided into three categories: private, protected and public. The private properties and methods can only be used in a class. The protected properties and methods can be utilized in both a class and its child classes. Furthermore, the public properties and methods are visible for all objects. Each class has a unique name and will produce response to the messages received. Communication between objects will through messages based on a set of predefined protocols.

In this chapter, we will discuss the software system architecture at first. Then the details of the kernel classes will be given. At last, design of the Graphical User Interface (GUI) will be explained. Some useful information about the Vector Network Analyzer (VNA) programming[12] and control has been presented in Appendix I.

## ***4.2 Measurement software system architecture***

The measurement software system architecture is shown in **Error! Reference source not found..** It can be seen that different measurement operations (i.e., empty cavity measurement, system calibration, sample measurement, etc.) are executed by the corresponding functional modules. The measurement modules will communicate with Vector Network Analyzer (VNA) via GPIB interface to perform the measurement



required using Virtual Instrument Software Architecture (VISA). A summary about VISA can be found in Appendix II. The measurement results will be saved in text files and also be displayed in the Graphical User Interface (GUI).

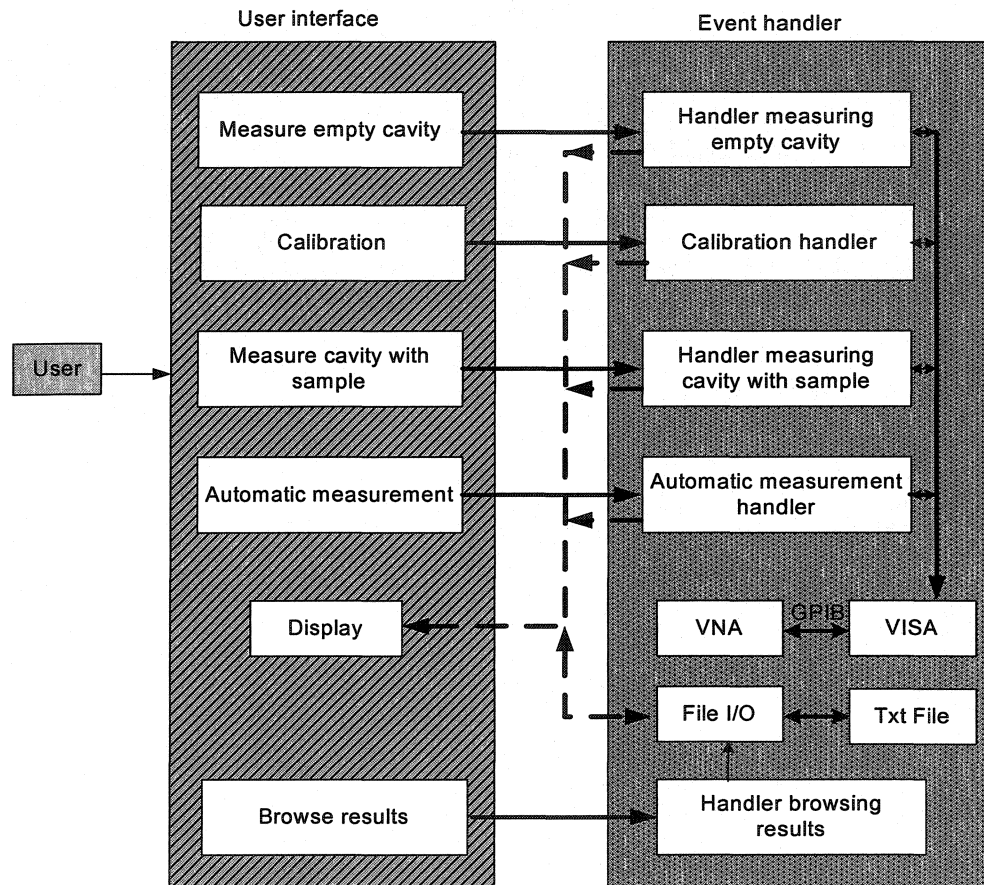


Figure 4.1 the measurement software system architecture

### 4.3 Main classes design

As described in section 4.1, classes are the foundation of OOP. A class is an abstract description of a set of objects that share common data structures and exhibit common

behaviors. It is composed of properties (member data) and methods (member functions). Comparing with a concrete object, it is not necessary for a class existing at run time. Several critical classes will be introduced as follows.

### **CVectorNetworkAnalyzer**

CVectorNetworkAnalyzer class inherits from CObject and is an abstraction of the Vector Network Analyzer (VNA). It encapsulates all of the communication functions that are necessary for the measurement application to communicate with VNA via GPIB interface. These communication functions call VISA functions directly to initialize VNA, send commands to VNA and acquire data from VNA. In this way, the application is independent to the GPIB card, which could be HPIB card or National Instrument GPIB card. It means the measurement software will be transplantable among the different PCs with different GPIB cards. The Class-Responsibilities-Collaborators (CRC) card of CVectorNetworkAnalyzer class is shown in Figure 4.2.

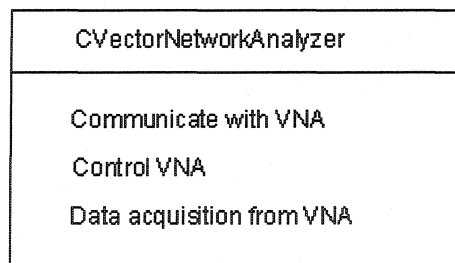


Figure 4.2 Class CVectorNetworkAnalyzer CRC card

### **CMeasurementResults**

When the resonant frequency, quality factor  $Q$ , resonant curve data and other parameters are acquired from VNA, these measurement results will be saved in an instance of CMeasurementResults class. The CRC card of CMeasurementResults class is shown in Figure 4.3.

CMeasurementResults
Save the measurement results

Figure 4.3 Class CMeasurementResults CRC card

### **CCurveData**

The resonant curve data read from VNA will include the frequency, rectangular and polar format  $S_{21}$ . All of these data will saved in an instance of class CCurveData for the future data processing with other methods. The CRC card of CCurveData class is shown in Figure 4.4.

CCurveData
Save the resonant curve data

Figure 4.4 Class CCurveData CRC card

### **COptionDlg**

The number of the sampling points and attenuation values will be setting in the option dialog (an instance of COptionDlg). These attenuation values will be used to decide the sweep frequency range so as to adjust the resolution of the sweep frequency.

The CRC card of COptionDlg class is shown in Figure 4.5.

COptionDlg
Setting frequency sweeping parameters

Figure 4.5 Class COptionDlg CRC card

### **CCalibrationDlg**

The permittivity and volume of standard sample will be setting in this dialog (an instance of class CCalibrationDlg) before executing the calibration process. Calibration results will also be displayed in this dialog. All calibration operations will be performed through this GUI. The CRC card of CCalibrationDlg class is shown in Figure 4.6.

CCalibrationDlg
Setting calibration parameters
Showing calibration results
Executing the calibration
Save calibration results

Figure 4.6 Class CCalibrationDlg CRC card

### **CAutoMeasurementDlg**

The measurement can be executed for many times automatically. The measurement times and the related information of the sample measured can be set in this dialog (an instance of class CAutoMeasurementDlg). The measurement results will be displayed in the main window. The CRC card of CAutoMeasurementDlg class is shown in Figure 4.7.

CAutoMeasurementDlg
Setting measurement times Setting the related information of the sample Executing automatic measurement

Figure 4.7 Class CAutoMeasurementDlg CRC card

### **CBrowseResultDlg**

The measurement results can be saved as a text format file. Then at any time these saved results can be browsed by this dialog (an instance of class CbrowseResultDlg). The CRC card of CBrowseResultDlg class is shown in Figure 4.8.

CBrowseResultDlg
Browsing the measurement results saved as in text format file

Figure 4.8 Class CBrowseResultDlg CRC card

### **CMeasurementPropertyPage1**

The cavity parameters and the sweeping frequency range should be set before measuring the quality factor  $Q$  and the resonant frequency of the empty cavity. These setting can be operated in this property page (an instance of class CMeasurementPropertyPage1). The CRC card of class CMeasurementPropertyPage1 is shown in Figure 4.9.

CMeasurementPropertyPage1
Setting cavity parameters Setting the sweep frequency range

Figure 4.9 Class CMeasurementPropertyPage2 CRC card

### **CMeasurementPropertyPage2**

This class will cooperate with class CMeasurementPropertyPage1 to perform the quality factor  $Q$  and the resonant frequency  $f$  measurement of the empty cavity. The CRC card of class CMeasurementPropertyPage2 is shown in Figure 4.10.

CMeasurementPropertyPage2
Performing quality factor $Q$ and resonant frequency $f$ measurement of empty cavity Displaying the resonant curve of empty cavity

Figure 4.10 Class CMeasurementPropertyPage2 CRC card

### **CMeasurementPropertyPage3**

This class is used to perform the quality factor  $Q$  and the resonant frequency  $f$  measurement of the cavity with sample. It will cooperate with class CMeasurementPropertyPage4 to get the complex permittivity of the sample measured. The CRC card of class CmeasurementPropertyPage3 is shown in Figure 4.11.

CMeasurementPropertyPage3
Performing quality factor $Q$ and resonant frequency $f$ measurement of cavity the cavity with sample
Displaying the resonant curve of the cavity with sample

Figure 4.11 Class CMeasurementPropertyPage3 CRC card

### **CMeasurementPropertyPage4**

After measuring the quality factors and the resonant frequencies of the empty cavity and the cavity with sample, the complex permittivity of the sample measured can be determined according to the perturbation theory. The quality factors, the resonant frequencies and the permittivity will be displayed in this property page (an instance of the class CMeasurementPropertyPage4). The CRC card of class CMeasurementPropertyPage4 is shown in Figure 4.12.

CMeasurementPropertyPage4
Calculating the complex permittivity Displaying permittivity, quality factors and resonant frequencies

Figure 4.12 Class CMeasurementPropertyPage4 CRC card

### CPermiSysDoc

A class CPermiSysDoc based on CDocument is needed to store the application data. The environment setting data, cavity parameters and the measurement results are saved in an instance of CPermiSysDoc. Its CRC card is shown in Figure 4.13.

Class: CPermiSysDoc Base: CDocument
Store the environment setting data Store the cavity parameters Store the measurement results

Figure 4.13 Class CPermiSysDoc CRC card

### CPermiSysMainView

A class CPermiSysMainView based on CView is needed to display the measurement results. Its CRC card is shown in Figure 4.14.



Class: CPermiSysMainView Base: CView
Setting the calibration methods  Displaying the measurement results

Figure 4.14 Class CPermiSysMainView CRC card

### **CMainFrame**

In MFC framework, class CMainFrame based on CFrameWnd is used to create and manage menu, toolbar and views. Its CRC card is shown in Figure 4.15.

Class: CMainFrame Base: CFrameWnd
Create menu and toolbar Create views Enable and disable some menus and toolbars Response the menu and toolbaar command

Figure 4.15 Class CMainFrame CRC card

### **CPermiSysApp**

Class CPermiSysApp includes the entry point of the MFC Windows application. It is responsible for creating document template and starting the application. Its CRC card is shown in Figure 4.16.

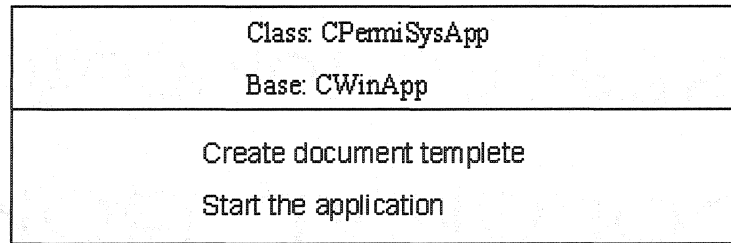


Figure 4.16 Class CPermiSysApp CRC card

## 4.4 Graphical User Interface (GUI) Design

### Main Window

The main window consists of menu, toolbar and the window client area[13]. The menu includes file, view, measurement tools, and help submenu. The toolbar includes a series of graphical shortcuts of some common commands such as automatic measurement, empty cavity measurement, sample measurement, measurement wizard and so on. An instance of class CPermiSysMainView is presented in the client area. The main window is shown in Figure 4.17.

### Empty cavity measurement wizard

Empty cavity measurement wizard consists of two steps. The first step is an instance of class CPropertyPage1, which is used to set the cavity parameters and the sweep frequency range. The second step is an instance of class CPropertyPage2, which is responsible for executing the measurement of the quality factor  $Q_0$  and the resonant

frequency  $f_0$  of the empty cavity and displaying the resonant curve of the empty cavity in this window. The wizard is shown in Figure 4.18.

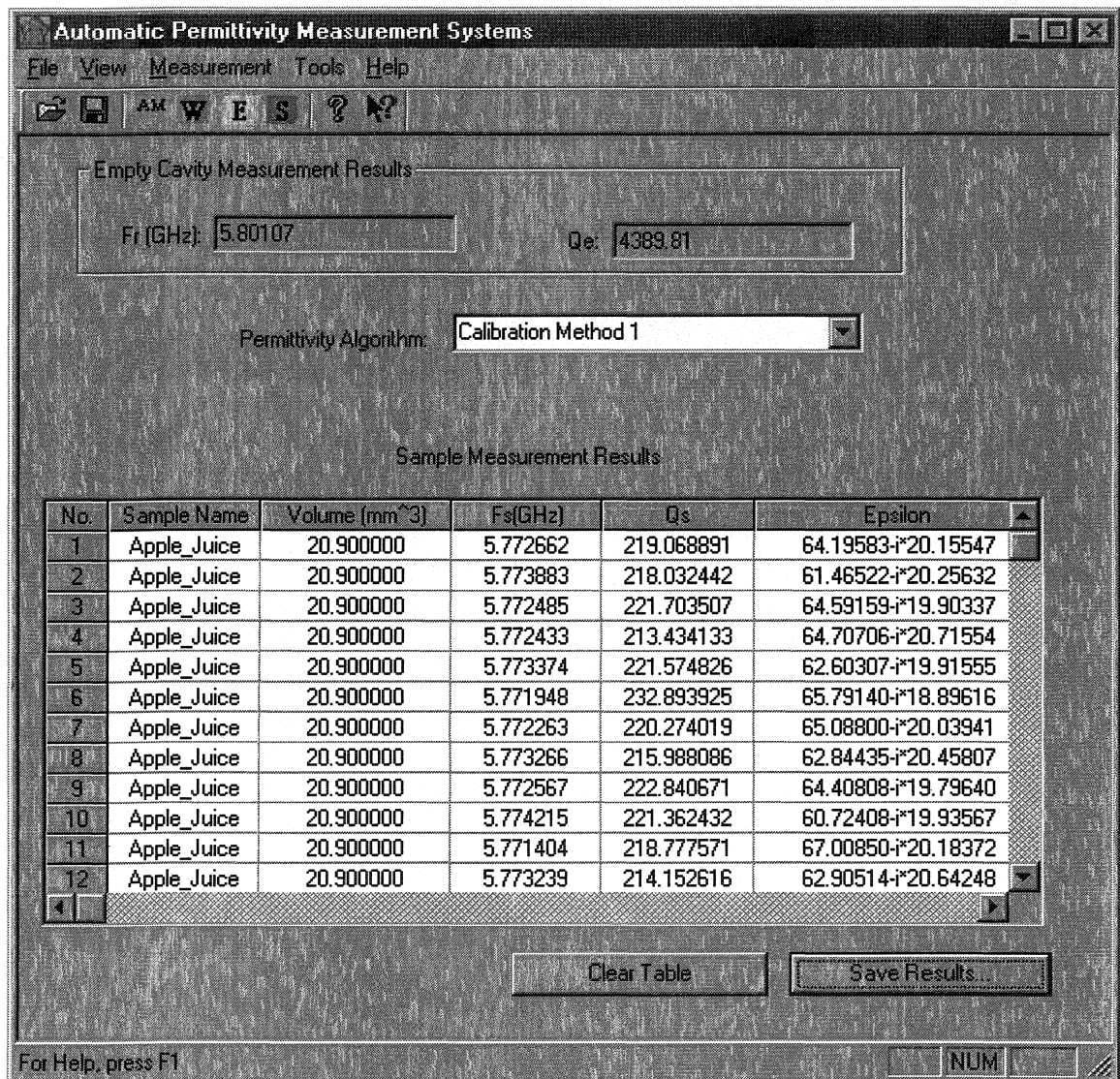


Figure 4.17 the main window of PermiSys

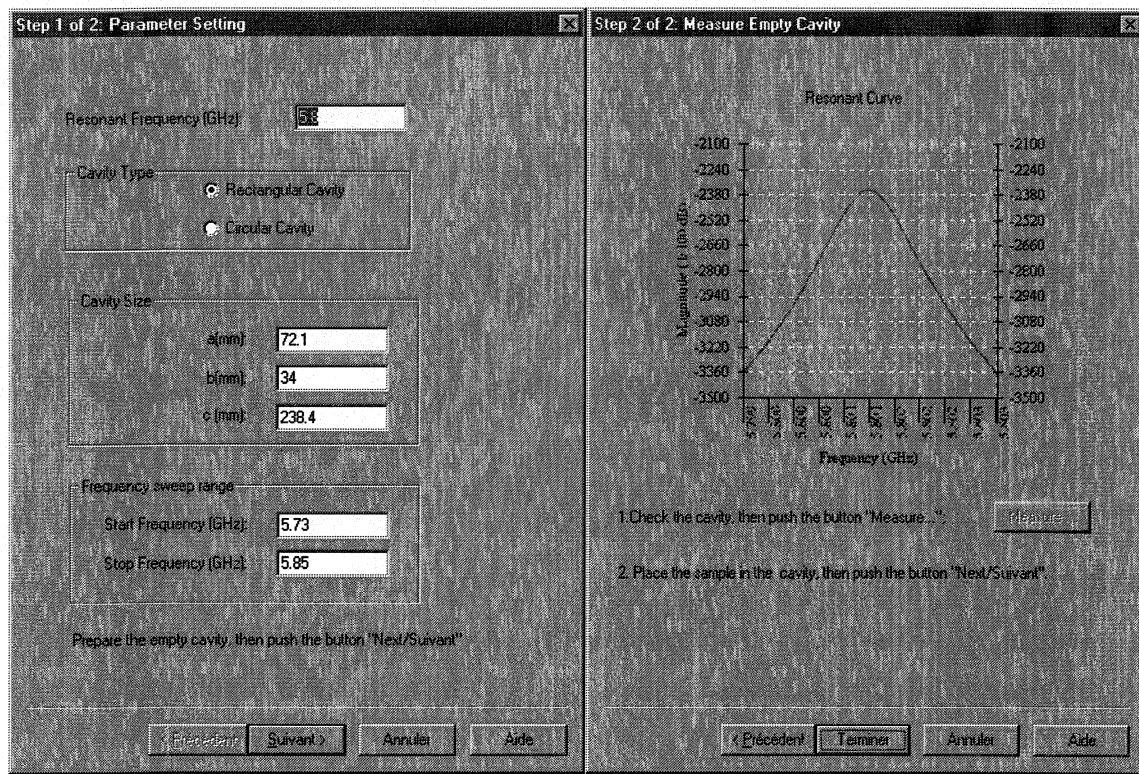


Figure 4.18 Empty cavity measurement wizard

### Calibration dialog

The calibration dialog is an instance of class CCalibrationDlg and is shown in Figure 4.19. The complex permittivity and name of the standard sample such as pure water are set in this dialog. The calibrate button is used to call the calibration method. The calibration results and the resonant curve are displayed in the dialog.

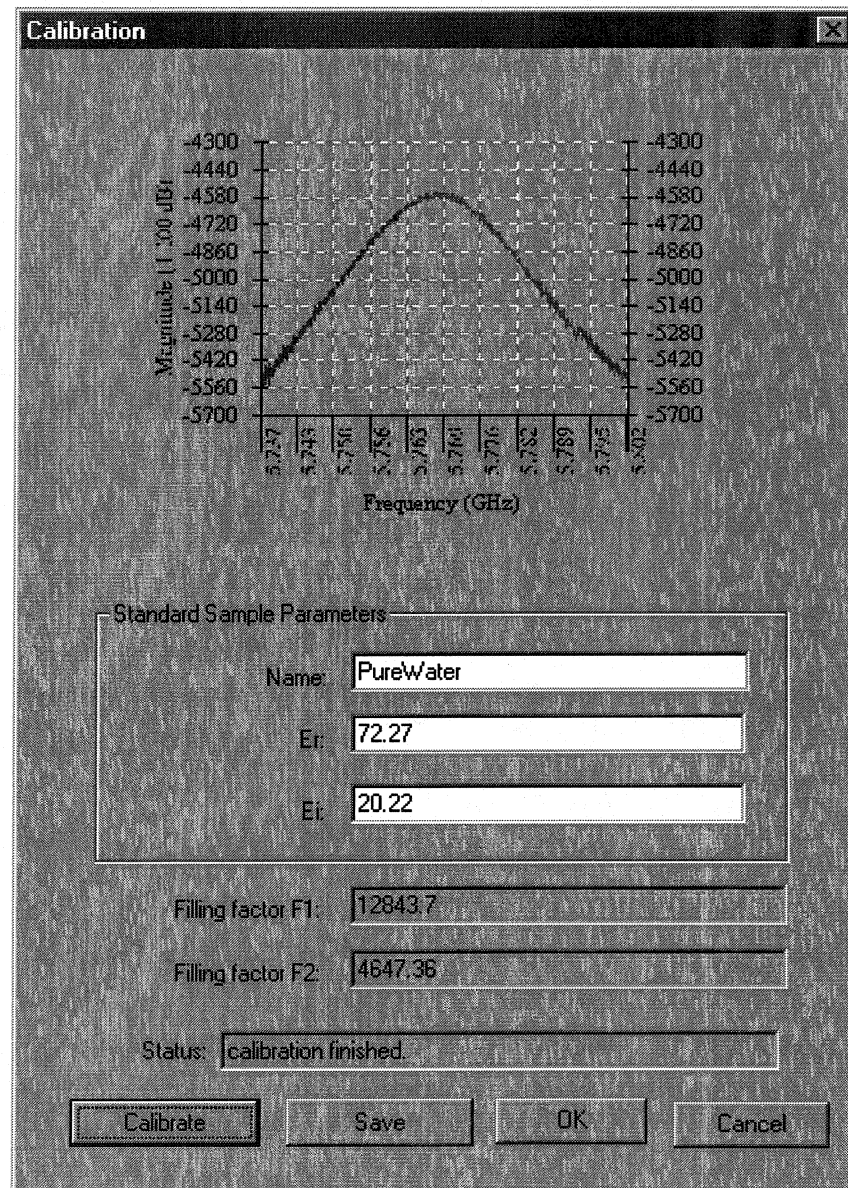


Figure 4.19 Calibration dialog

### Sample measurement wizard

Sample cavity measurement wizard also consists of two steps. The first step is an instance of class `CPropertyPage3`, which is used to set the sample parameters, execute



the measurement of the quality factor  $Q_s$  and the resonant frequency  $f_s$  of the cavity with sample and display the resonant curve of the cavity with sample in this window. The second step is an instance of class `CPropertyPage4`, which is responsible for calculating the complex permittivity of the measured sample and displaying the measurement results in this property page. The save button is used to call a method to save the measured results to a text format file. The “Add to table” will call a method to add the measurement results to the table in the main window. The wizard is shown in Figure 4.20.

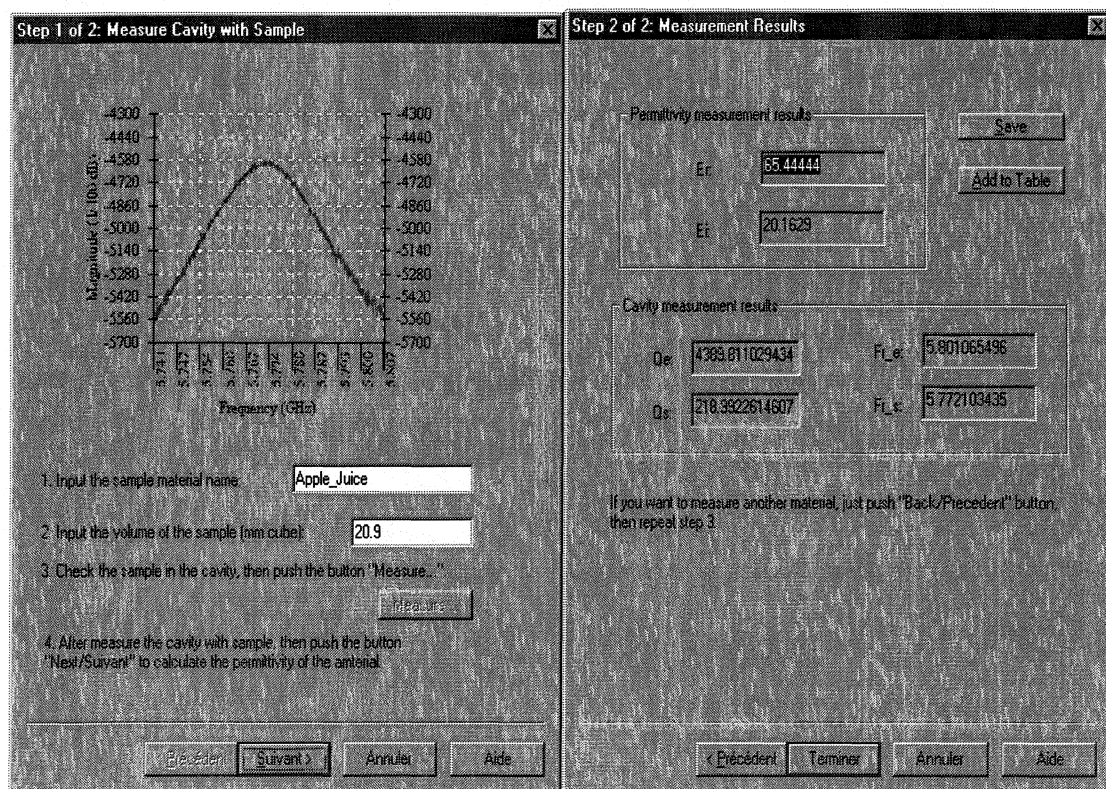


Figure 4.20 Sample measurement wizard

### Automatic measurement dialog

The automatic measurement dialog is shown in Figure 4. 21. Sample material name and volume can be set in this dialog. The repeat measurement times should be given before pushing “Measure” button to start the measurement process. The permittivity and the resonant curve will be updated during the measurement process. The status will display how many measurements have completed in order that user can know the measurement progress.

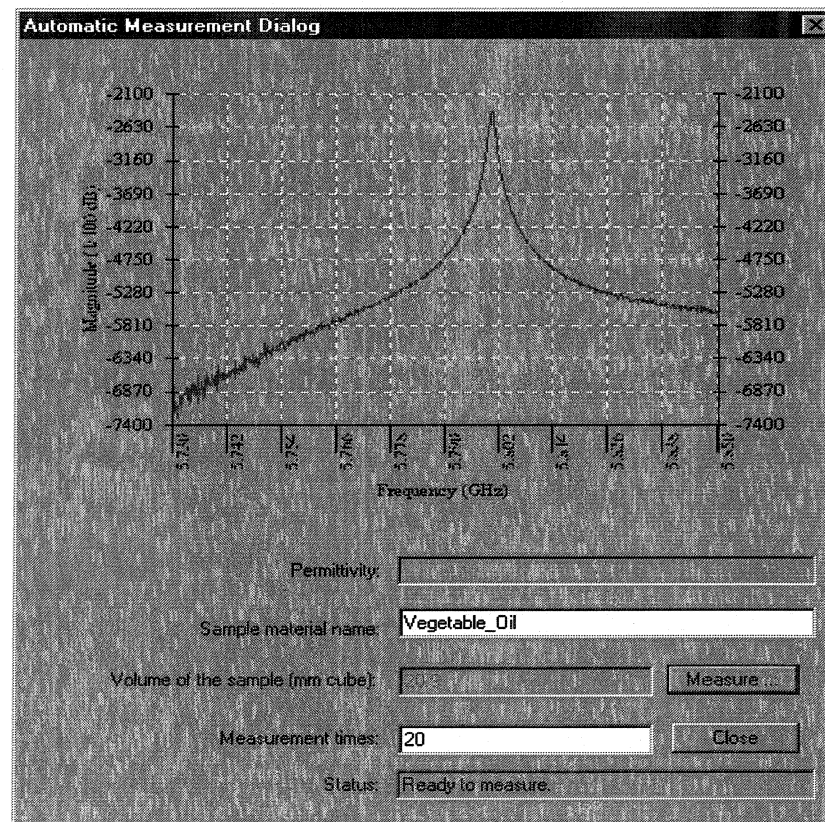


Figure 4. 21 automatic measurement dialog

### Option setting dialog

The option setting dialog is shown in Figure 4.22. The sample point in the sweep range can be set in this dialog. Attenuate value 1 is used to make a large range sweep so as to catch the resonant frequency easily. Attenuate value 2 is used to improve the measurement resolution around the resonant frequency.

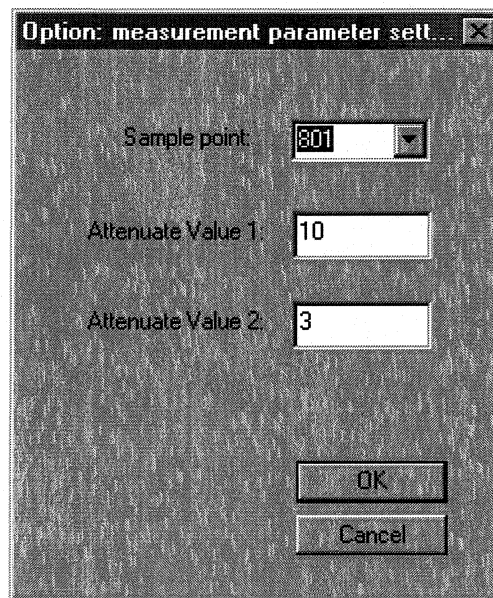


Figure 4.22 Option setting dialog

### Browsing results dialog

Browse result dialog is shown in Figure 4.23. As the name suggested, this dialog is used to display different measurement results saved in text format file before.



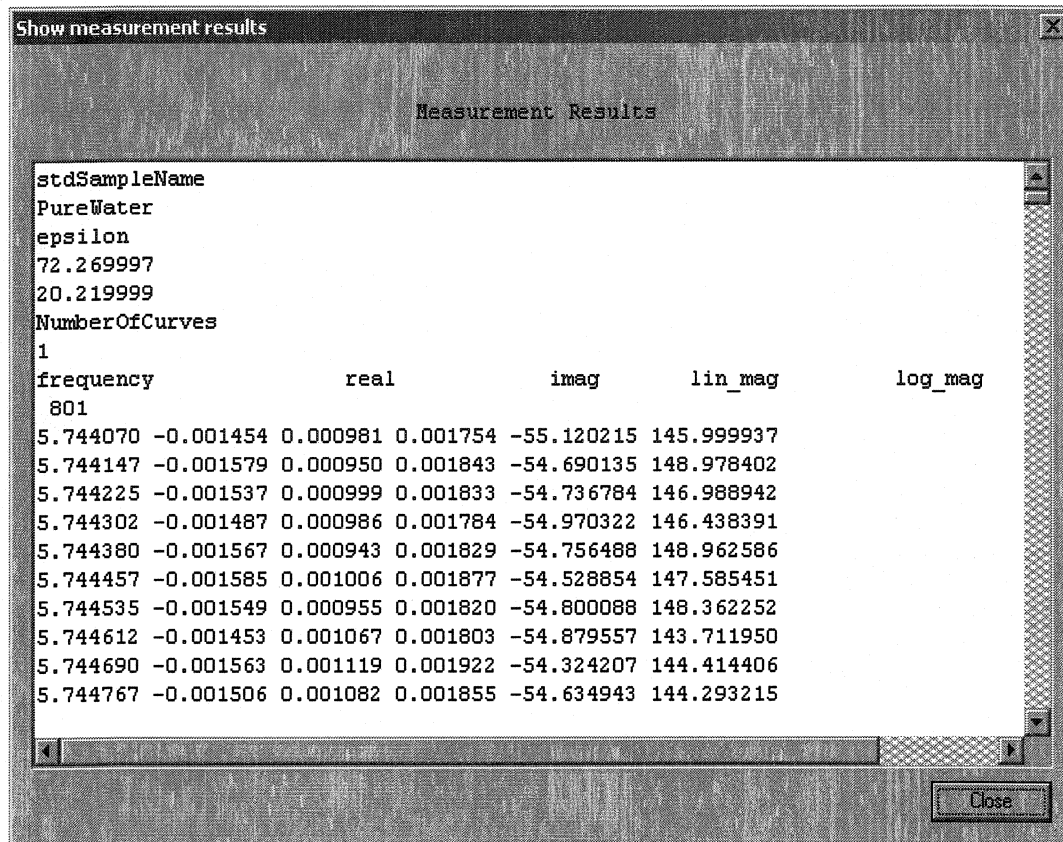


Figure 4.23 Browse result dialog

**Reference:**

- [1] J. Prosise, Programming Windows 95 with MFC: Create Programs for Windows Quickly with Microsoft Foundation Class Library, Microsoft Press, 1996.
- [2] G. Booch, Object-Oriented Analysis and Design with Applications, The Benjamin/Cummings Publishing Company, Inc. 1994.

- [3] J. Martin and J. J. Odell, Object-Oriented Analysis and Design, Prentice Hall, 1995.
- [4] T. Budd, An Introduction to Object-Oriented Programming, Addison-Wesley Pub. Co, 1997.
- [5] J. P. Cohoon and J. W. Davidson, C++ Program Design: An Introduction to Programming and Objected-Oriented Design, Richard D. Irwin Inc., 1997
- [6] R. Decker and S. Hirshfield, The Object Concept: An Introduction to Computer Programming Using C++, PWS Pub. Co., 1995.
- [7] S. Morris, Object-Oriented Programming under Windows, Butterworth Heinemann, 1995.
- [8] C. Walnum and P. Robichaux, Using MFC and ATL, Que, 1997.
- [9] M. Andrews, Visual C++ Object-Oriented Programming, Sams Publishing, 1994.
- [10] G. Perry, Teach Yourself Object-Oriented Programming with Visual C++ 1.5 in 21 days, Sams Publishing, 1994.
- [11] Microsoft Corporation, Win32 Programmer's Reference, Remond, WA: Microsoft Press, 1995.
- [12] HP8510B Network Analyzer, Operating and programming manual, September 1990.
- [13] Microsoft Corporation, The Windows Interface Guidelines for Software Design, Remond, WA: Microsoft Press, 1995.

## Chapter 5 Measurement data processing

### 5.1 Introduction

As described in Chapter 2, the complex permittivity is calculated in terms of the resonant frequency  $f$  and the quality factor  $Q$  of the resonant cavity with and without sample. Hence the measurement accuracy of the complex permittivity is fully dependent on the accuracy of the resonant frequency  $f_0$  and the quality factor  $Q$  measured.

For a VNA, such as HP8753D or HP8510B that are available in our lab, the maximum sweep point is 801 points. That means only 801 frequency-sampling points are available for a signal measurement. Thus it determines the measurement frequency resolution. For example, for a frequency sweep from 5.75 GHz to 5.85 GHz, the frequency resolution is 124.844KHz. Such a large frequency ambiguity is not suitable for the complex permittivity measurement with cavity perturbation method since the resonant frequency shift caused by the sample loaded could be at the same order as the frequency resolution. In order to increase the frequency resolution, the frequency sweep range should be as small as possible.

Although narrowing the frequency sweep range can effectively improve the accuracy of the resonant frequency, the reduction of the sweep range will lead to a large measurement error of the quality factor  $Q$  of the resonant cavity since the measured  $Q$  is based on the frequency measurements directly. There is a group of the measurement results of the

resonant frequency  $f_0$  and the quality factor  $Q$  shown in Table 5.1. From Table 5.1, we can clearly see that there is a large deviation of the resonant frequency  $f_0$  and the quality factor  $Q$ .

Therefore, we have to find a solution to accurately compute the resonant frequency  $f_0$  and the quality factor  $Q$ . In this chapter we will introduce the cursor method first. Then two accurate resonant frequency and quality factor measurement methods, Lorentzian fit method and Resonance Curve Area (RCA) method, will be discussed in details.

Table 5.1 Typical measurement results the resonant frequency  $f_0$  and the quality factor  $Q$

Times	F0(GHz)	DltaF0 (MHz)	Q	deltaQ
1	5.806564	-0.0122	4273.149703	5.4516224
2	5.806594	0.0178	4264.693729	-3.0043516
3	5.806583	0.0068	4261.714374	-5.9837066
4	5.806593	0.0168	4262.650051	-5.0480296
5	5.806587	0.0108	4268.03493	0.3368494
6	5.806581	0.0048	4267.310488	-0.3875926
7	5.806575	-0.0012	4257.620854	-10.0772266
8	5.806575	-0.0012	4275.630272	7.9321914
9	5.806581	0.0048	4262.574953	-5.1231276
10	5.806556	-0.0202	4267.744699	0.0466184

11	5.806583	0.0068	4266.03263	-1.6654506
12	5.806588	0.0118	4264.908775	-2.7893056
13	5.806574	-0.0022	4270.37211	2.6740294
14	5.806553	-0.0232	4273.529715	5.8316344
15	5.806572	-0.0042	4277.253998	9.5559174
16	5.806557	-0.0192	4274.159827	6.4617464
17	5.806588	0.0118	4263.907401	-3.7906796
18	5.806593	0.0168	4263.289744	-4.4083366
19	5.806581	0.0048	4276.159119	8.4610384
20	5.806546	-0.0302	4263.22424	-4.4738406
Average	5.8065762		4267.698081	
Maximum	5.806594	0.0178	4277.253998	9.5559174
Minimum	5.806546	-0.0302	4257.620854	-10.0772266
Standard deviation	1.4215E-05	0.014214892	5.62516	5.62516

## 5.2 Cursor method

For a network analyzer such as HP8753 or HP8510, there is an internal function that can show the peak value and the bandwidth of the resonant curve at a designated value with a cursor operation. This function has been widely employed to evaluate the resonance frequency and quality factor  $Q$  of the resonant curve measured. As shown in **Error!**

**Reference source not found.**, suppose the attenuation is decreased by  $\alpha$  dB and the corresponding limit frequencies are  $(f_2)_\alpha$  and  $(f_1)_\alpha$ . The quality factor is determined by[1]:

$$Q = \frac{f_0 \times BW(\alpha)}{(f_2)_\alpha - (f_1)_\alpha} \quad (5.1)$$

where

$$BW(\alpha) = (10^{\alpha/10} - 1)^{1/2} \quad (5.2)$$

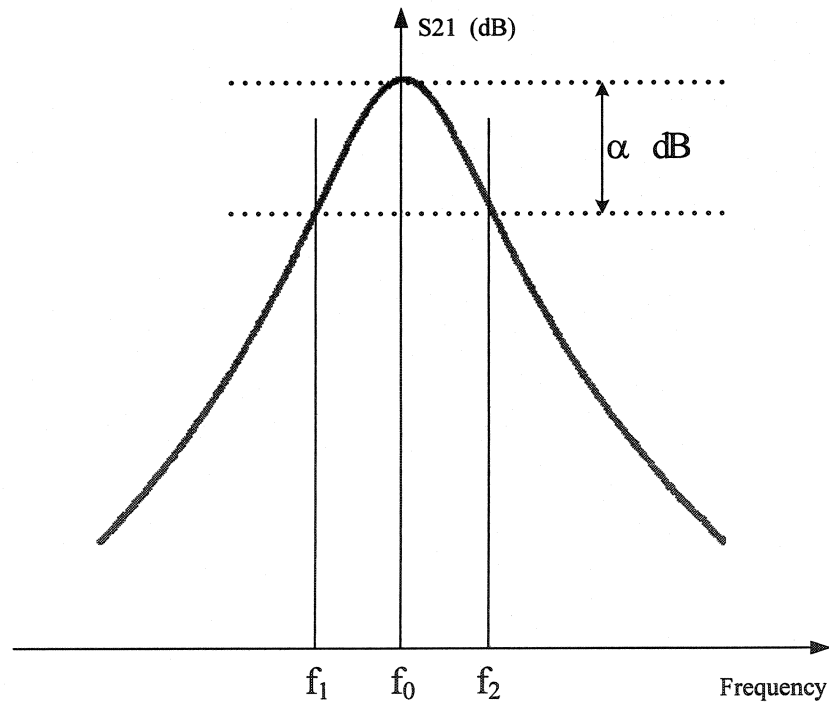


Figure 5. 1 Cursor method

This method is simple and easy to implement. It doesn't need complicate data processing as the following two other methods. Thus it is implemented in the

measurement software directly using VC++. However, it has the worst accuracy for frequency and quality factor  $Q$  measurement comparing with the following two methods.

### 5.3 Lorentzian fit method

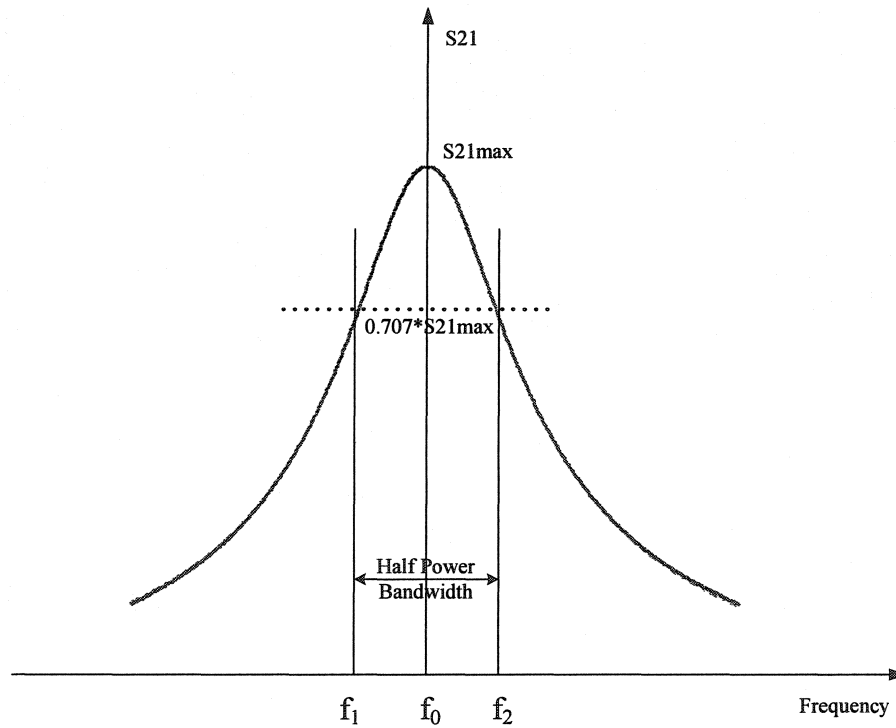


Figure 5.2 Lorentzian resonance curve

For the Lorentzian fit method, the resonant curve data ( $|S_{21}|$  verse frequency) is fit to a Lorentzian curve as shown in Figure 5.2 using a nonlinear least-square fit[2]. The Lorentzian formula for curve fitting is as follows:

$$|S_{21}(f)| = A_1 + A_2 f + \frac{|S_{\max}| + A_3 f}{\sqrt{1 + 4 \left( \frac{f - f_0}{\Delta f_{\text{Lorentz}}} \right)^2}} \quad (5.3)$$

where  $f_0$  is the resonant frequency;  $\Delta f_{\text{Lorentz}}$  is the half-power bandwidth;  $A_1$  is a bias constant;  $A_2$  is a first order coefficient;  $A_3$  is skew coefficient; and  $|S_{\max}|$  is the maximum magnitude. All of these parameters are used as the fitting parameters during the curve fitting process.

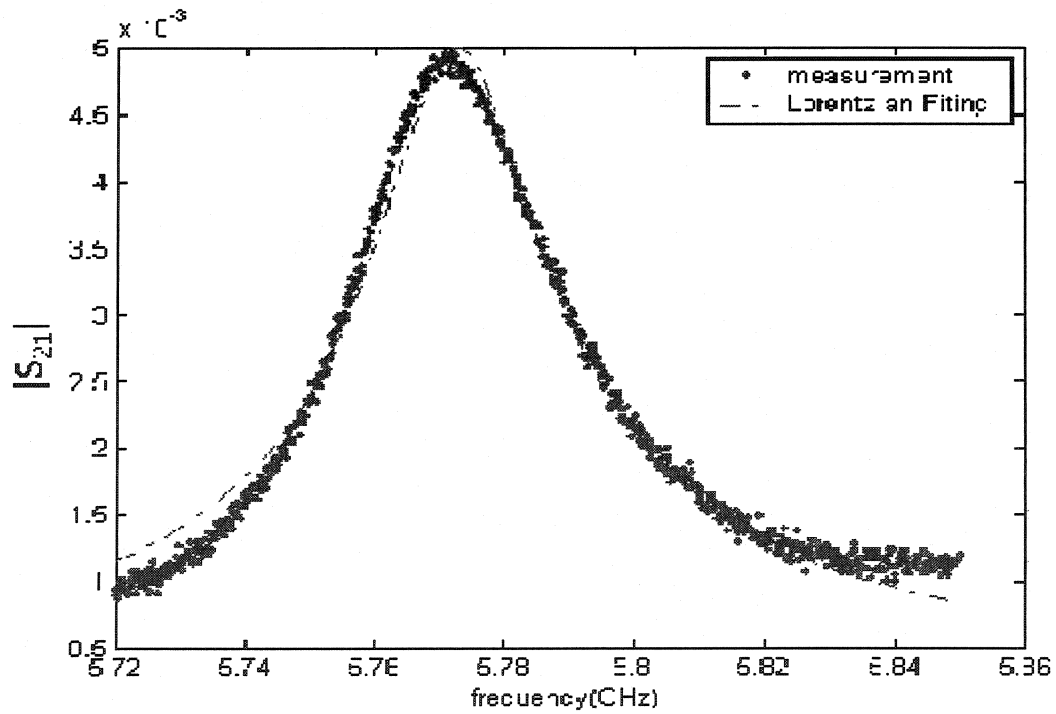


Figure 5.3 A typical Lorentzian fit curve



After fitting the measurement data, all of the coefficients in equation (5.3) were determined. Then the equation (5.3) can be used to calculate a new set of  $|S_{21}(f)|$ . A typical Lorentzian fit curve is shown in Figure 5.3. We can observe that the Lorentzian fit curve is noise free and can correct the asymmetry of the measurement data. In order to get a high resolution so as to increase the accuracy, this new data set can be very large. For example, there are only 801 data for the measurement data from VNA, which is limited by the resolution of the network analyzer, but the new data set derived from equation (5.3) could be larger than 10000. The resonant frequency  $f_0$  was given by the mean value of the frequencies corresponding to two half-power points. The frequencies  $f_1$  and  $f_2$  corresponding to two half-power points can be obtained from the fit curve. Since the absolute magnitude  $|S_{21}(f)|$  is used here, the half-power points locate at  $\sqrt{2}/2|S_{21}(f)|_{\max} \approx 0.707|S_{21}(f)|_{\max}$ . The quality factor  $Q$  can be calculated as follows:

$$Q = \frac{f_0}{f_2 - f_1} \quad (5.4)$$

This method is substantially more robust in the presence of noise than the cursor method.

## 5.4 RCA method

### 5.4.1 Principle of RCA method

For the above two measurement methods, there is a problem, which is how to obtain the half power bandwidth accurately. Currently the half power bandwidth is got by computing

the frequency difference corresponding to the two half-power points around the peak value directly [3]. However, the errors exist for determining the half-power points, and furthermore, they will cause a large error in the bandwidth obtained due to the subtraction of the two half-power frequencies. Consequently, this will decrease the accuracy of the Q evaluation.

To increase the accuracy of the Q evaluation, the Resonance Curve Area (RCA) method was proposed[4][5]. RCA method is based on that the loss factor of a resonance circuit is equivalent to the frequency domain integral of its resonance power curve. Hence it can utilize all of the measurement data from VNA and also minimize the effects of the noise at the same time. The output power of a resonant cavity can be described as follows:

$$\begin{aligned} P(f) &= |S_{21}(f)|^2 \\ &= \frac{P_0}{1 + \left( \frac{2Q(f - f_0)}{f_0} \right)^2} \end{aligned} \quad (5.5)$$

$P_0$  is the peak power of the resonant curve,  $f_0$  is the resonant frequency and  $f$  is the signal frequency feeding into the resonant cavity from VNA.

Let

$$x = \frac{2Q(f - f_0)}{f_0} \quad (5.6)$$

Then we have

$$P(x) = \frac{P_0}{1+x^2} \quad (5.7)$$

The resonant curve area in the frequency domain  $S$  can be obtained as follows:

$$\begin{aligned} S &= \int_{-\infty}^{\infty} P(f) df \\ &= \int_{-\infty}^{+\infty} P(x) \frac{f_0}{2Q} dx \\ &= \frac{\pi f_0 P_0}{2Q} \end{aligned} \quad (5.8)$$

Consequently, the  $Q$ -factor can be deduced from equation (5.8) as follows:

$$Q = \pi f_0 \frac{P_0}{2S} \quad (5.9)$$

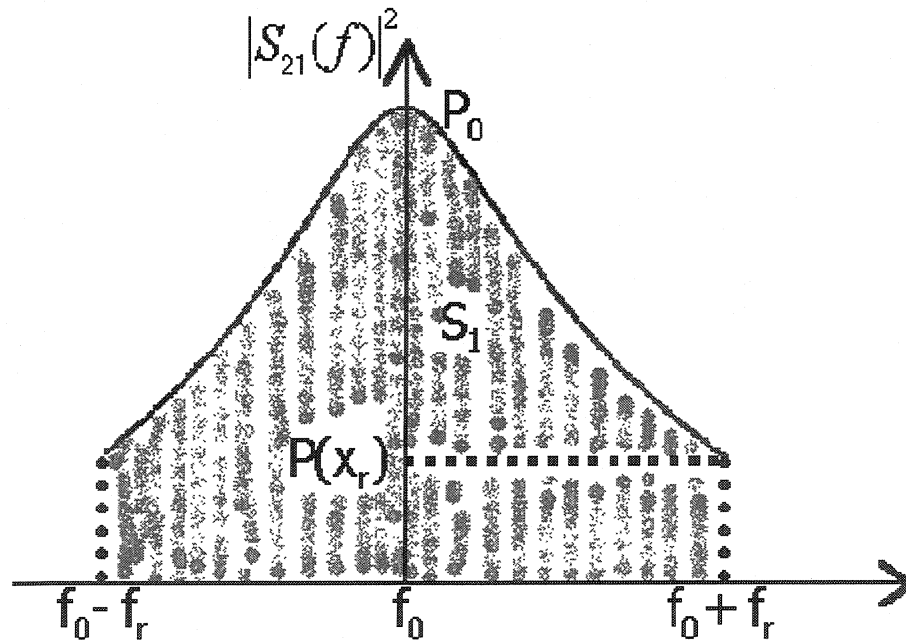


Figure 5.4 Finite range integration for RCA method

In a practical frequency sweep measurement, the frequency range will be in a finite range around the resonant frequency  $f_0$  as shown in Figure 5.4. Hence equation (5.8) should be modified as

$$\begin{aligned}
 S_1 &= \int_{-x_r}^{+x_r} \frac{P_0}{1+x^2} \left( \frac{f_0}{2Q} \right) dx \\
 &= f_0 \frac{P_0}{Q} \tan^{-1}(x_r) \\
 &= f_0 \frac{P_0}{Q} \tan^{-1} \sqrt{\frac{P_0}{P(x_r)} - 1}
 \end{aligned} \tag{5.10}$$

where

$$x_r = \frac{2Qf_r}{f_0} \tag{5.11}$$

$f_0 + f_r$  is the frequency corresponding to the right end of the resonant curve;

$f_0 - f_r$  is the frequency corresponding to the left end of the resonant curve.

Substituting  $x_0$  into equation (5.5), the final result is obtained as follows:

$$Q = f_0 \frac{P_0}{S_1} \tan^{-1} \sqrt{\frac{P_0}{P(x_r)} - 1} \tag{5.12}$$

We can rewrite equation (5.9) as:

$$Q = 2\pi f_0 \frac{\frac{P_0}{2\pi S_1}}{\tan^{-1} \sqrt{\frac{P_0}{P(x_r)} - 1}} = 2\pi f_0 \frac{P_0}{S_1'} \tag{5.13}$$

The definition of the quality factor  $Q$  of a resonance circuit is

$$Q = 2\pi f_0 \frac{\text{Average stored energy}}{\text{Energy loss per second}} \quad (5.14)$$

Comparing this definition with equation (5.13), it is noticed that the peak power  $P_0$  corresponds to the average stored energy, and the equivalent resonance curve area  $S_1'$  corresponds to the energy loss per second of the resonant circuit.

#### 5.4.2 Software implementation of RCA method

For RCA method, the area under the  $|S_{21}(f)|^2$  curve is integrated to compute the value of the quality factor  $Q$  using equation (5.12). In order to implement RCA method, we should make the squared magnitude data of the transmission coefficient,  $|S_{21}(f)|^2$ , versus frequency fit to a Lorentzian curve:

$$|S_{21}(f)|^2 = \frac{P_0}{1 + 4\left(\frac{f - f_0}{\Delta f_{RCA}}\right)^2} \quad (5.15)$$

Here the fitting parameters are the resonant frequency  $f_0$ , the maximum power  $P_0$ , and the bandwidth  $\Delta f_{RCA}$ .

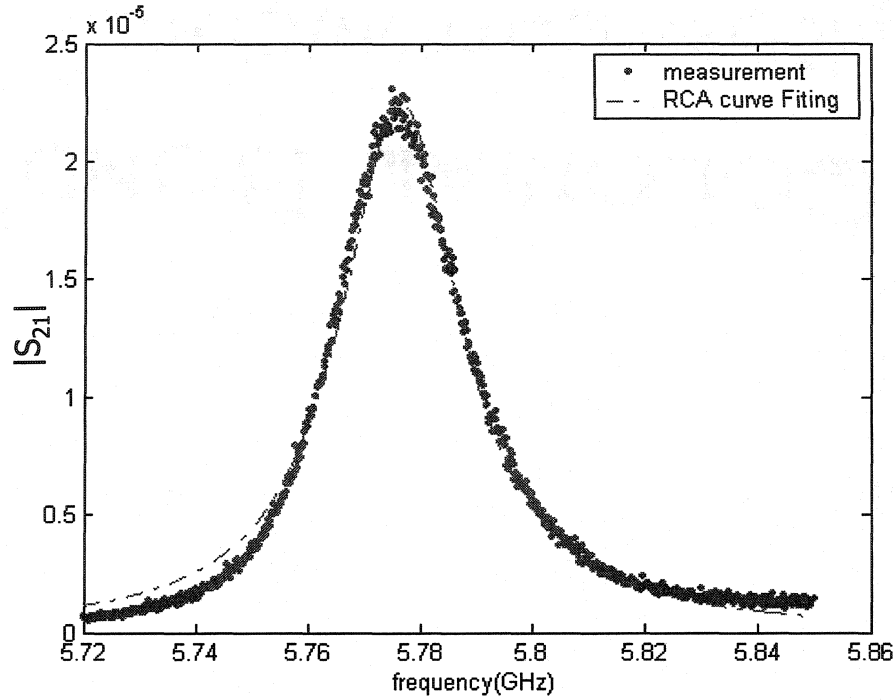


Figure 5.5 A typical curve fit for RCA

Secondly, with the fitting parameters obtained, the Lorentzian curve presented by equation (5.15) becomes the best approximate resonant curve according to the measurement data. A typical resonant curve fit results is shown in Figure 5.5. It is noted that this resonant curve is noise free and also reduces the effects of the random measurement errors. As shown in Figure 5.4, the values of the driving power  $|S_{21}(f)|^2$  corresponding to all frequencies located between  $f_o - f_r$  to  $f_o + f_r$  can be calculated using equation (5.15) with the fitting parameters obtained. Then the area under the fitting curve,  $S_1$ , from  $f_o - f_r$  to  $f_o + f_r$  can be computed using the trapezoidal rule[6] as follows:

$$\begin{aligned}
S_1 &= \int_{f_0 - f_r}^{f_0 + f_r} |S_{21, fitting}(f)|^2 df \\
&= \sum_{f_0 - f_r}^{f_0 + f_r} \frac{\Delta f}{2} \left( |S_{21, fitting}(n)|^2 + |S_{21, fitting}(n+1)|^2 \right)
\end{aligned} \tag{5.16}$$

where  $|S_{21, fitting}(n)|^2$  stands for the driving power corresponding to the  $n$ -th frequency point, and  $\Delta f$  is the frequency difference between two consecutive frequency points. In order to improve the accuracy of the numerical integral in equation (5.16), the number of the frequency points between  $f_0 - f_r$  and  $f_0 + f_r$  should be as large as possible. For example, 50001 points was used in our Matlab program. In this way the resolution is largely increased, comparing with the maximum 801 measurement data from the vector network analyzer HP8753

Consequently, the quality factor  $Q$  can be calculated from the area  $S_1$  as follows:

$$Q = f_0 \frac{P_0}{S_1} \tan^{-1} \sqrt{\frac{P_0}{|S_{21}(f_0 \pm f_r)|^2} - 1} \tag{5.17}$$

It should be noted that  $f_r$  ought to be large enough to make both  $f_0 - f_r$  and  $f_0 + f_r$  far from the resonant frequency  $f_0$  so as to improve the accuracy of  $Q$  evaluation. In fact, by making integration over a broad frequency band, the errors derived from the frequency measurement and noise can be reduced, so we can obtain an improvement in the accuracy of  $Q$  measurement. Since RCA method utilizes all of the resonant curve data in the integral with equation (5.16), it is claimed that this method is more robust against noise than the Lorentzian fit method [5].

## **5.5 Software design**

Matlab is a powerful software tool for numerical computation, visualization, programming, research, engineering, and communication, which was developed by Mathworks Inc. It includes cutting-edge algorithms, enormous data handling abilities, and powerful programming tools. It also provides a graphical user interface design tool for user to design a friendly windows interface. This provides more convenient for end user to use the programs developed by Matlab. Moreover, Mathworks also provides a compiler to compile the m files to a stand-alone executable program. In this way, the application program developed by Matlab can run separately from Matlab environment. In fact, it can run in a PC not installed Matlab, once including the entire necessary supporting library while releasing the application software. Hence Matlab was selected to develop the data processing program in this project. Therefore, it is no necessary for us to write the complicate algorithms such as curve fit from scratch. This largely simplifies the development process of the post data processing.

### **5.5.1 Graphical User interface (GUI) Design**

The graphical user interface of the data processing is shown in Figure 5.6. The sample point field is used to set the new sampling point that is used to find the resonant frequency and compute the quality factor after fitting the measurement data. The calibration algorithm should be set in the algorithm field. RCA method or Lorentzian fit method can be selected in the curve fitting method field.



There are three frame areas following these three fields, which are empty cavity area, standard sample area, and measurement sample area. In the empty cavity area, the curve data name field and the “Browse” button are used to select the measurement curve data file of the empty cavity. The “Run” button will call the resonant frequency  $f_0$  and the quality factor  $Q_0$  calculation function. The calculation results will be shown in the field  $f_0$  and  $Q_0$ .

In the standard sample area, the curve data name field and the “Browse” button are also used to select the measurement curve data file of the cavity with standard sample. The permittivity of the standard sample will be displayed in the Epsilon\_r and Epsilon\_i fields after loading the data from the data file. The “Calibrate” button will call the calibration function.  $f_0$  and  $Q_0$  of the empty cavity obtained early will be utilized during calibration process. At the end of the calibration calculation, the results will be stored in the “Filling factor  $F_1$ ” and “Filling factor  $F_2$ ” fields.

In the measurement sample area, the curve data name field and the “Browse” button are used to select the measurement curve data file of the cavity with sample measured. The sample name will be put in the sample name field after loading the measurement data from the data file. The “Run” button will call the permittivity calculation function.  $f_0$  and  $Q_0$  of the empty cavity, and the filling factors  $F_1$  and  $F_2$  will be used during the permittivity calculation process. The calculation results will be displayed in the “Measurement results” list and be saved to a text file automatically.

### 5.5.2 Post data processing flow chart

The post data processing flow chart is shown in Figure 5.7. The data processing procedure can be divided into 5 steps as follows:

- Step 1: set the sampling points, select the calibration method and the curve fit method.
- Step 2: Calculating the resonant frequency  $f_0$  and the quality factor  $Q_0$  of the empty cavity. Firstly, select the curve data file of the empty cavity by clicking the “Browse” button in the empty cavity area. Then click the “Run” button in the same area to call  $f_0$  and  $Q_0$  calibration functions to compute  $f_0$  and  $Q_0$ .
- Step 3: Calculating the filling factors  $F_1$  and  $F_2$ . At first, select the curve data file of the cavity with standard sample by clicking the “Browse” button in the standard sample area. Then click the “Calibrate” button in the same area to call calibration function to compute the filling factors  $F_1$  and  $F_2$ .
- Step 4: Calculating the complex permittivity of the sample. As above operation process, select the curve data file of the cavity with the sample measured by clicking the “Browse” button in the measurement sample area at first. Then click the “Run” button in the same area to call the permittivity calculation function to compute the complex permittivity of the sample measured.
- Step 5: If we want to calculate the permittivity of another sample with the same sampling points, and the same calibration algorithm and curve fit method as those selected early, then just go back to step 4. If we want to process another sample with different sampling points, calibration algorithm or curve fit method, then we need to go to step 1 and repeat all steps from step 1 to step 4.

**PermiSys Post Data Processing** Author: Yan Ye

Sample Point:  Algorithm:  Curve Fitting Method:

**Empty Cavity**

Curve Data Name:

FQ(GHz):  Q0:

**Standard Sample**

Curve Data Name:

Sample Name:

Epsilon\_r:  Epsilon\_i:

Filling Factor F1:  Filling Factor F2:

**Measurement Sample**

Curve Data Name:

Sample Name:

**Measurement Results**

Fs	Qs	Epsilon1	Epsilon2	tan delta
5.772600000	220.4084969787	62.5355700000	20.7011300000	0.3310296844
5.772696000	220.5912635364	62.3270700000	20.6830700000	0.3318473017
5.772648000	220.3908169683	62.4313200000	20.7028800000	0.3316104801
5.772648000	220.5487720046	62.4313200000	20.6872600000	0.3313602852
5.772672000	218.9290232659	62.3791900000	20.8484600000	0.3342213966
5.772648000	219.8749441111	62.4313200000	20.7540300000	0.3324297804
5.772696000	220.4217519668	62.3270700000	20.6998200000	0.3321160452
5.772696000	218.0220715263	62.3270700000	20.9397600000	0.3359657369

Figure 5.6 Post data processing GUI

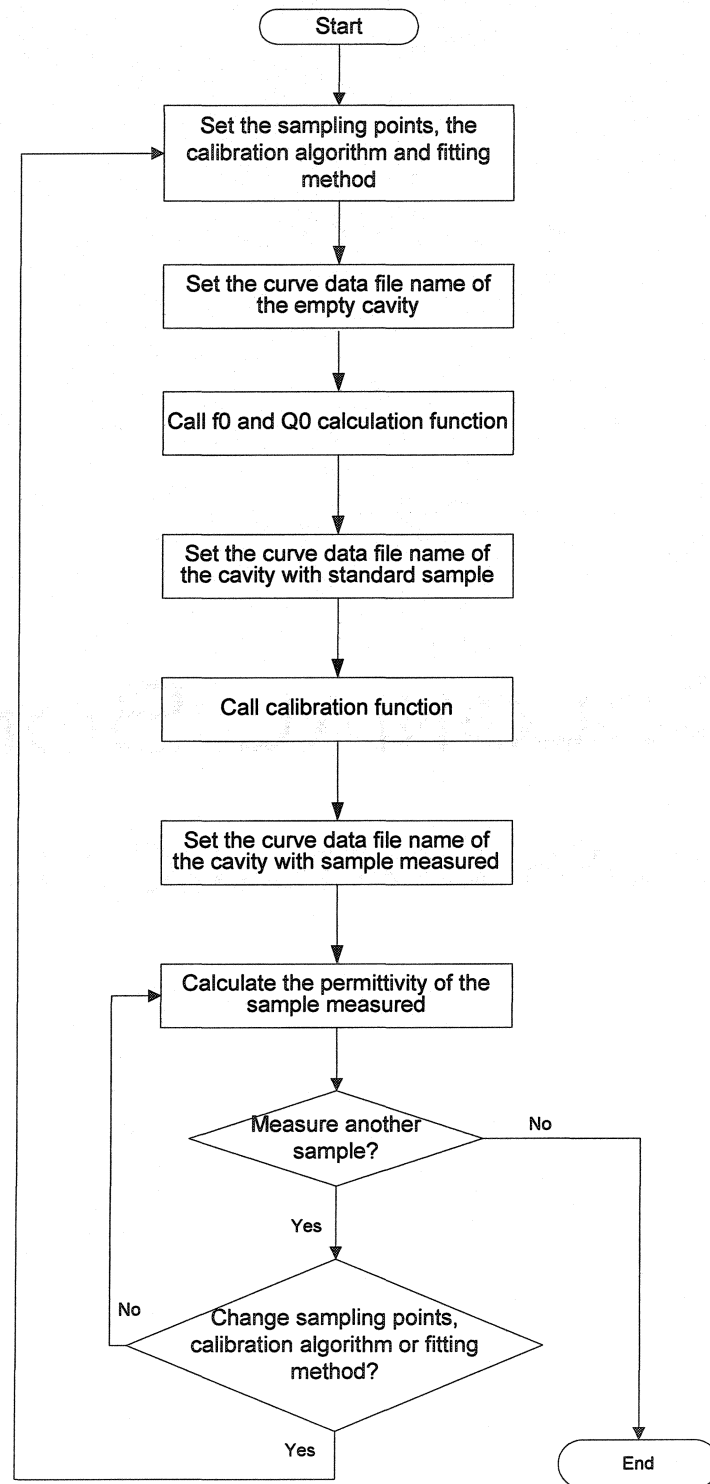


Figure 5.7 Post data processing flow chart

## References:

- [1] C. Akyel, and R. G. Bosisio, "New developments on automated-active circuits for permittivity measurements at microwave frequencies", IEEE Trans. Instrum. Meas., vol.38, no.2, pp.496-504, April 1989
- [2] P.R. Bevington, Data Reduction and error Analysis for the Physical Sciences, pp.237-240, McGraw-Hill, New York, 1969
- [3] D. Kajfez, "Q Factor", Vector Fields, 1994.
- [4] H. Yanai, M. Ogi, "Measurments of Q and dielectric losses by the resonance area method", Jour. ICE, vol.36, no.3, pp.121-125, Mar. 1953.
- [5] T. Miura, T. Takahashi, and M. Kobayashi, "Accurate Q-factor evaluation by resonance curve area method and its application to the cavity pertubation", IEICE Trans. Electron., E77-C, no.6, pp.900-907, June1994.
- [6] W.H. Press, B.P. Flannery, S.A. Teukolsky, and W.T. Vetterling, *Numerical recipes*, pp.105,202,203,523-528, Cambridge University Press, New York, 1989.

## Chapter 6 Measurement procedures, results and Discussion

### 6.1 *The Automatic Permittivity Measurement System*

The diagram of the automatic permittivity measurement system and the photo of the system are shown in Figure 6.1 and Figure 6.2, respectively. We use the vector network analyzer HP8753 to measure  $S_{21}$  of the cavity in a frequency range interested in order to get the resonant curve of the resonant cavity. The measurement process is fully controlled by PermiSys through the GPIB interface. For the GPIB programming, since the current popular Virtual Instrument Software Architecture (VISA) has been used, the PermiSys has good transplant property for supporting the different GPIB cards. Whatever the GPIB cards are made by HP, NI or others, PermiSys can work well with them if they support VISA.

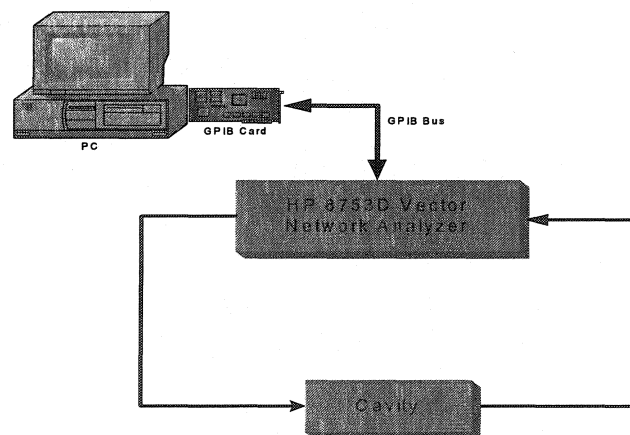


Figure 6.1 the diagram of the automatic permittivity measurement system

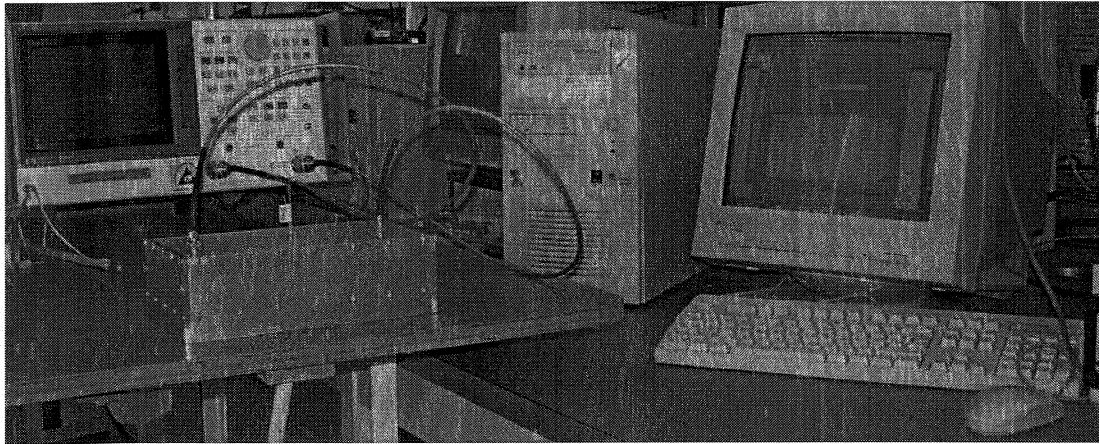


Figure 6.2 the photo of the automatic permittivity measurement system

## 6.2 *Permittivity measurement procedures*

The measurement procedure includes following four steps:

- ❑ parameter setting;
- ❑ measuring the resonant frequency and  $Q$  factor of empty cavity;
- ❑ calibrating the measurement system with a standard sample;
- ❑ measuring the resonant frequency and  $Q$  factor of the cavity with a sample and calculation the complex permittivity of the sample.

### 6.2.1 Parameter setting

As shown in Figure 6.3, the parameters listed in this dialog should be set if the resonant cavity changes. Here the resonant frequency is the quota resonant frequency of the empty cavity. The resonant cavity is limited to a rectangular cavity or a circular

cavity. For a rectangular cavity, the length  $a$ , width  $b$  and height  $c$  should be given. For a circular cavity, the diameter  $d$  and the height  $h$  should be defined. Moreover, the initial frequency sweep range should be given, i.e., for the 5.8 GHz resonant cavity in this project, the default values are  $f_{\text{start}}=5.73$  GHz and  $f_{\text{stop}}=5.85$  GHz. Therefore, this automatic permittivity measurement software can be used in any frequency if the proper parameters are set accordingly when the resonant cavity is replaced. Since these parameters will be saved in a file and are loaded automatically at the software start, they only need to be set one time except the cavity is changed.

**Step 1 of 2: Parameter Setting**

Resonant Frequency (GHz):

Cavity Type

☒ Rectangular Cavity

☐ Circular Cavity

Cavity Size

a(mm):

b(mm):

c (mm):

Frequency sweep range

Start Frequency (GHz):

Stop Frequency (GHz):

Prepare the empty cavity, then push the button "Next/Suivant"

Figure 6.3 Parameter setting



### 6.2.2 Measuring the empty cavity

The resonant curve of the empty cavity is shown in Figure 6.4. The resonant curve data are read from the VNA and are saved in a txt file for further data processing later. Then the resonant frequency  $f_{0e}$  is measured by VNA and is sent to PC. In the same way, the  $(f_1)_\alpha$  and  $(f_2)_\alpha$  are measured (e.g., select  $\alpha=3\text{dB}$ ) and are delivered to PC. The Q-factor of the empty cavity can be obtained by [1]:

$$Q = \frac{f_0 \times BW(\alpha)}{(f_2)_\alpha - (f_1)_\alpha} \quad (6.1)$$

where

$$BW(\alpha) = \left(10^{\alpha/10} - 1\right)^{1/2} \quad (6.2)$$

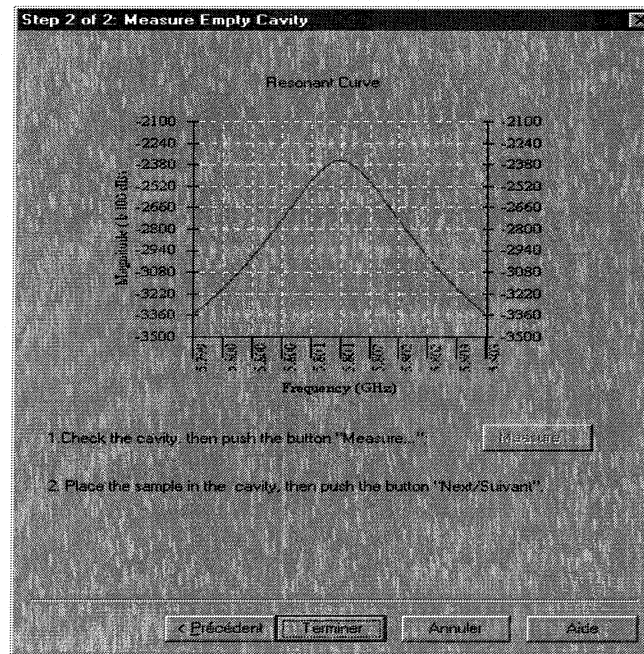


Figure 6.4 Empty cavity measurement

### 6.2.3 Measurement system calibration

The measurement system should be calibrated with a known permittivity sample such as distilled water. In this project, distilled water will be used as the standard sample since the samples measured are liquid and they should have the same shape and volume as that the standard sample. The calibration dialog, which can be activated by clicking the menu item “Calibrate with Standard Sample” in Tools menu, is shown in Figure 6.5. The filling factors can be calculated by

$$F_1'' = \frac{\varepsilon_r' - 1}{\left(1 - \frac{f}{f_0}\right)} \quad (6.3)$$

$$F_2'' = \frac{\varepsilon_r''}{\left(\frac{1}{Q} - \frac{1}{Q_0}\right)} \quad (6.4)$$

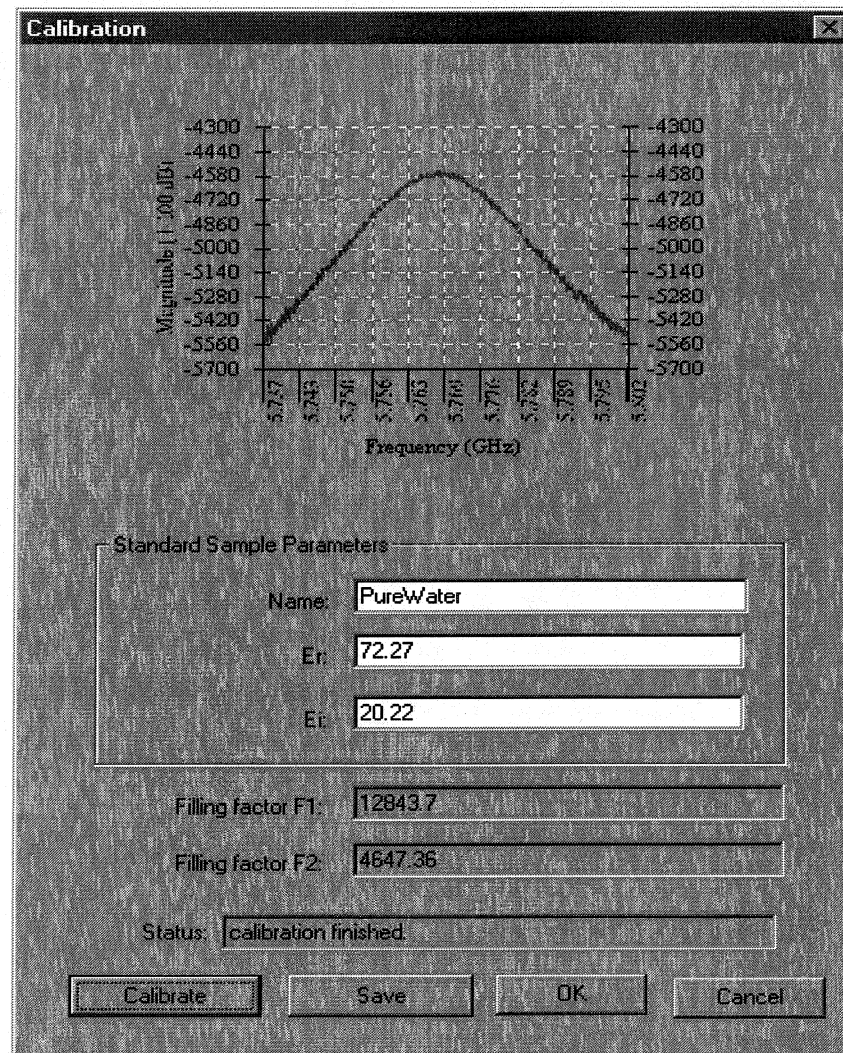


Figure 6.5 Calibration dialog

### 6.2.4 Measuring the permittivity of the sample

After the previous three steps, the system is ready to measure the permittivity of the sample. There are two approaches to make the measurement. One is guided by measurement wizard and another one is conducted by automatic multi-time measurement dialog.

### ***Measurement wizard***

The resonant curve of the cavity with a sample is shown in Figure 6.6 (a). The name of the sample should be given before measuring. The volume of the sample is also needed when the calibration method 2 is used. The resonant frequency  $f_{0s}$  is measured at first, then  $(f_{1s})_{\alpha}$  and  $(f_{2s})_{\alpha}$  are measured (here we select  $\alpha=3\text{dB}$ ). From the equation (6.1) the Q-factor of the empty cavity can be obtained. At last, the permittivity of the sample is calculated by

$$\varepsilon_r' = 1 + F_1'' \left( 1 - \frac{f}{f_0} \right) \quad (6.5)$$

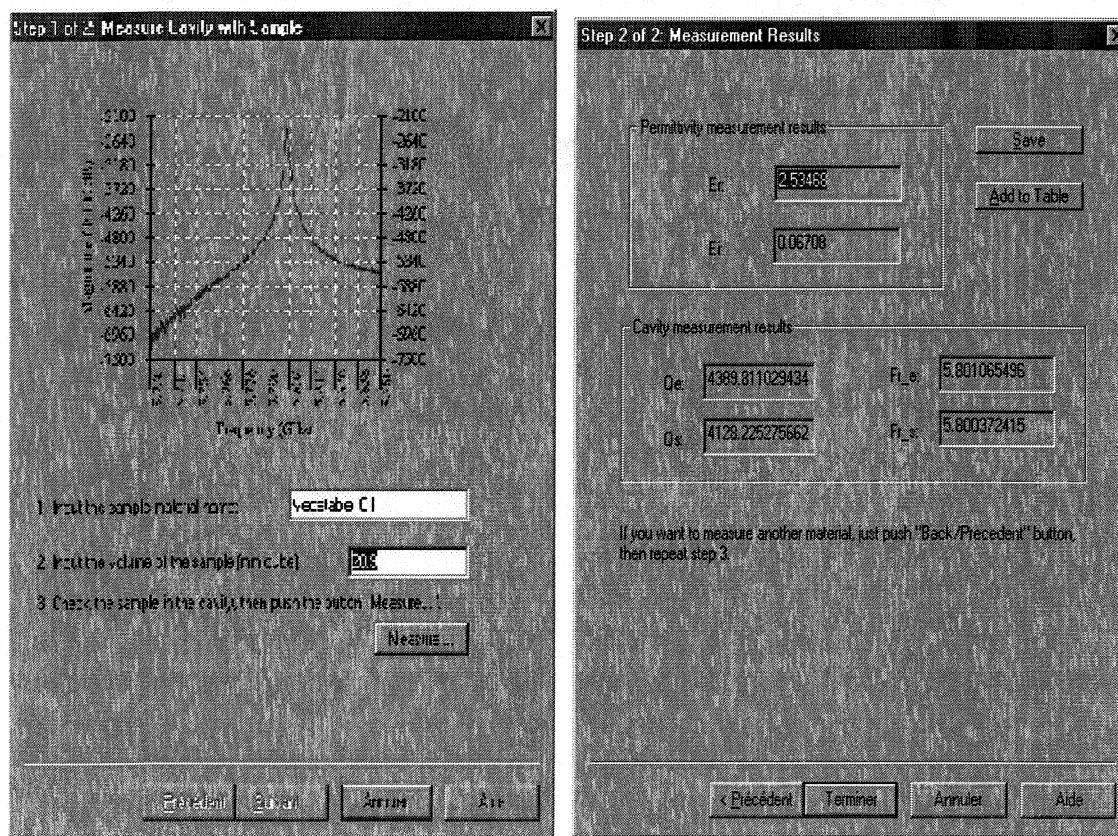
$$\varepsilon_r'' = F_2'' \left( \frac{1}{Q} - \frac{1}{Q_0} \right) \quad (6.6)$$

The permittivity will be displayed in Figure 6.6 (b) and also can be saved to a file. These measurement results can also be added to the table in the main window by clicking the push-button “Add to Table”. If there is another material needed to measure, just click the “Précédent” button and repeat this measurement process.

### ***Automatic multi-time measurement***

In order to increase the accuracy of the measurement, it is necessary to measure a sample for many times under the same condition. This kind of measurement can be done by the automatic multi-time measurement program. The automatic multi-time measurement dialog is shown in Figure 6.7. We can set the measurement times directly in

this dialog. During the measurement process, the resonant curves and measurement results will be displayed in this dialog continuously. The measurement results are also added to the table in the main window as shown in Figure 6.8. In this case, all of the resonant curves will be saved as a text file for post-data processing.



(a)

(b)

Figure 6.6 Permittivity measurement wizard (a) measure cavity with sample (b) calculate the permittivity

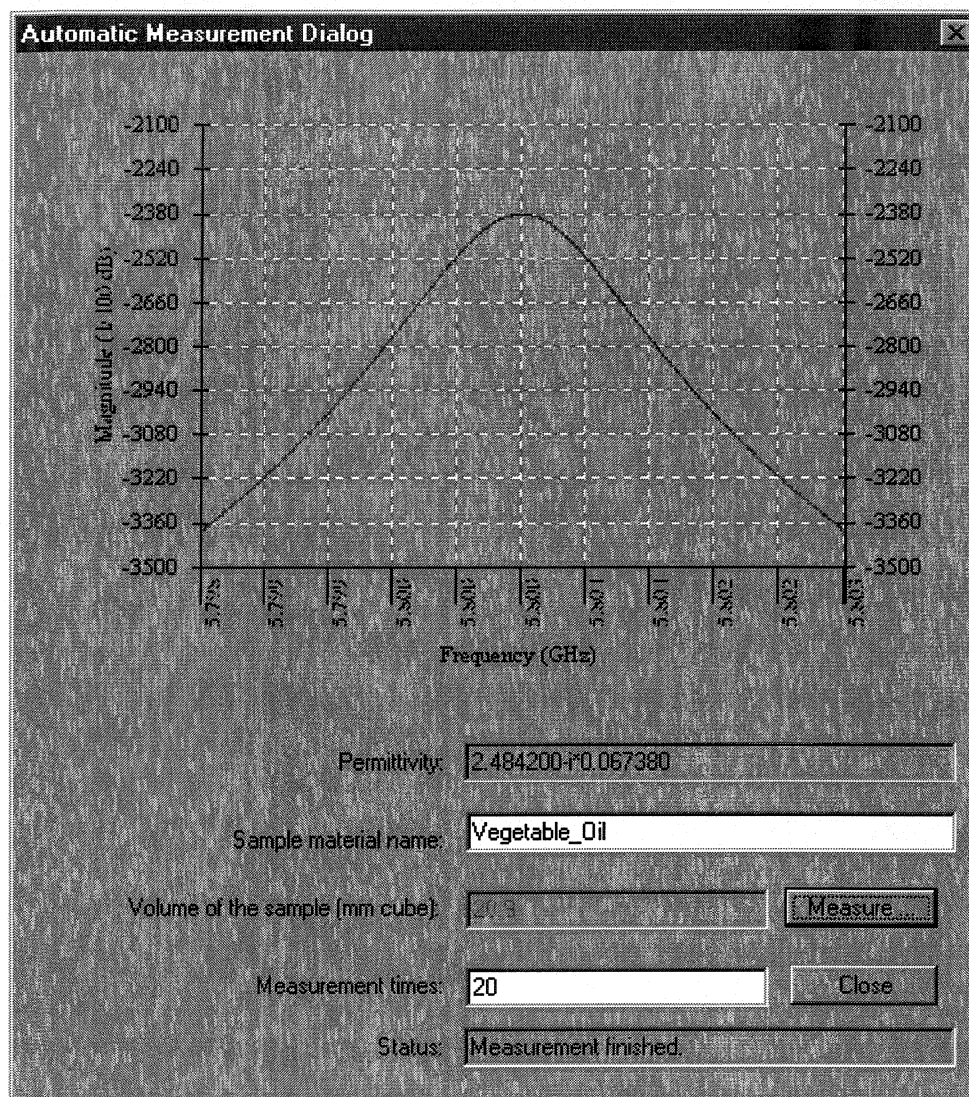


Figure 6.7 Automatic multi-time measurement



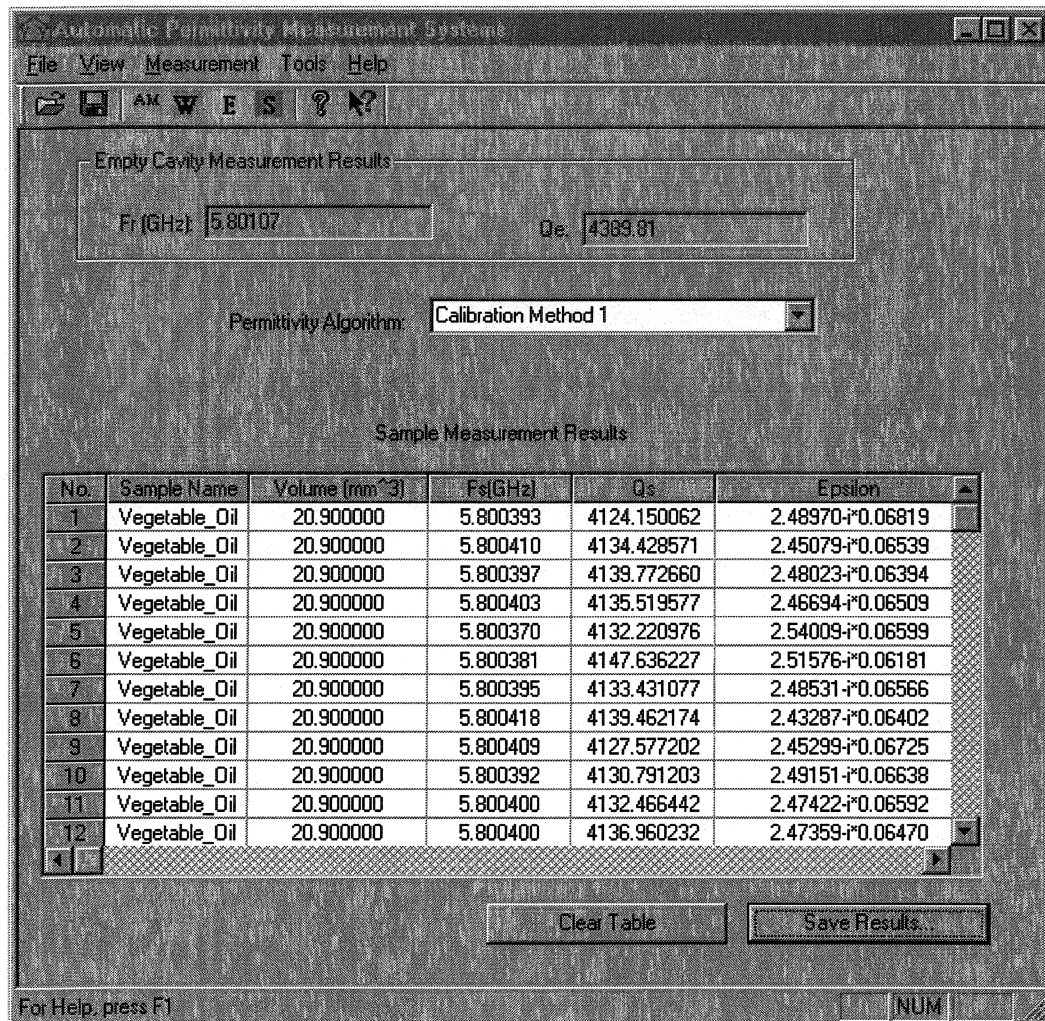


Figure 6.8 The measurement results displayed in the main window

### 6.3 Measurement Results and Discussion

Distilled water was used as the standard sample to calibrate the measurement system. Its permittivity at 25°C is  $72.27 - j*20.22$  for 5.8 GHz work frequency[2][4][5]. Some liquid samples were used to validate this measurement system. These samples can be categorized as three classes: high loss, median loss and low loss liquids. These liquid

samples were injected into a standard corning micro-pipette (100ul) made of borosilicate glass. Even though the loss of the pipettes is very low, in order to improve the measurement accuracy an empty pipette should be insert in the sample hole of the cavity while the empty cavity was measured.

Since most of the permittivity measurements for liquid samples have been made at 915 MHz and 2.45 GHz and permittivity measurement has been rarely made at 5.8 GHz, it is very difficult to find a reference to validate the accuracy of our measurement results. In order to get a reference value, HP85070 dielectric probe kit, which is an open-ended coaxial probe measurement system consisting of the probe, related software and calibration standards, was utilized to measure the same sample at 5.8 GHz to get a reference value while the sample was measured with our measurement system. Since a coaxial probe system cannot accurately measure permittivity, the results measured with hp85070 coaxial probe system cannot be used as the standard references, they only can be taken as reference results for comparison.

### **6.3.1 High loss liquid**

#### **6.3.1.1 *Distilled water***

Although the distilled water (québec.O<sup>®</sup>), which mineral salts content is less than 10ppm, was taken as the standard sample to calibrate the system, it was measured again by the automatic multi-time measurement program to check the repeatability of the



measurement system. The permittivities measured with different methods were listed in the Table 6.1. The dielectric constant  $\epsilon'$  and loss factor  $\epsilon''$  were plotted in Figure 6.9 and Figure 6.10 respectively. It was noted that both RCA method and Lorentzian fitting method lead to get a dielectric constant  $\epsilon'$  with very low deviation, but there was a large deviation for the dielectric constant  $\epsilon'$  with the Cursor method. For the dielectric loss factor  $\epsilon''$ , even though there are some deviation for both RCA method and Lorentzian fitting method, the deviation is much smaller than that of the Cursor method. The permittivity measurement result was  $68.45 - j*12.50$  at 5.8 GHz for hp85070 coaxial probe system. We know that the permittivity of water at 25°C is  $72.27 - j*20.22$  for 5.8 GHz operation frequency[2][4][5]. Thus, both of the dielectric constant  $\epsilon'$  and the dielectric loss factor  $\epsilon''$  are smaller than those of water in the literature. Especially for the dielectric loss factor  $\epsilon''$ , the relative deviation from the value in literature is as high as 61.8%. Accordingly, hp85070 coaxial probe system cannot accurately measure the dielectric loss factor  $\epsilon''$ .

Table 6.1 Permittivity of distilled water at 5.8 GHz

No	Cursor		RCA		Lorentzian Fit	
	$\epsilon'$	$\epsilon''$	$\epsilon'$	$\epsilon''$	$\epsilon'$	$\epsilon''$
1	81.45	20.42	72.07	20.41	72.09	20.32
2	73.20	20.37	72.11	20.41	72.12	20.34
3	73.91	19.15	72.24	20.33	72.29	20.30
4	74.52	19.35	72.24	20.44	72.25	20.38
5	72.29	19.72	72.13	20.47	72.14	20.38
6	76.90	19.83	72.20	20.41	72.19	20.41
7	76.78	20.38	72.16	20.31	72.22	20.29
8	74.37	18.94	72.15	20.45	72.20	20.42
9	72.79	19.90	72.18	20.49	72.22	20.44
10	71.43	20.31	72.12	20.39	72.21	20.39
11	72.13	19.93	72.15	20.43	72.15	20.42
12	74.47	20.06	72.14	20.35	72.13	20.36
13	73.19	19.06	72.10	20.39	72.13	20.36
14	75.52	19.57	72.22	20.50	72.22	20.44
15	74.19	19.86	72.20	20.44	72.26	20.38
16	76.18	19.97	72.24	20.41	72.26	20.32
17	72.71	19.82	72.29	20.44	72.28	20.43
18	75.13	19.51	72.19	20.48	72.17	20.43
19	70.73	20.28	72.18	20.44	72.20	20.32
20	73.55	20.23	72.16	20.50	72.20	20.51
Average	74.27	19.83	72.17	20.42	72.20	20.38
Standard Deviation	2.38	0.45	0.05	0.05	0.06	0.06

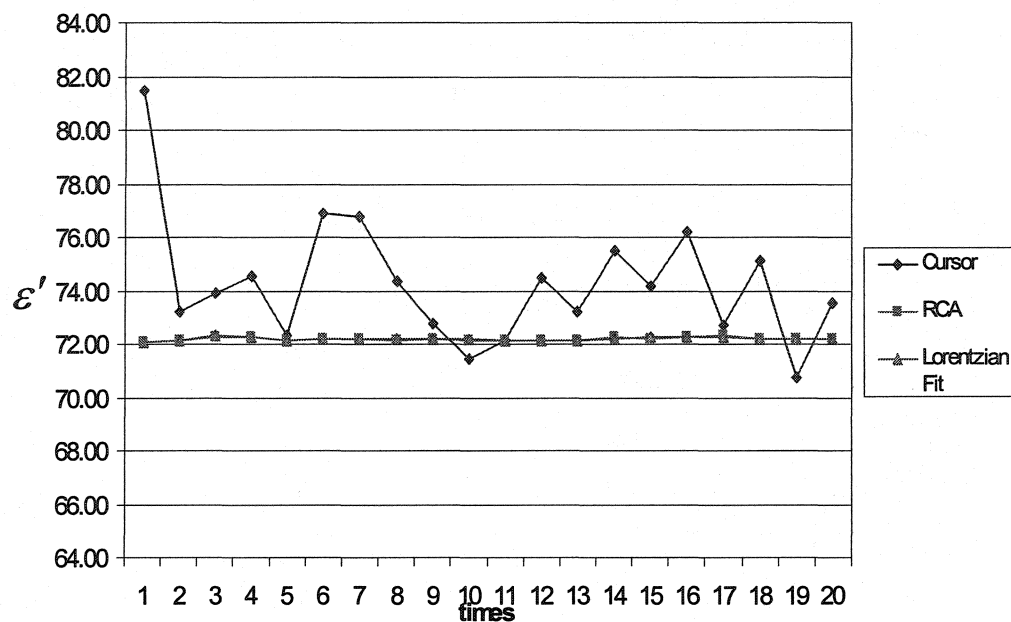


Figure 6.9 Dielectric constant of distilled water at 5.8 GHz

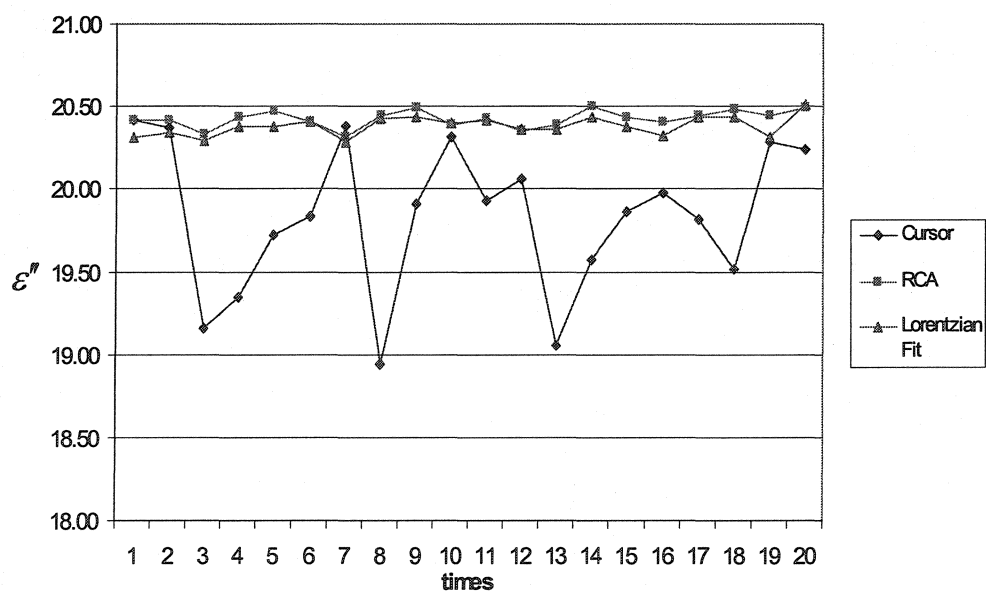


Figure 6.10 Dielectric loss factor of distilled water at 5.8 GHz

### 6.3.1.2 3.25%-fat milk

The homogenised milk (Quebon<sup>®</sup>: 3.25% fat) was bought from the local super market and stored in the refrigerator. Small amount of milk were drawn and kept in ambient conditions for about 1 and half hours before the beginning of the dielectric measurement. The measurement results with different methods were listed in Table 6.2 and plotted in Figure 6.11 and Figure 6.12, respectively.

Similar as the distilled water, for the dielectric constant  $\epsilon'$ , both RCA method and Lorentzian fit method produced results with very small deviation, however, the Cursor method resulted in outcome with large deviation. For the dielectric loss factor  $\epsilon''$ , even though there are some deviation for both RCA method and Lorentzian fit method, the deviation is still smaller than that of the Cursor method. The results demonstrated that RCA method and Lorentzian fit method have much better repeatability than the Cursor method.

The permittivity measurement result was  $56.88 - j*25.87$  at 5.8 GHz for hp85070 coaxial probe system. As shown in Table 6.2, the permittivity of milk with our measurement system is  $55.63-j*22.10$ ,  $53.64-j*22.87$  and  $53.54-j*21.81$  for cursor method, RCA method and Lorentzian fit method, respectively.

Table 6.2 Permittivity of 3.25%-fat milk at 5.8 GHz

No	Cursor		RCA		Lorentzian Fit	
	$\epsilon'$	$\epsilon''$	$\epsilon'$	$\epsilon''$	$\epsilon'$	$\epsilon''$
1	54.71	21.49	53.71	22.49	53.63	21.63
2	52.94	21.82	53.76	22.47	53.65	21.59
3	55.22	21.71	53.71	22.64	53.64	21.71
4	53.67	22.07	53.68	22.73	53.60	21.72
5	55.67	21.96	53.66	22.70	53.56	21.70
6	55.61	22.17	53.56	22.83	53.50	21.75
7	54.73	22.06	53.65	22.88	53.55	21.71
8	57.77	22.20	53.63	22.87	53.53	21.80
9	56.20	22.11	53.58	22.86	53.45	21.80
10	56.26	22.32	53.60	22.92	53.52	21.87
11	56.67	22.32	53.61	22.93	53.51	21.77
12	56.09	22.23	53.65	22.95	53.53	21.93
13	56.38	22.26	53.64	22.97	53.54	21.80
14	56.81	22.38	53.62	22.94	53.55	21.91
15	54.44	22.16	53.66	23.04	53.56	21.84
16	56.52	22.33	53.64	22.97	53.59	21.89
17	56.64	22.01	53.55	23.12	53.47	21.91
18	55.27	21.94	53.58	23.03	53.48	21.91
19	54.37	22.44	53.59	23.04	53.48	21.90
20	56.62	22.03	53.61	23.01	53.53	21.99
Average	55.63	22.10	53.64	22.87	53.54	21.81
Standard Deviation	1.20	0.24	0.05	0.18	0.06	0.11

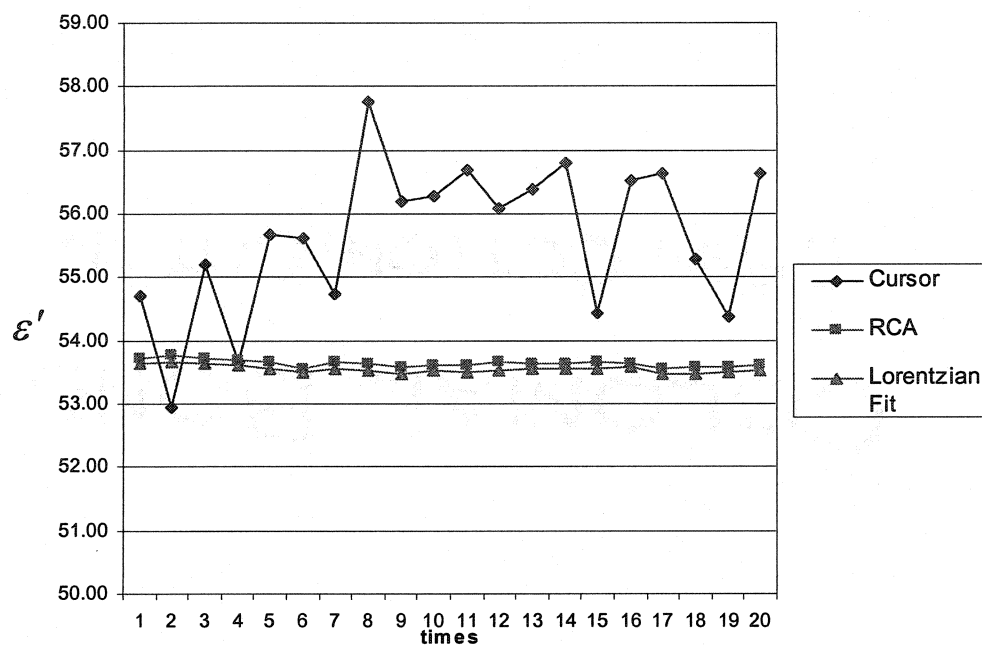


Figure 6.11 Dielectric constant of 3.25% milk at 5.8 GHz

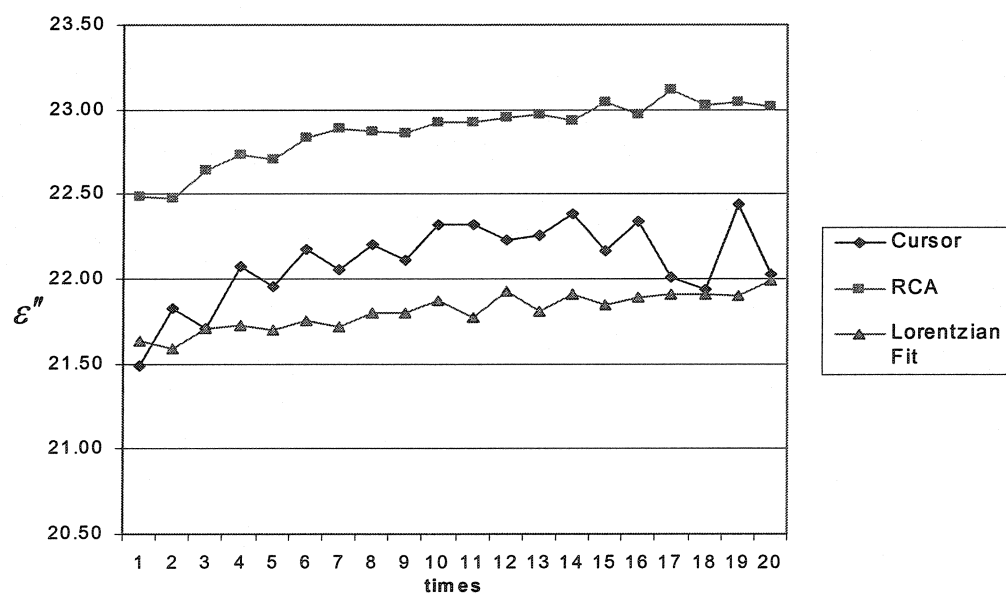


Figure 6.12 Dielectric loss factor of 3.25% milk at 5.8 GHz

### 6.3.1.3 *Orange juice*

Like milk, orange juice (Fruite<sup>®</sup>: 1% sodium, 2% potassium and 9% carbohydrate) was also bought from the local super market and stored in the refrigerator. Small amount of juice were drawn and kept in room temperature (25°C) for about 1 and half hours before the start of the dielectric measurement. The measurement results with different methods were listed in Table 6.3 and plotted in Figure 6.13 and Figure 6.14, respectively.

As shown in Figure 6.13 and Figure 6.14, for the dielectric constant  $\varepsilon'$ , both RCA method and Lorentzian fit method produced results with very small deviation, however, the Cursor method resulted in outcome with large deviation. Moreover,  $\varepsilon'$  from RCA method and Lorentzian fit method are almost same, in fact, the average values for both methods are 64.15. For the dielectric loss factor  $\varepsilon''$ , the deviation is very small for RCA method; even though there are some deviation for Lorentzian fit method, the deviation is still smaller than that of the Cursor method. Hence the results demonstrated that RCA method and Lorentzian fit method have much better repeatability than the Cursor method too.

The permittivity measurement result was  $64.51 - j*15.92$  at 5.8 GHz for hp85070 coaxial probe system. As shown in Table 6.3, the permittivity of orange juice with our measurement system is  $65.40-j*20.30$ ,  $64.15-j*21.01$  and  $64.15-j*20.75$  for cursor method, RCA method and Lorentzian fit method, respectively.

Table 6.3 Permittivity of orange juice at 5.8 GHz

No	Cursor		RCA		Lorentzian Fit	
	$\epsilon'$	$\epsilon''$	$\epsilon'$	$\epsilon''$	$\epsilon'$	$\epsilon''$
1	64.48	20.79	64.20	20.92	64.21	20.76
2	63.23	20.56	64.15	20.98	64.13	20.71
3	67.98	20.18	64.17	21.04	64.18	20.85
4	64.87	19.46	64.28	21.02	64.27	20.69
5	66.56	19.52	64.14	20.99	64.16	20.76
6	63.74	20.47	64.27	20.92	64.29	20.66
7	66.76	19.63	64.13	21.06	64.13	20.83
8	63.02	20.35	64.05	21.02	64.03	20.65
9	66.65	20.14	64.21	21.00	64.20	20.95
10	63.32	20.94	64.06	20.96	64.05	20.63
11	65.73	19.40	64.19	21.03	64.23	20.87
12	68.35	20.37	64.18	20.91	64.19	20.77
13	68.77	20.21	64.26	21.00	64.24	20.53
14	65.33	20.85	64.14	20.98	64.14	20.75
15	67.29	19.92	64.07	21.04	64.10	20.85
16	64.23	20.61	64.15	21.04	64.14	20.61
17	68.00	21.15	64.16	21.11	64.15	20.82
18	63.43	20.48	63.98	21.04	63.97	20.76
19	64.20	20.70	64.09	21.10	64.07	20.87
20	62.13	20.34	64.04	21.06	64.07	20.76
Average	65.40	20.30	64.15	21.01	64.15	20.75
Standard Deviation	2.02	0.50	0.08	0.05	0.08	0.10



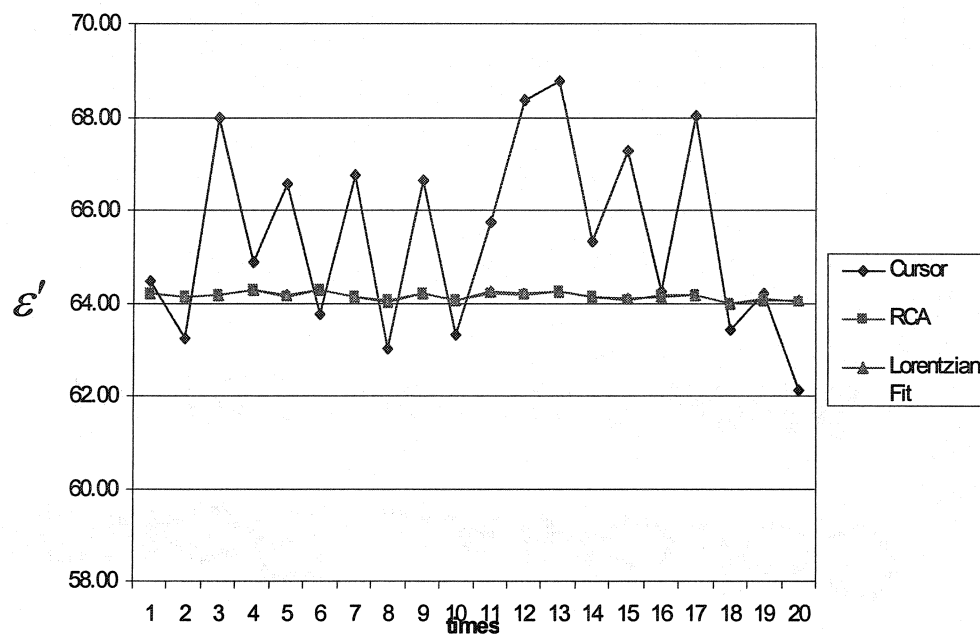


Figure 6.13 Dielectric constant of orange juice at 5.8 GHz

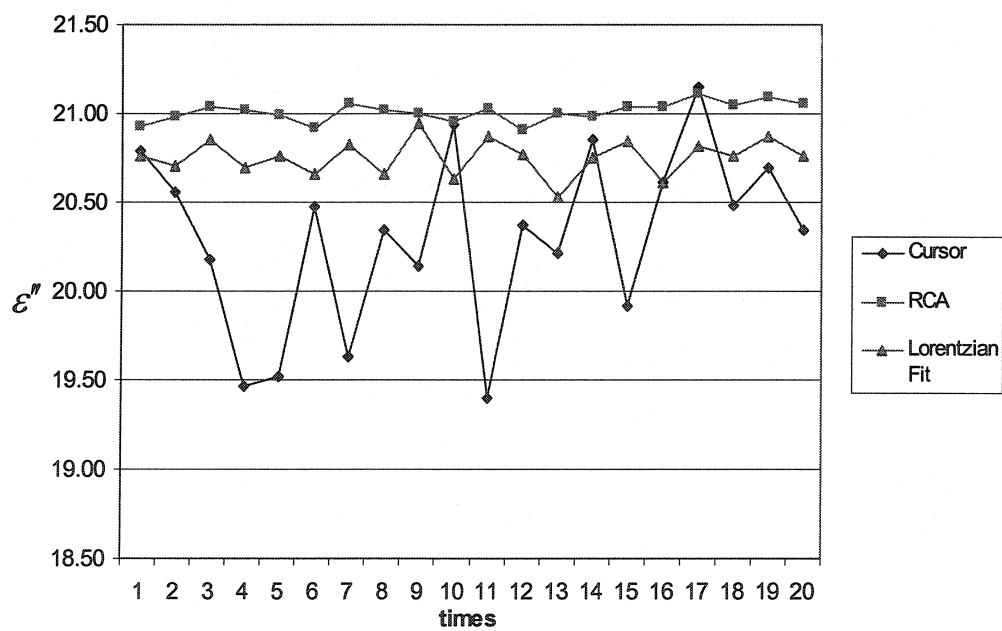


Figure 6.14 Dielectric loss factor of orange juice at 5.8 GHz

#### 6.3.1.4 *Apple juice*

Apple juice (Rougemont<sup>®</sup>: 21g carbohydrate, 19g sugars, 10mg sodium, 240mg potassium, and 110% vitamin C in every 200ml apple juice) was bought from the local super market and stored in the refrigerator. Apple juice sample was prepared as orange juice. The measurement results with different methods were listed in Table 6.4 and plotted in Figure 6.15 and Figure 6.16, respectively.

From the measurement results, we have noted that the characterizations of apple juice in the permittivity for different measurement methods are very similar to those of orange juice. As shown in Table 6.4, for dielectric constant  $\epsilon'$ , both RCA method and Lorentzian fit method gave almost same results, 62.50 and 62.54, respectively. The cursor method produced a larger value, 63.60. Hp85070 gave a very close value, 62.75, with RCA and Lorentzian fit method. For the dielectric loss factor  $\epsilon''$ , the results from Cursor, RCA and Lorentzian fit method are close, they are 20.10, 20.83 and 20.42, respectively. However, hp85070 gave a smaller value, 14.82.

As shown in Figure 6.15, for dielectric constant  $\epsilon'$ , both RCA method and Lorentzian fit method exhibit excellent repeatability (very small deviation). The Cursor method resulted in very poor repeatability, a very large deviation exist for different measurement. The standard deviation is as large as 2.44, which is at least 30 times larger than those of RCA method and Lorentzian fit method (0.08 and 0.07).

As shown in Figure 6.16, for loss factor  $\epsilon''$ , RCA method exhibits best repeatability (smallest deviation, 0.08). The Cursor method resulted in the worst repeatability, its standard deviation is 0.42, four times as large as the standard deviation of Lorentzian fit method, and five times as large as that of RCA method. The loss factors  $\epsilon''$  from RCA method are the largest among the three methods. However, the differences among the average values for the three methods are very small, less than 3.6%.

Table 6.4 Permittivity of apple juice at 5.8 GHz

No	Cursor		RCA		Lorentzian Fit	
	$\epsilon'$	$\epsilon''$	$\epsilon'$	$\epsilon''$	$\epsilon'$	$\epsilon''$
1	64.20	20.16	62.65	20.82	62.70	20.45
2	61.47	20.26	62.50	20.80	62.52	20.47
3	64.59	19.90	62.42	20.76	62.53	20.39
4	64.71	20.72	62.64	20.68	62.68	20.29
5	62.60	19.92	62.48	20.73	62.50	20.50
6	65.79	18.90	62.47	20.75	62.50	20.44
7	65.09	20.04	62.56	20.72	62.59	20.33
8	62.84	20.46	62.43	20.82	62.48	20.45
9	64.41	19.80	62.50	20.81	62.53	20.34
10	60.72	19.94	62.53	20.86	62.58	20.48
11	67.01	20.18	62.65	20.84	62.64	20.37
12	62.91	20.64	62.55	20.83	62.58	20.38
13	60.77	19.92	62.59	20.82	62.62	20.41
14	60.19	20.56	62.43	20.84	62.44	20.31
15	60.74	19.97	62.47	20.87	62.57	20.28
16	66.09	20.01	62.40	20.92	62.46	20.50
17	64.54	19.69	62.47	21.04	62.53	20.60
18	59.62	20.16	62.43	20.81	62.49	20.34
19	68.27	20.71	62.51	20.95	62.49	20.55
20	65.54	20.17	62.40	20.82	62.46	20.44
Average	63.60	20.10	62.50	20.83	62.54	20.42
Standard Deviation	2.44	0.42	0.08	0.08	0.07	0.09

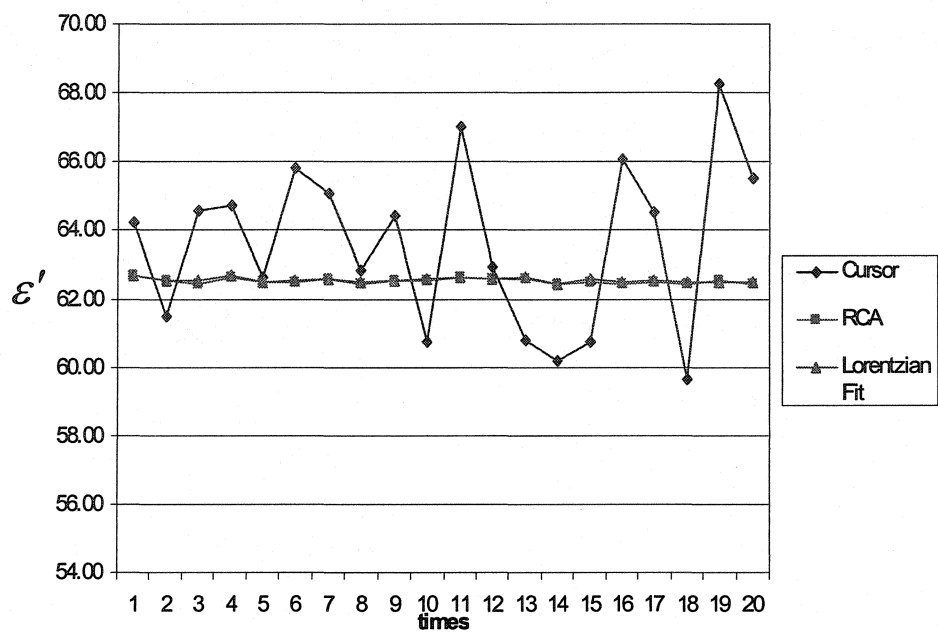


Figure 6.15 Dielectric constant of apple juice at 5.8 GHz

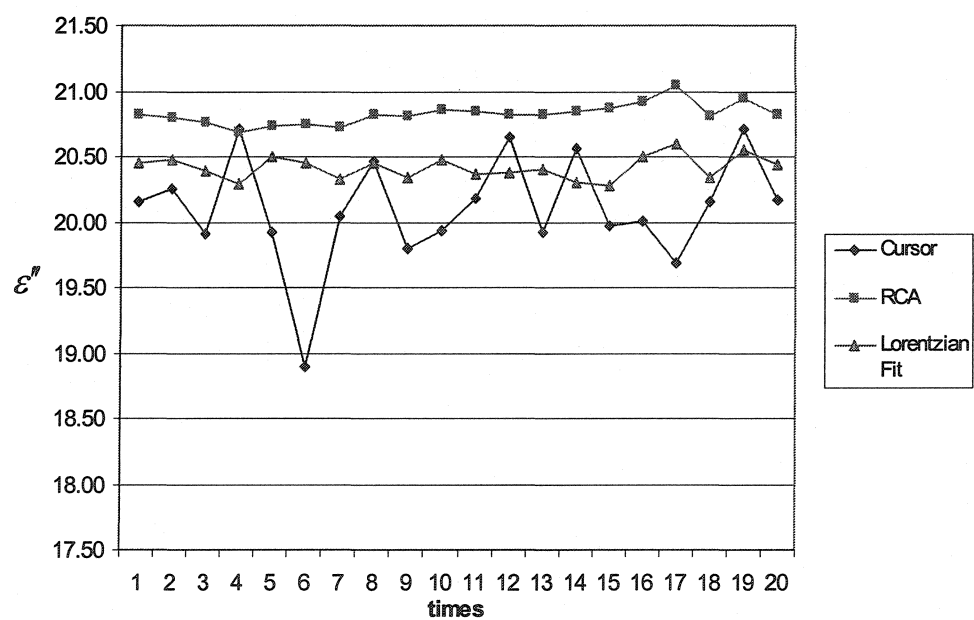


Figure 6.16 Dielectric loss factor of apple juice at 5.8 GHz

### 6.3.2 Median loss liquid

#### 6.3.2.1 *Methanol*

Absolute methanol (Anachemia<sup>®</sup>: AC-5732, UN-1230) was used as a median loss sample to validate the measurement system. It was injected into a standard corning micro-pipette (100ul) made of borosilicate glass and then was insert into the cavity for measuring. The measurement results with different methods were listed in Table 6.5 and plotted in Figure 6.17 and Figure 6.18, respectively.

As shown in Figure 6.17 and Figure 6.18, for the dielectric constant  $\epsilon'$ , both RCA method and Lorentzian fit method produced results with very small deviation (as low as 0.02), however, the Cursor method resulted in outcome with large deviation (0.45). Moreover,  $\epsilon'$  from RCA method and Lorentzian fit method are almost same. For the dielectric loss factor  $\epsilon''$ , the deviation is small for both RCA method and Lorentzian fit method. Whatever both RCA method and Lorentzian fit method exhibit much better repeatability than the Cursor method.

The permittivity measurement result was  $12.32 - j*10.33$  at 5.8 GHz for hp85070 coaxial probe system. As shown in Table 6.5, the permittivity of methanol with our measurement system is  $9.08 - j*7.01$ ,  $8.85 - j*7.53$  and  $8.88 - j*7.07$  for cursor method, RCA method and Lorentzian fit method, respectively.

Table 6.5 Permittivity of methanol at 5.8 GHz

No	Cursor		RCA		Lorentzian Fit	
	$\epsilon'$	$\epsilon''$	$\epsilon'$	$\epsilon''$	$\epsilon'$	$\epsilon''$
1	9.41	7.02	8.88	7.53	8.92	7.07
2	8.55	6.99	8.86	7.53	8.89	7.08
3	9.10	7.00	8.83	7.52	8.87	7.07
4	9.62	7.00	8.83	7.53	8.87	7.08
5	9.13	7.01	8.83	7.54	8.86	7.09
6	9.21	7.10	8.85	7.52	8.88	7.06
7	9.23	6.91	8.82	7.54	8.85	7.07
8	8.58	6.98	8.87	7.53	8.90	7.07
9	9.17	7.03	8.83	7.54	8.86	7.09
10	8.83	6.95	8.85	7.53	8.88	7.07
11	8.66	7.10	8.84	7.51	8.87	7.05
12	8.78	7.03	8.86	7.51	8.89	7.05
13	9.15	7.12	8.87	7.51	8.90	7.05
14	10.20	7.01	8.85	7.54	8.89	7.08
15	9.47	7.02	8.86	7.53	8.89	7.06
16	8.87	7.06	8.86	7.51	8.88	7.05
17	8.95	7.03	8.87	7.52	8.91	7.06
18	9.68	7.06	8.82	7.53	8.84	7.08
19	8.27	6.86	8.86	7.53	8.89	7.07
20	8.76	6.84	8.84	7.52	8.87	7.06
Average	9.08	7.01	8.85	7.53	8.88	7.07
Standard Deviation	0.45	0.07	0.02	0.01	0.02	0.01

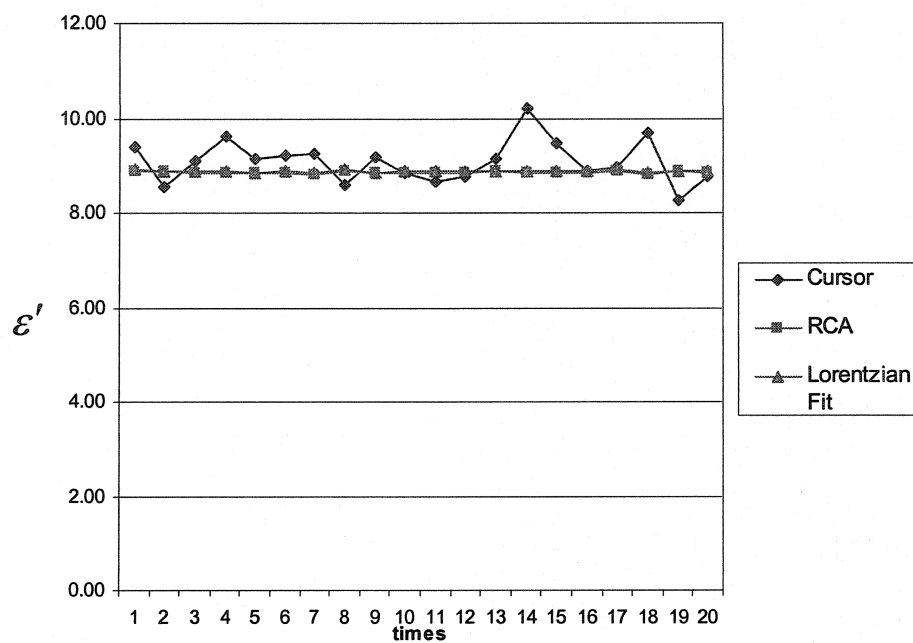


Figure 6.17 Dielectric constant of methanol at 5.8 GHz

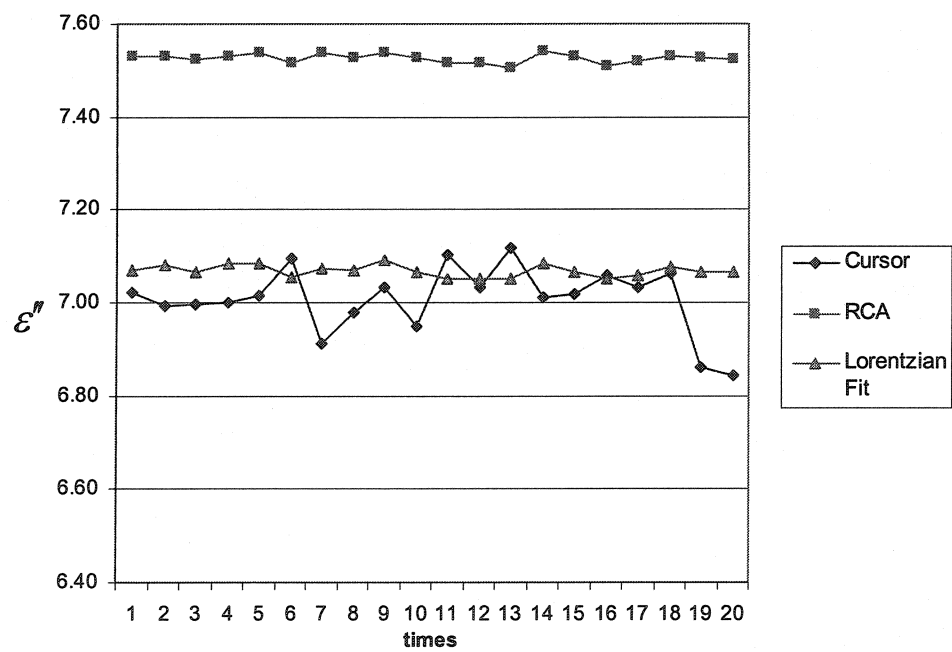


Figure 6.18 Dielectric loss factor of methanol at 5.8 GHz

### 6.3.2.2 *Alcohol*

Isopropyl rubbing alcohol (70%) was used as another median loss sample to validate the measurement system. It was injected into a standard corning micro-pipette (100ul) made of borosilicate glass and then was insert into the cavity for measuring. The measurement results with different methods were listed in Table 6.6 and plotted in Figure 6.19 and Figure 6.20, respectively.

From the measurement results, we have noted that the characterizations of alcohol in the permittivity for different measurement methods are similar to those of methanol. As shown in Table 6.6, for dielectric constant  $\epsilon'$ , Cursor method, RCA method and Lorentzian fit method produced similar results, 9.21, 9.09 and 9.13, respectively. Hp85070 gave the largest value, 13.51. For the dielectric loss factor  $\epsilon''$ , the results from Cursor and Lorentzian fit method are very close, they are 6.51 and 6.58, respectively. RCA method produced a little bit larger value, 6.99. However, hp85070 gave a much larger value, 9.76.

As shown in Figure 6.19, for the dielectric constant  $\epsilon'$ , both RCA method and Lorentzian fit method exhibit excellent repeatability (very small deviation, 0.02). Moreover, both methods gave very close results. The Cursor method resulted in very poor repeatability, a very large deviation exist for different measurement. The standard deviation is as large as 0.43, which is twenty-one times larger than those of RCA method and Lorentzian fit method (0.02).



As shown in Figure 6.20, for the loss factor  $\epsilon''$ , both RCA method and Lorentzian fit method exhibit excellent repeatability (very small deviation, 0.01). The Cursor method resulted in the worst repeatability, its standard deviation is 0.09, nine times as large as the standard deviation of RCA and Lorentzian fit method. The loss factors from RCA method are the largest among the three methods. The difference between the average value of RCA method and the Cursor method is about 7.4%.

Table 6.6 Permittivity of 70% alcohol at 5.8 GHz

No	Cursor		RCA		Lorentzian Fit	
	$\epsilon'$	$\epsilon''$	$\epsilon'$	$\epsilon''$	$\epsilon'$	$\epsilon''$
1	10.08	6.55	9.10	7.00	9.13	6.59
2	8.98	6.54	9.08	6.99	9.11	6.58
3	8.94	6.49	9.08	6.99	9.11	6.58
4	9.28	6.62	9.11	6.99	9.16	6.58
5	9.12	6.52	9.09	7.01	9.12	6.60
6	9.55	6.65	9.12	6.99	9.16	6.57
7	9.71	6.48	9.11	6.97	9.15	6.55
8	9.57	6.48	9.08	6.99	9.12	6.58
9	9.61	6.49	9.08	7.00	9.12	6.59
10	8.91	6.41	9.08	6.99	9.11	6.57
11	9.08	6.49	9.12	7.00	9.15	6.59
12	9.16	6.51	9.07	7.00	9.11	6.60
13	9.13	6.47	9.09	6.99	9.14	6.59
14	9.48	6.47	9.09	6.96	9.13	6.55
15	8.59	6.55	9.09	6.97	9.12	6.57
16	9.54	6.63	9.07	6.98	9.10	6.57
17	9.50	6.64	9.10	7.00	9.13	6.58
18	8.43	6.44	9.10	6.99	9.14	6.59
19	8.59	6.57	9.08	6.98	9.13	6.56
20	8.84	6.28	9.05	6.98	9.08	6.57
Average	9.21	6.51	9.09	6.99	9.13	6.58
Standard Deviation	0.43	0.09	0.02	0.01	0.02	0.01

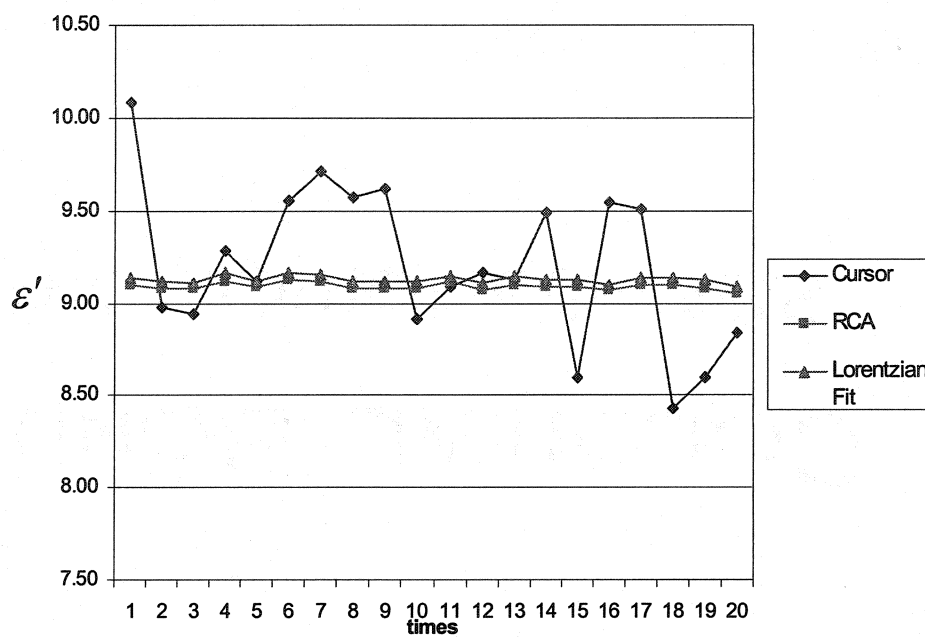


Figure 6.19 Dielectric constant of 70% alcohol at 5.8 GHz

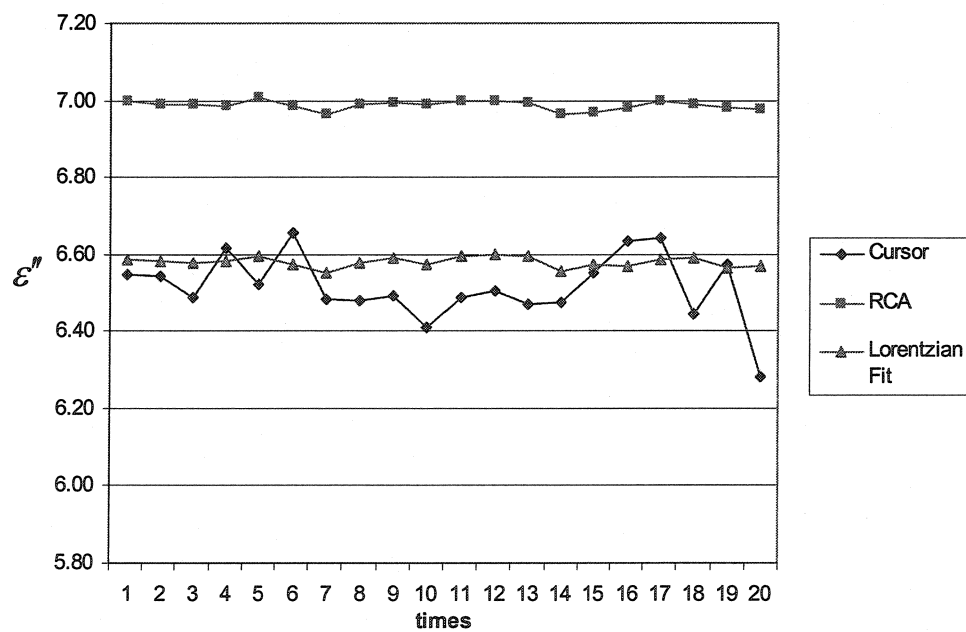


Figure 6.20 Dielectric loss factor of 70% alcohol at 5.8 GHz

### 6.3.3 Low loss liquid

#### 6.3.3.1 *Canola oil*

Canola oil (no name<sup>©</sup> : 2.8g Polyunsaturates, 5.8g Monounsaturates and 0.6g saturates ) was used as a low loss sample to validate the measurement system. It was injected into a standard corning micro-pipette (100ul) made of borosilicate glass and then was insert into the cavity for measuring. The measurement results with different methods were listed in Table 6.7 and plotted in Figure 6.21 and Figure 6.22, respectively.

As shown in Figure 6.21 and Figure 6.22, for the dielectric constant  $\varepsilon'$ , both RCA method and Lorentzian fit method produced results with very small deviation (as low as 0.001), however, the Cursor method resulted in outcome with large deviation (0.036). Moreover,  $\varepsilon'$  from RCA method and Lorentzian fit method are almost same. For the dielectric loss factor  $\varepsilon''$ , the deviations are small for both RCA method and Lorentzian fit method. Whatever both RCA method and Lorentzian fit method exhibit much better repeatability than the Cursor method.

The permittivity measurement result was  $2.694 - j*0.010$  at 5.8 GHz for hp85070 coaxial probe system. As shown in Table 6.7, the permittivity of canola oil with our measurement system is  $2.322-j*0.066$ ,  $2.298-j*0.064$  and  $2.301-j*0.062$  for cursor method, RCA method and Lorentzian fit method, respectively.

Table 6.7 Permittivity of Canola oil at 5.8 GHz

No	Cursor		RCA		Lorentzian Fit	
	$\epsilon'$	$\epsilon''$	$\epsilon'$	$\epsilon''$	$\epsilon'$	$\epsilon''$
1	2314	0.064	2297	0.065	2299	0.062
2	2312	0.065	2297	0.065	2299	0.062
3	2327	0.063	2296	0.065	2301	0.063
4	2276	0.065	2296	0.064	2300	0.061
5	2335	0.061	2297	0.065	2301	0.062
6	2246	0.067	2297	0.065	2301	0.063
7	2327	0.066	2298	0.064	2300	0.062
8	2326	0.066	2297	0.064	2300	0.061
9	2332	0.067	2296	0.064	2300	0.062
10	2409	0.065	2299	0.064	2301	0.062
11	2325	0.067	2298	0.065	2300	0.062
12	2337	0.070	2299	0.065	2301	0.062
13	2315	0.065	2298	0.064	2302	0.062
14	2282	0.066	2298	0.065	2301	0.062
15	2398	0.068	2298	0.064	2302	0.061
16	2294	0.065	2299	0.065	2303	0.062
17	2322	0.066	2299	0.064	2302	0.062
18	2299	0.069	2301	0.064	2303	0.061
19	2321	0.063	2300	0.064	2302	0.062
20	2343	0.066	2300	0.064	2304	0.062
Average	2322	0.066	2298	0.064	2301	0.062
Standard Deviation	0.036	0.002	0.001	0.000	0.001	0.001

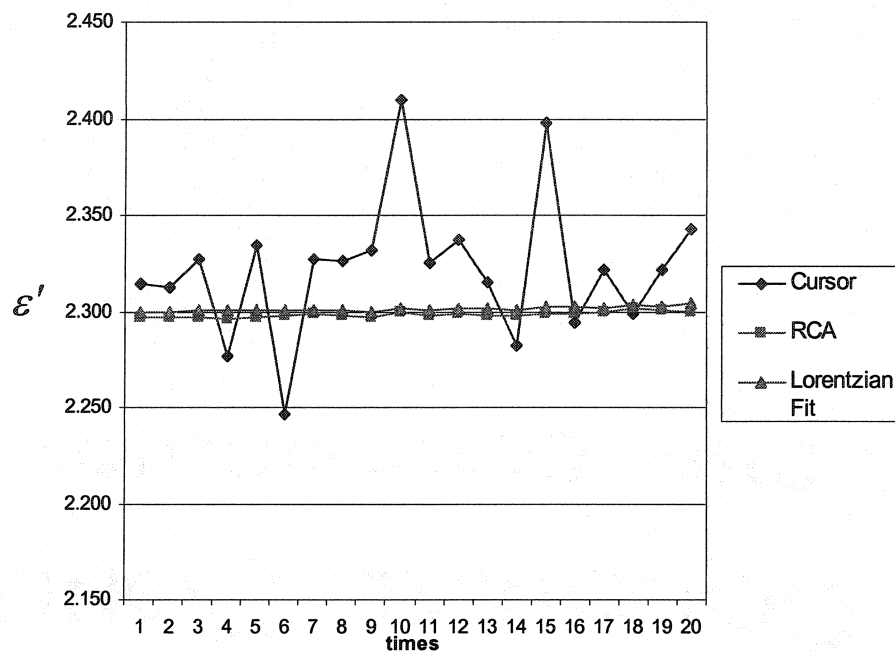


Figure 6.21 Dielectric constant of Canola oil at 5.8 GHz

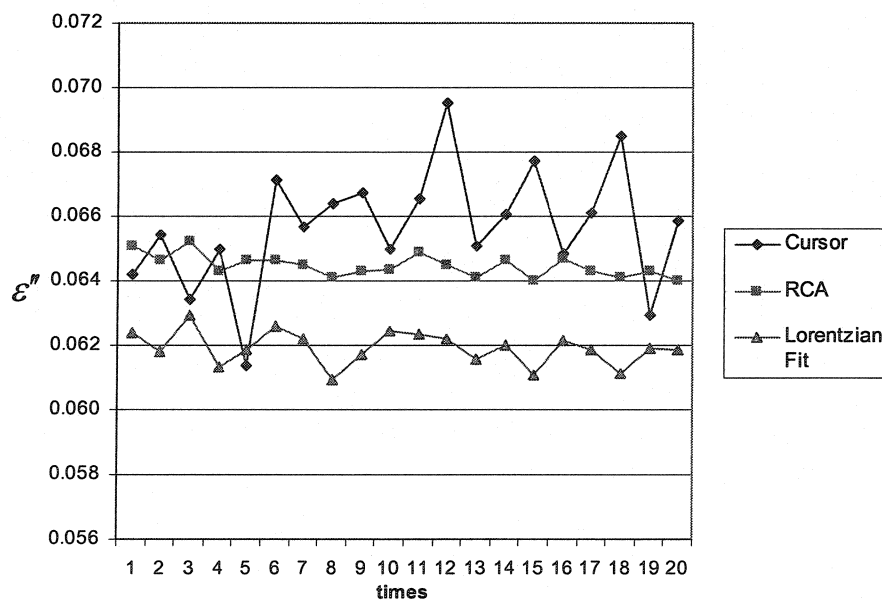


Figure 6.22 Dielectric loss factor of Canola oil at 5.8 GHz

### 6.3.3.2 *Vegetable oil*

Vegetable oil (no name<sup>®</sup> : 9.2g Polyunsaturates, 2.3g Monounsaturates and 1.4g saturates) was used as another low loss sample to validate the measurement system. It was also injected into a standard corning micro-pipette (100ul) made of borosilicate glass and then was insert into the cavity for measuring. The measurement results with different methods were listed in Table 6.8 and plotted in Figure 6.23 and Figure 6.24, respectively.

From the measurement results, it is noted that the characterizations of vegetable oil in the permittivity for different measurement methods are similar to those of canola oil. For dielectric constant  $\epsilon'$ , RCA method and Lorentzian fit method produced very close results, 2.450 and 2.454, respectively. The Cursor method presented larger result, 2.490. Hp85070 gave the largest value, 2.716. For the dielectric loss factor  $\epsilon''$ , the results from Cursor, RCA and Lorentzian fit methods are very close, they are 0.065, 0.064 and 0.062, respectively. However, hp85070 gave a much smaller value, 0.013.

As shown in Figure 6.23, for the dielectric constant  $\epsilon'$ , both RCA method and Lorentzian fit method exhibit excellent repeatability (very small deviation, 0.002 and 0.001). Moreover, both methods gave very close results. The Cursor method resulted in very poor repeatability, very large deviations exist for different measurements. The standard deviation is as large as 0.029, which is twenty-nine times larger than that of Lorentzian fit method (0.001).

As shown in Figure 6.24, for the loss factor  $\epsilon''$ , both RCA method and Lorentzian fit method exhibit excellent repeatability, the standard deviations of both RCA method and the Lorentzian fit method are smaller than 0.001. The Cursor method resulted in poorer repeatability, its standard deviation is 0.002. The loss factors from Lorentzian fit method are the smallest among the three methods. The difference between the average value of Lorentzian fit method and the Cursor method is about 4.8%.

Table 6.8 Permittivity of vegetable oil at 5.8 GHz

No	Cursor		RCA		Lorentzian Fit	
	$\epsilon'$	$\epsilon''$	$\epsilon'$	$\epsilon''$	$\epsilon'$	$\epsilon''$
1	2.490	0.068	2.449	0.064	2.453	0.062
2	2.451	0.065	2.449	0.064	2.452	0.061
3	2.480	0.064	2.448	0.064	2.452	0.061
4	2.467	0.065	2.449	0.064	2.452	0.061
5	2.540	0.066	2.448	0.064	2.452	0.061
6	2.516	0.062	2.449	0.065	2.451	0.062
7	2.485	0.066	2.448	0.064	2.452	0.061
8	2.433	0.064	2.449	0.065	2.453	0.062
9	2.453	0.067	2.451	0.065	2.454	0.062
10	2.492	0.066	2.449	0.065	2.453	0.062
11	2.474	0.066	2.450	0.064	2.454	0.062
12	2.474	0.065	2.450	0.065	2.454	0.062
13	2.471	0.065	2.450	0.065	2.454	0.062
14	2.536	0.064	2.452	0.064	2.454	0.062
15	2.536	0.064	2.452	0.064	2.455	0.062
16	2.509	0.067	2.452	0.064	2.455	0.062
17	2.514	0.064	2.453	0.064	2.456	0.062
18	2.490	0.063	2.451	0.064	2.456	0.062
19	2.502	0.063	2.451	0.064	2.456	0.062
20	2.484	0.067	2.451	0.065	2.455	0.062
Average	2.490	0.065	2.450	0.064	2.454	0.062
Standard Deviation	0.029	0.002	0.002	0.000	0.001	0.000

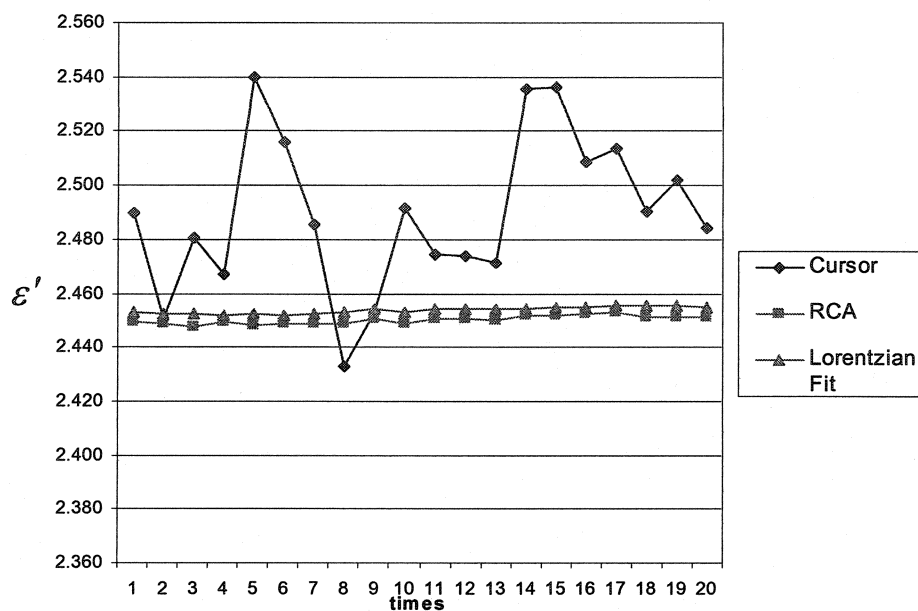


Figure 6.23 Dielectric constant of vegetable oil at 5.8 GHz

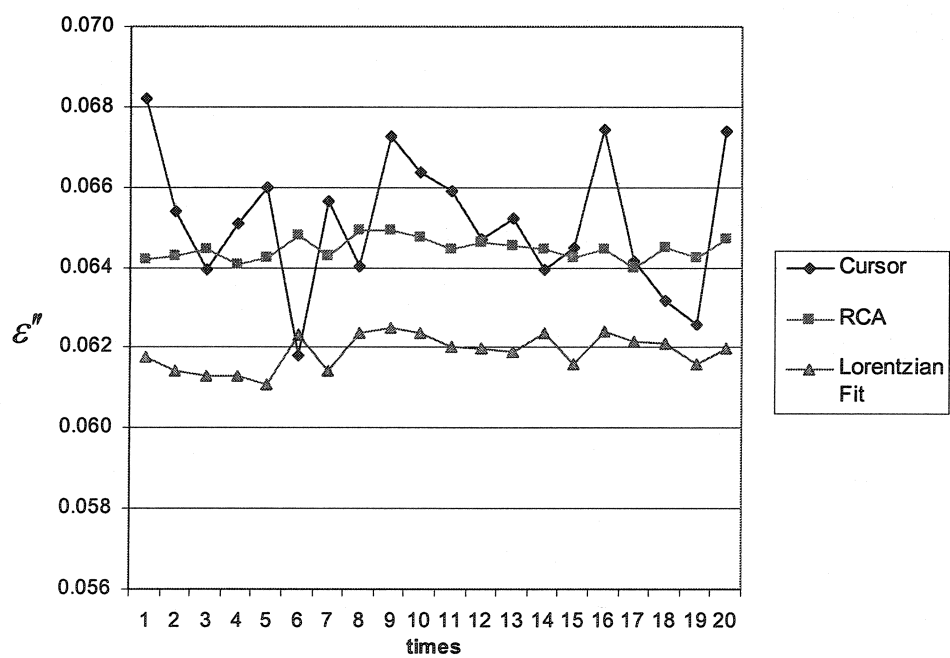


Figure 6.24 Dielectric loss factor of vegetable oil at 5.8 GHz



## References:

- [1] C. Akyel, and R. G. Bosisio, "New developments on automated-active circuits for permittivity measurements at microwave frequencies", IEEE Trans. Instrum. Meas., vol.38, no.2, pp.496-504, April 1989.
- [2] Martin Chaplin , Water structure and behaviour,  
<http://www.sbu.ac.uk/water/index.html>
- [3] J. B. Hasted, Liquid water: Dielectric properties, in F. Franks (Ed), *Water A comprehensive treatise*, Vol 1, (Plenum Press, New York, 1972) pp. 255-309.
- [4] R. Buchner, J. Barthel and J. Stauber, The dielectric relaxation of water between 0° C and 35° C, *Chem. Phys. Lett.* 306, 1999.
- [5] Kaatze, U. and V. Uhlendorf, The Dielectric Properties of Water at Microwave Frequencies, *Zeitsch f Physik. Chemie Neue Folge*, 1981.

## Chapter 7 Conclusion and future work

The aim of this research was to design and implement an automatic permittivity measurement system in order to measure the permittivity of the dielectric materials at the frequency band of ISM 5.8 GHz. The permittivity measurement was based on the cavity perturbation theory and utilized a rectangular cavity operating in the  $TE_{315}$  mode.

A new calibration permittivity measurement method, suitable for any resonant mode of rectangular or circular cavity, was proposed and implemented in an automatic permittivity measurement system at 5.8 GHz. Consequently, it was not necessary to calculate the sample filling factors with a complicated high-order mode electromagnetic analysis. These filling factors were obtained via the calibration with some known permittivity samples such as pure water. In addition, compared with the traditional calibration method which only uses one filling factor, two filling factors were used in the calibration process in order to improve the accuracy of the dielectric loss factor.

$TE_{315}$  mode is selected as the work resonant mode. An optimization design approach of the high-order resonant mode for a rectangular cavity was proposed and implemented. The resonant frequency of the empty cavity measured is 5.8066GHz. Hence there was only a 6.6MHz frequency deviation from the design target of 5.8 GHz. The measurement results of the resonant modes at approximately 5.8 GHz demonstrated the

effectiveness of this optimization method. The cavity exhibited a high Q-factor ( $>4000$ ) in the empty cavity condition and, thereby, indicated an accurate and reliable measurement.

An automatic complex permittivity measurement system controlled completely by PC was established. The measurement software PermiSys, which provided a friendly GUI, was developed using VC++ and MFC. The communication between PC and VNA was through the GPIB interface. The Virtual Instrument Software Architecture (VISA) was adopted in the communication program so as to maintain compatibility between PermiSys and different GPIB cards. The PermiSys provided a visual mode to configure and control the measurement system. Following the prompt of the measurement wizard, it was possible for the measurement to be executed step by step. Moreover, a multi-time measurement was carried out automatically to get a more precise measurement result. The resonant curve data and the permittivity measured by the Cursor method are saved in a PC.

These resonant curve data can be further processed by a Matlab program with the RCA method or the Lorentzian fit method to get more accurate results. This data processing Matlab program also has a graphical user interface to make operation more convenient. It can be invoked from the menu of PermiSys or be directly started up by clicking on the icon on the desktop of Windows.

The measurement results of three kinds of liquid samples (high-loss, intermediate-loss and low-loss) validated the effectiveness of the measurement system. The data processing results demonstrated that the RCA and Lorentzian methods are more accurate than the Cursor method.

## **Future work**

In order to improve the performance of the system, we can do some further works in the following aspects. First of all, as we describe in the thesis, the cavity design was based on the traditional electromagnetic analysis and optimization. This can only determine the position of the transformers of the waveguide-to-coaxial at the input and the output ports. However, by the help of Ansoft HFSS, we can design the transformers so that the coupling coefficients of the input and the output ports can be optimized.

Secondly, the RCA method and the Lorentzian fit method can be implemented in PermiSys with VC++. In this way, all of the results with different data processing methods can be obtained immediately after the raw data are acquired from VNA.

Finally, even though only liquid samples were used to validate the measurement system in this project, solid samples can also be measured with this system. A solid sample with known permittivity, such as Teflon, can be used as the standard sample to calibrate the measurement system. However, it should be noted that the samples measured should have same volume and same shape with the standard sample. Hence it requires more sample preparation work.

## Appendix I VNA Programming

How can we automate measurement using VNA HP8753/HP8510 with an external controller (PC) via the GPIB? The internal microprocessor of the VNA controls the system instrument via its system bus and calculates all data internally. However, we also can connect an external controller such as a PC to the VNA's GPIB interface to fully control VNA remotely. In this way, we can control the system state of VNA, transfer data between PC and VNA memory, and control the instruments connected to the VNA system bus via the PC. These capabilities provide the possibility to construct an automated permittivity measurement system with a VNA easily.

Generally speaking, the same sequences as pressing VNA front panel hard-keys and soft-keys can be employed to program the VNA system state through the standard GPIB protocol. The default GPIB address of the VNA is 16.

### COMMAND FORMAT

The basic command format of VNA HP8753/HP8510 consists of a four- to eight-character followed by a numeric in the basic measurement units when required. For example, the *START* key is programmed using *STAR*. Several commands can be written in logical sequences, separated by the semicolon. For example, string

*"PRES;STAR5.75E9; STOP5.85E9;S21;LINP;MARK5.8E9;"* represents to Preset the system, select a 5.75GHz to 5.85GHz sweep, display S21 using the polar format, and then position the measurement maker at 5.8GHz. The semicolon (;) is used to terminate each individual command. Numeric entries with no unit terminator are equivalent to pressing the x1 key in the entry area.

In order to improve the readability, it is allowed to include the actual units for frequency, time and voltage values following the numeric. For example, in the previous command string *"PRES; STAR5.75GHz; STOP5.85GHz; S21; LINP; MARK5.8GHz;"* GHz is used as the frequency unit. The units could be GHz, MHz, KHz, or Hz for frequency entries, fs, ps, ns, us, ms, or s for time entries, and V or mV for voltage entries. Both uppercase and lowercase characters are allowed to use.

### **READ THE RESONANT CURVE DATA**

A complete resonant curve data can be read from VNA memory using following command sequences:

*"STAR5.75GHz; STOP5.85GHz;"*

*"CHAN1; S21; LOGM; SING; REFP 9;"*

*"FORM3; OUTPDATA;"*

Here *"STAR5.75GHz; STOP5.85GHz;"* stands for sweeping from 5.75GHz to

5.85GHz. "CHAN1; S21; LOGM;" represents to select channel 1, to display S21 using the LOG format. "SING;" command is used to synchronize data output with completion of data acquisition.

FORM3 is a typical method used in this project. It adopts IEEE 64 bit floating point format (16bytes/point). For FORM3 data transmission format, the data is transferred in a sequence consisting of a preamble, the two ASCII Characters #A, a two byte ASCII integer which give the total number of bytes to be transferred, and practical data pairs of real, imaginary numbers. The total number of output pairs corresponds to the number of points currently selected, such as 801.

"FORM3; OUTPDATA;" prepares the VNA to transfer the resonant curve data from the Corrected Data array for the currently selected channel. To read data, we can use a real array variable such as Data(\*), where Data is a two-dimensional array (n elements by 2 elements where n is the current number of points selected), to receive the real/imaginary data pairs that make up the resonant curve.



## Appendix II Virtual Instrument Software Architecture (VISA)

This Virtual Instrument Software Architecture (VISA) is a special software technique used for configuring, programming instrument systems with GPIB, GPIB-VXI, VXI, MXI, Ethernet TCP/IP and/or Serial bus interfaces. It supplies with a common foundation for the interoperation of the high-level multi-vendor system software components, such as instrument drivers, soft front panels, and application software. The VISA framework standardizes the I/O layer between instrument drivers and controllers.

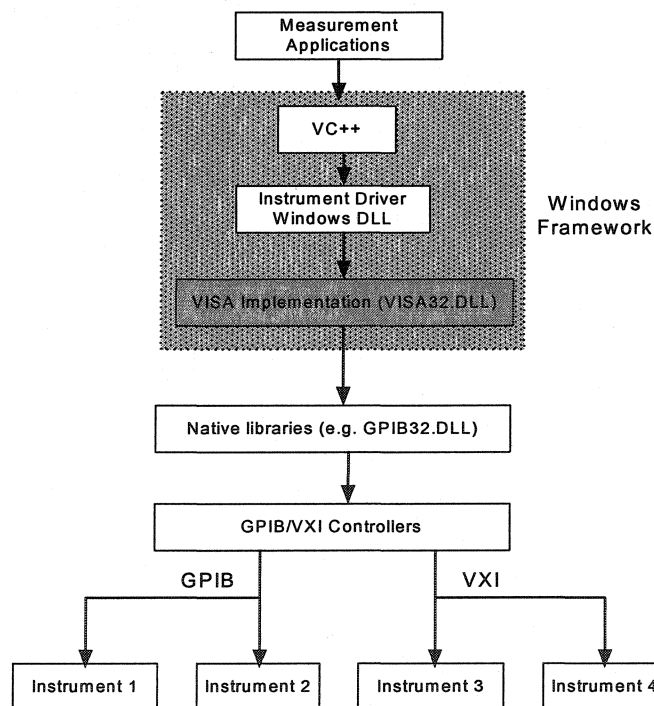


Figure A-1 VISA implementation context

The VISA specification was defined by the VXI Plug-n-Play Alliance. The

specification describes an abstraction layer and a set of interface functions as shown in Figure A-1. Figure A-1 shows the context for a VISA implementation. VISA virtualizes instruments, interfaces, backplanes, and low-level access to devices. It defines the following mandatory resource types for GPIB:

- ❑ INSTR (Instrument);
- ❑ INTFC (Interface);

The optional/recommended resource types are:

- ❑ BACKPLANE;
- ❑ SERVANT.

Each resource has attributes, events and operations. A Resource Manager is designed to manage these resource types. A default resource manager must be implemented for identifying and registering resources, managing sessions, controlling access and addressing. Resources are accessed through sessions. Multiple sessions may be initiated with the same VISA resource.

The search and navigation for a resource must be supported through a resource list of the available resources. There are 14 types of resource strings that have been defined for addressing devices on various interfaces. Translations between these resource strings and interface-specific formats are done by a function of the VISA implementation.

Implementing the VISA specification is not an easy task. Fortunately, the manufacturers of GPIB interface card, such as Agilent and National Instrument, have supported VISA. They have implemented the VISA specification. Therefore, we can use the VISA instead of the GPIB functions in the measurement software development process. This makes the measurement software system independent of a specific GPIB card. In this way, the application software has higher flexibility.